Università degli Studi di Napoli "Federico II"

Università di Camerino Consiglio Nazionale delle Ricerche

Optimal parent Hamiltonians for many-body systems

Dottorato di ricerca in Quantum Technologies
Ciclo XXXV
Anni 2019/2022
Coordinatore: Prof. Francesco Tafuri

Settore scientifico disciplinare FIS/03

Dottorando:
Davide Rattacaso

Tutori:
Prof. Rosario Fazio
Prof. Procolo Lucignano

Author:
Davide Rattacaso

Supervisors:
Prof. Rosario Fazio
Prof. Procolo Lucignano

Institute:
Università di Napoli Federico II, Naples, Italy

DEDICATION

To my parents

CONTENTS

1 INTRODUCTION

1.1 MOTIVATIONS AND GOALS

Given a quantum state, the inverse problem consists in the determination of a realistic Hamiltonian, called parent Hamiltonian, that captures the physics of the system, i.e. a Hamiltonian having such state as an eigenstate or ground state or, in the case of time-dependent states, generating the observed time evolution. We call *realistic* a Hamiltonian consisting in a superposition of a set of interactions fulfilling some constraint that depend on the system under exam, such as being local or engineerable.

The search for efficient strategies for finding parent Hamiltonians represents an important step towards the development of novel quantum technologies, especially in this noisy intermediate-scale quantum era. This search is indeed intimately related to quantum state control, verification, and benchmarking of quantum devices, and design of annealing schedules. More specifically, the ability to learn a Hamiltonian from the results of measurements, and therefore from a total or partial knowledge of the system's state, is a necessary skill for verifying the correct functioning of new quantum devices. Furthermore, knowing which Hamiltonian is compatible with a given evolution allows us to tune the control parameters of these devices to control their state. This allows for the implementation of states that serve as building blocks for quantum algorithms, such as graph states, or that encode important characteristics of condensed matter systems, such as the Jastrow-Gutzwiller wave functions.

In the context of many-body quantum systems, where the space of states increases exponentially in the system size while the space of realistic Hamiltonians increases polynomially, defining new methods to build suitable parent Hamiltonians represents a major challenge. The necessary effort to reach this goal is strictly related to stimulating theoretical questions in the context of quantum information. For example, it can help us to understand the relationship between the information content of a given quantum state (correlation length, entanglement, complexity...) and the system resources in terms of interactions (range and weight of the interactions, size, and oscillations of the couplings...).

From a computational point of view, the need to reconstruct the system's Hamiltonian is faced with the exponential growth of the complexity of this task in the size of the systems under examination. As a consequence, the greater the computational advantage we can obtain through these quantum devices, the greater the difficulty we encounter in verifying their correct functioning and controlling their state. For this reason, in this era of rapid development of quantum technologies, it is necessary to increase efforts to develop optimal

strategies for searching for parent Hamiltonians. In recent years, numerous optimization strategies have been proposed that apply to different situations, from benchmarking to optimal control, from measurements on time-independent states to the study of the dynamics of observables.

In this thesis, we propose optimal strategies to search for realistic parent Hamiltonians for time-dependent states. As we will see, the possible applications of this approach range from quantum state control to the selection of optimal strategies for learning. Furthermore, by considering the adiabatic limit of our strategy, we can dynamically obtain parent Hamiltonians from their ground states, swapping the role of the Hamiltonian and the state in quantum annealing.

We can divide our original contributions to the search for parent Hamiltonians in three parts, corresponding to three different but strictly related points of view on this problem

- *Finding an optimal generator for a time-dependent state.*

  We propose a method to define a realistic time-dependent Hamiltonian capable of generating a target time-dependent state by minimizing a suitable cost functional on a space of allowed interactions. This approach can be exploited to drive many-body states in synthetic quantum systems and to define a geometric measure of the accessibility of a path of states depending on the locality of allowed interactions. We also show the direct relationship between our result and shortcuts to adiabaticity.

- *Learning the Hamiltonian of a quantum device from a time-dependent state.*

  We extend the optimization approach to Hamiltonian learning of quantum devices, showing how it is possible to reconstruct the unknown Hamiltonian couplings of a synthetic quantum system from measurements on a single time-dependent quantum state and proving that the ergodic behavior of time-evolution is a resource for Hamiltonian learning.

- *Adiabatic limit of the time-dependent inverse problem.*

  We consider the adiabatic limit of the time-dependent inverse problem: given a path of many-body quantum states, we want to find a local Hamiltonian having the target states as ground states, i.e., a *proper* parent Hamiltonian. This task generally is exponentially hard in the system size. In analogy with standard adiabatic quantum computation, we define evolution in the space of local Hamiltonians that, in the adiabatic limit, generates an approximated proper parent Hamiltonians for the target states. Remarkably, this evolution can be integrated in a polynomial amount of time in the system size, allowing an efficient reconstruction of proper parent Hamiltonians.

An additional part of this thesis work, is dedicated to the evolution of non-stabilizerness in integrable spin systems, with a focus on the transverse-field Ising model. This part is not connected directly to the rest of the thesis. Non-stabilizerness is a resource for quantum computation, encoding the inability to efficiently simulate a given evolution using a classical computer through the stabilizer formalism. It represents, along with entanglement, a necessary ingredient for quantum speed-up. We estimate how non-stabilizerness evolves

after a quantum quench in subsystems of a large quantum system. This allows to evaluate the Hamiltonian's ability to generate this resource, and to elaborate on the connection between this ability and the integrable or chaotic behavior of the system. Finally, we study how dynamics affects the additivity that characterizes non-stabilizerness. This additivity seems to be connected to the presence of area-law entanglement, a property that disappears ballistically during evolution. In this way, we examine the interplay between entanglement and non-stabilizerness, which seems to underlie the impossibility of efficiently simulating quantum algorithms using classical computers.

1.2 THESIS OUTLINE

The remaining part of this thesis is structured as follows:

In Chapter 2 , we define the many-body quantum inverse problem [1]. We introduce the notion of realistic Hamiltonians and its connection with locality and engineerability. Given a many-body quantum state, we introduce the space of symmetries, i.e. the space of realistic Hamiltonians for which the state is an eigenstate, and the space of proper parent Hamiltonians, having the state as a ground state. Finally, we survey recent contribution in literature about the inverse problem, with a focus on the construction of realistic parent Hamiltonians from eigenstates and from ground states. Furthermore, we review some important contributions to the inverse problem for time-dependent state and related topics, such as Hamiltonian learning and quantum optimal control.

In Chapter 3 , we illustrate the first original contribution of this work. Following [2], we define an engineerable time-dependent parent Hamiltonian capable of driving an initial state through a target time evolution. We analyze the problem from a geometric point of view, introducing a measure for the accessibility of the target path of states and showing connections with shortcuts to adiabaticity.

In Chapter 4 , we extend results from the previous chapter to Hamiltonian learning, where the time-dependent state is actually implemented on a synthetic quantum device and the goal is to reconstruct the system Hamiltonian. Following [3], we show that the tentative of reconstructing the Hamiltonian is successful when the system state ergodically explores the Hilbert space: ergodicity is a resource for Hamiltonian learning.

In Chapter 5 , we face the reconstruction of local Hamiltonians from their ground state. To reach this goal, we introduce a novel and efficient approach called inverse quantum annealing [4], where the proper parent Hamiltonian is reconstructed through an adiabatic dynamic in the space of local operators.

In Chapter 6 , we investigate the non-stabilizerness evolution in an integrable spin chain [5]. In this way, we estimate the capability of the Hamiltonian of generating

states that are a resource for quantum computation. We also argue on how this capability is connected with the integrability of the system. Finally, we introduce a measure of localization of non-stabilizerness and examine how locality is destroyed by time evolution.

In Chapter 7 , the main results of this work are summarized, with a particular focus on open questions and future perspectives.

1.3 CONTRIBUTIONS

The results of this thesis are based on the following original contributions:

- **Davide Rattacaso**, Patrizia Vitale, and Alioscia Hamma. Quantum geometric tensor away from equilibrium. Journal of Physics Communications, 4(5). (2020) [[6]].
- **Davide Rattacaso**, Patrizia Vitale, and Alioscia Hamma. Towards a Geometrization of Quantum Complexity and Chaos. In: Lecture Notes in Computer Science. Springer International Publishing. (2021) [[7]].
- **Davide Rattacaso**, Gianluca Passarelli, Antonio Mezzacapo, Procolo Lucignano, and Rosario Fazio. Optimal parent Hamiltonians for time-dependent states. Physical Review A, 104(2). (2021) [[2]]. Discussed in Chapter 2.
- **Davide Rattacaso**, Gianluca Passarelli, Procolo Lucignano, and Rosario Fazio. *Optimal Parent Hamiltonians for Many-Body States.* In: Bayat, A., Bose, S., Johannesson, H. (eds) Entanglement in Spin Chains. Quantum Science and Technology. Springer, Cham. (2022) [[1]]. Discussed in Chapter 3.
- **Davide Rattacaso**, Gianluca Passarelli, and Procolo Lucignano. High-accuracy Hamiltonian learning via delocalized quantum state evolutions. Quantum, 7(905). (2023) [[3]]. Discussed in Chapter 4.
- **Davide Rattacaso**, Gianluca Passarelli, Angelo Russomanno, Giuseppe Santoro, Procolo Lucignano, and Rosario Fazio. Optimal parent Hamiltonians for time-dependent states. *Parent Hamiltonian searching by inverse quantum annealing.* (In preparation) [[4]]. Discussed in Chapter 5.
- **Davide Rattacaso**, Lorenzo Leone, Salvatore F.E. Oliviero, Procolo Lucignano, Rosario Fazio, Alioscia Hamma. *Non-stabilizerness dynamics in quantum spin chains.* (In preparation) [[5]]. Discussed in Chapter 6.

2

PARENT HAMILTONIANS FOR MANY-BODY STATES

2.1 INTRODUCTION

Many-body quantum systems are characterized by fascinating emerging behaviors, such as spontaneous symmetry breaking and long-range entanglement, that can not be efficiently simulated by classical computers. The idea of using synthetic quantum systems to simulate generic many-body quantum systems was proposed for the first time in a pioneering work by Feynman [8]. At the same time, it has been shown that the computational complexity of several problems can be exponentially reduced by implementing quantum algorithms on synthetic quantum systems [9]. Motivated by this close connection between many-body physics and quantum computation, a tremendous amount of work has been put forward in recent years to produce increasingly tunable artificial quantum systems, where a variety of observables can be measured and interaction couplings can be controlled with great precision [10–13].

Some of the most promising quantum platforms are based on trapped ions [14–18] or Rydberg atoms [19, 20]. These systems use electric and magnetic fields to confine and manipulate atoms, which can be used to encode and process quantum information. Superconducting circuits are another promising platform for quantum devices [21–23]. These circuits use superconducting materials to create microwave cavities that can trap and control individual photons. Superconducting circuits are often used to build quantum computers and other quantum devices, such as quantum sensors and quantum communication systems. Finally, photonic systems use light to encode and process quantum information [24]. Photons can be transmitted over long distances without being absorbed or scattered, which makes them an attractive choice for building quantum communication systems.

Once quantum devices are realized, we need to verify their proper functioning. This task is called quantum verification [25–30] and is crucial in the field of quantum computing and other quantum technologies, as quantum systems are prone to errors and can be difficult to evaluate and control. There are several techniques that are involved in verification, such as quantum state tomography, quantum process tomography, randomized benchmarking, and Hamiltonian learning. This latter consists in inferring the Hamiltonian generating the evolution of the systems from a collection of experiments on the systems, each of them ends with the measurement of certain observables [31–37].

The capability of controlling the Hamiltonian of a quantum system does not directly imply the ability to prepare and control an arbitrary quantum state with high precision. This is an important problem in quantum computing and other quantum technologies, as the performance of these systems depends on the ability to control their quantum state. Moreover, there are several many-body states that one wants to realize because of their properties, as for example Laughlin states[38], and would like to understand how to generate. In general, quantum state control can be obtained through adiabatic driving, or through the application of suitable quantum gates and measurements. The task of finding the control fields that will produce the desired evolution of the quantum state in the shortest amount of time, or with the least amount of resources is called optimal quantum control [39–51].

The need for controlling the state of these engineered systems through an optimal control strategy and the need for verifying their actual functioning by Hamiltonian learning are both related to a fundamental problem, the so-called *quantum inverse problem*. The inverse problem refers to the problem of reconstructing an unknown quantity from observations or measurements. In the context of quantum physics, the inverse problem consists in reconstructing the parent Hamiltonian of a quantum system from measurements of the system's dynamics. This generally allows us to understand the underlying physical mechanisms of a quantum system and to predict its behavior.

In this work, we deal with the search for parent Hamiltonians in many-body systems, consisting of numerous interacting particles capable of exhibiting a wide range of behaviors, including phase transitions and emergent collective phenomena. In this context, the inverse problem can be more challenging to solve because of the complexity of the system, which is reflected by the space of possible configurations whose dimension increases exponentially in the system size. At the same time, the amount of available resources, i.e., the size of the space of realistic Hamiltonians that can act on the system, increases polynomially either due to fundamental constraints like locality or because of technological limitations. As can be deduced from this premise, some fundamental aspect of many-body quantum theory and quantum information can be investigated in close relation with the inverse problem. Examples include whether a complete description of the system state is required to determine the physical laws governing the system, how many models are compatible with a set of measurements, whether a quantum system's high energy behavior may be deduced from its time-independent state or from its low energy behavior [52], or which portion of the Hilbert space is actually accessible in a world governed by local interactions [53]. All these questions are related to the search for parent Hamiltonians in some form, and will have a pivotal role in this work.

We focus our attention only on the inverse problem for unitary evolutions, anyway extensions to open quantum systems, consisting in the search for an unknown Lindbladian, have been recently proposed [54, 55]. To assort the several recent papers that investigated the problem with different methods and purposes, we can consider three statements of the problem, corresponding to different physical situations.

- In the first case, the system state is time-independent, being an eigenstate of the unknown Hamiltonian. Therefore, one wants to reconstruct a realistic Hamiltonian starting from one of its eigenstates [56–61]. We call this Hamiltonian **symmetry** of the state. Finding symmetries is an important step towards Hamiltonian learning for time-independent systems and a fundamental resource to perform quantum state preparation through adiabatic processes.
- In the second case, one tries to reconstruct a local Hamiltonian from one of its ground states [62–65]. We refer to this class of Hamiltonians as **proper parent Hamiltonians** (PPH). In low-temperature systems the capability of reconstructing PPHs allows to prepare target states [66–69] and to reconstruct system interactions.
- In the latter case, one tries to reconstruct the parent Hamiltonian for a time-dependent state. The time-dependent state can be not an eigenstate of the parent Hamiltonian, that can be thought as the **generator** of the evolution. In this form, the inverse problem has been especially investigated because of its relation with Hamiltonian learning and quantum state control [2, 70, 71].

In the first sections of this chapter, we illustrate some preliminary aspects of the inverse problem in many-body physics. The constraints that characterize realistic and engineerable Hamiltonians that are candidate parent Hamiltonians are described in Section 2.2. In Section 2.3 we wonder if a complete description of the state of the system is necessary to reconstruct its parent Hamiltonian. Finally, in Section 2.4 we analyze the relationship between inverse problem and Hamiltonian learning. Successively, we briefly survey the recent literature about the different forms of the problem. Section 2.5 is devoted to discussing the search for local or engineerable symmetries, while techniques for the reconstruction of PPHs are illustrated in Section 2.6. In Section 2.7 we focus on the search for generators of quantum dynamics and its relation to Hamiltonian learning and quantum state control. Based on the illustrated results, in Section 2.8 we propose an overall point of view on the inverse problem as a constrained optimization problem.

2.2 LOCAL AND ENGINEERABLE HAMILTONIANS

In large quantum systems, numerous constraints on possible interactions drastically limit the set of Hermitian operators representing realistic Hamiltonians. Some of these constraints are general, being intimately related to fundamental physical properties such as the principle of locality or the thermodynamic stability of matter[72]. Other constraints, such as symmetries and interaction range, depend on the considered system and the features of its constituents, for example, Rydberg atoms [19, 20] or superconducting transmons [21–23]. In practice, effective Hamiltonians representing systems in condensed matter or engineerable quantum devices can be written as the span of a small set $\mathcal{L}$ of Hermitian operators representing some elementary interactions. Since the identity operator only evolve a quantum system by a physically meaningless phase factor, from now on we

will assume that the set $\mathcal{L}$ does not include the identity operator. This is equivalent to ask that operators in $\mathcal{L}$, and consequently any considered Hamiltonian, are traceless.

In condensed matter systems, along with the symmetries, locality represents the most significant constraint: elementary interactions happen only between bodies within a finite distance l, called interactions *range*, that does not depend on the number of bodies. If bodies, as usually happens, are scattered in the space, this means that each of them can only interact with a finite number of the other ones. In this way, the number of elementary interactions remains linear in the system size.

Another ubiquitous constraint in many-body systems is the existence of finite interactions *weight* w. An interaction has weight w if it can not be written as the linear superposition of n-bodies interactions with $n < w$. The vast majority of condensed matter Hamiltonians are low-energy effective Hamiltonians of electromagnetically interacting electrons and protons Hamiltonians, where the interactions have weight 2. As a consequence, weight 2 interactions are very common in condensed matter. Having a Hamiltonian where the weight of elementary interactions scales with the system size, as it happens for a randomly chosen Hermitian operator, is unrealistic. Due to constraints on interactions weight, the number of elementary interactions is at most polynomial in the system size.

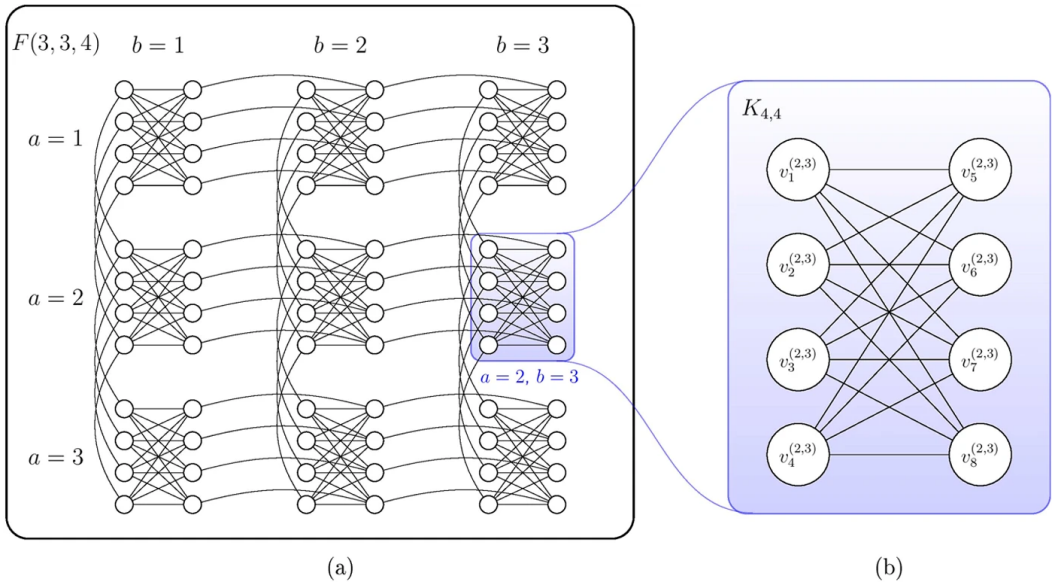

Figure 2.1: The Chimera graph that represents the qubit connectivity of D-Wave hardware. Each circle represents a different qubit and each line represents an interaction between qubits. Image from Ref. [73]

What about synthetic quantum systems, such as solid-state quantum circuits, trapped ions and photonic or atomic systems? Each of these devices is characterized by a fixed set of tunable interactions that can be used to simulate the effective Hamiltonians of condensed matter systems [14, 74, 75], to engineer quantum annealers capable of attaching NP-hard problems [76–80], or to build the fundamental gates needed for universal quantum computation [81]. In many cases, such as in quantum computers, all the interactions are designed to have weight 2 and range 2, since adjacent qubits CNOT gates and single spin gates are sufficient to arbitrarily approximate any unitary evolution [9]. In other cases, such

as in quantum annealing, the capability to realize all-to-all long-range interactions is fundamental to achieving important goals, such as finding solutions to the traveler salesman problem [80] or set covering problems [73]. In a large system, where realizing this kind of interaction is impossible, a compromise is made by resorting to effective long-range interactions [82] or to optimal device typologies such as the Chimera graph in D-Wave devices [83], which is shown in Figure 2.1. At any rate, all these synthetic quantum systems are ultimately characterized by some tunable interactions that are polynomial in the system size for large systems.

All these constraints can be taken into account considering a vector subspace of the Hermitian operators, spanned by the realistic interactions in $\mathcal{L}$, as the space of realistic Hamiltonians in which parent Hamiltonians must be searched. Other constraints, that are not taken into account in this work, can affect the couplings associated with the interactions in $\mathcal{L}$. The most important examples in this direction are the upper bounds on the magnitude of the couplings and on the rate at which they can change in time. These bounds reflect the experimental impossibility of generating signals with an arbitrarily large amplitude or frequency. At the same time, the tunable Hamiltonians acting on synthetic systems are effective Hamiltonians, that well approximate the device behavior only when the control fields are in a suitable range.

2.3 DO WE REALLY NEED FULL STATE TOMOGRAPHY?

Although the original formulation of the inverse problem consists in reconstructing a parent Hamiltonian from full knowledge of a quantum state, in most cases, one can collect and manage only partial information about the system. In Hamiltonian learning, for example, this is because performing a full reconstruction of the state, i.e., a *state tomography*, requires measuring an exponential number of observables in the system size. This requirement reflects the exponential number of degrees of freedom that define a many-body quantum state. Analogously, representing a generic quantum state on a classical computer requires exponential memory. The characterization of the actual functioning of quantum devices without resorting to a complete tomography is investigated in many cases in Ref. [53] and represents a fundamental step towards the realization of these devices. For this reason, in several applications, one aims to reconstruct the Hamiltonian without state tomography or, in other words, without the full knowledge of the state.

The possibility of reconstructing the parent Hamiltonian(s) from partial knowledge of the state is ultimately related to the locality (or to the engineerability) constraints that make the space of realistic Hamiltonians polynomial in the system size. As a consequence, a polynomial amount of information about the state determines the Hamiltonian. In some cases, the knowledge of the expectation values of a polynomial set $\{O_i\}$ of observables is sufficient to identify the unknown Hamiltonian, even if this does not imply that we are aware of this set in advance. However, since we often deal with local Hamiltonians, the set of local observables is a good candidate for this aim. This choice gives different results based on the specific inverse problem, i.e., the search for symmetries, PPHs, and

generators. A more sophisticated approach to the search for an optimal set of observables involves active learning strategies and will be introduced in the next section.

As argued in Refs. [60, 61], the possibility of reconstructing a time-independent parent Hamiltonian, i.e., a symmetry or a PPH, from local expectation values seems to be related to the existence of a unique solution for the quantum marginal problem [62, 84, 85], i.e. the determination of a quantum state starting from its local expectation values. The stationary behavior of a quantum state indeed implies the conservation of both local and non-local expectation values. Hence, if non-local expectation values can be determined from the local ones, the stationary behavior can be verified. As we are going to show in Section. 2.6, this is always possible if the state is the non-degenerate ground state of some local PH. Accordingly to this observation, in Refs. [60, 61] the authors observe that the capability of reconstructing Hamiltonian from their time-independent state decreases when the energy level of the state increases.

When the inverse problem has a unique solution, it is also possible in principle to reconstruct Hamiltonians from local expectation values of time-independent states. However, previous applications of this approach in the literature are characterized by strong assumptions, such as the applicability of the Bisognano-Wichmann theorem [64, 65], or by computationally hard tasks, such as the minimization of extremely complicated cost functions [60, 61]. This behavior is consistent with the quantum marginal problem: even if some states are completely determined by local expectation values, reconstructing these states can be exponentially hard in the system size.

The situation changes drastically in the time-dependent inverse problem, in which one aims to find the Hamiltonian that governs the observed evolution. In this setting, it has been shown [86] that a polynomial number of expectation values, i.e., the local expectation values, is generally sufficient to reconstruct a local Hamiltonian with arbitrary precision, without resorting to a computationally hard data post-processing. This is ultimately due to the Lieb-Robinson bound, showing that the evolution generated by local Hamiltonians propagates information at a finite velocity. Starting from this bound, the authors of Ref. [86] have shown that the error committed when approximating the evolution of local expectation values as a function only of other expectation values does not depend on the system size. This happens even though the Hamiltonian norm depends on the system size. As a consequence, the effect of a local Hamiltonian on the evolution of local operators only depends on local operators and can be quantified by measuring the corresponding observables to infer the system Hamiltonian.

2.4 INVERSE PROBLEM AND HAMILTONIAN LEARNING

Hamiltonian learning inherits most features, challenges, and techniques from the inverse problem, to the point that it can be considered as the secondary topic of this thesis. Therefore, it is fundamental to clarify here the conceptual differences between these two research fields and their main consequences.

We presented the inverse problem as the reconstruction of the system Hamiltonian from its state or, in some cases, from partial information about this state. In Hamiltonian learning instead, the source of information is not the system state, but an entire quantum device whose dynamics is governed by the unknown Hamiltonian. This device can be seen as a black box, on which some operations - state preparation, unitary operators, time evolution, and measurements - can be performed to infer the internal mechanism. The experimenter freely chose the functions to perform and collects information about the system. In other words, he is an active agent.

The most straightforward consequence of this freedom is that one can prepare several initial states, and solve the inverse problem simultaneously for all these states to collect faster the information about the Hamiltonian. In this way, methods originally intended as solutions to the inverse problem for a single state can be improved for Hamiltonian learning [70, 71].

Besides the freedom in state preparation, if we consider also the freedom in evolution time, unitary operations, and measurements, we end up with a vast collection of queries that can be executed on the device to collect information. In this context, the choice of the minimum set of queries capable of maximizing the amount of information becomes a fundamental challenge both for the experimenter and the quantum information theorist. Indeed, while in quantum experiments optimal management of resources is essential to avoid the need for unrealistic execution times, in quantum information theory the search for an optimal set of queries allows for the investigation of quantum advantage, as exemplified from Ref. [87] in Section 2.7.

2.5 TIME-INDEPENDENT INVERSE PROBLEM: RECONSTRUCTING SYMMETRIES

In the field of Hamiltonian learning, a valuable goal is to reconstruct the system Hamiltonian from measurements on a time-independent state. At the same time, finding the Hamiltonian that makes a given state time-independent is a fundamental step towards implementation of such state. For pure quantum states, this is equivalent to the search for symmetries: given a state $|\psi\rangle$, we look for the realistic Hamiltonians for which $|\psi\rangle$ is an eigenstate.

In this section, we briefly summarize some important results in literature about this topic. Firstly, we show that the space of symmetries can be efficiently and exactly reconstructed starting from the knowledge of the correlation functions between the elementary interactions in the Hamiltonian [56–58]. Finally, we show how symmetries can be approximately reconstructed also using only local expectation values [59–61].

2.5.1 *Correlation functions and symmetries*

In the context of Hamiltonian learning, where the state is already implemented on the quantum device, correlation functions can be efficiently measured. Other relevant cases in

which correlation functions are easy to calculate are Gaussian states, where one can exploit Wick's theorem, and matrix product states [88].

The key point in reconstructing symmetries from correlations is that a realistic Hamiltonian $H = \sum_i h_i L_i$, with $L_i \in \mathcal{L}$, is a symmetry for the state $|\psi\rangle$ if and only if the variance of H on $|\psi\rangle$ is zero [56, 57]:

$$\langle\psi|H^2|\psi\rangle - \langle\psi|H|\psi\rangle^2 = 0.$$

Replacing $H = \sum_i h_i L_i$ in the latter equation, we obtain

$$\sum_{ij} h_i h_j C_{ij} = 0, \tag{2.1}$$

where

$$C_{ij} := \langle\psi|\{L_i, L_j\}|\psi\rangle - 2\langle\psi|L_i|\psi\rangle\langle\psi|L_j|\psi\rangle \tag{2.2}$$

is a semi-definite positive matrix. We call this matrix, which has a central role in the inverse problem, *quantum covariance matrix* (QCM).

When the coefficients h_i of a Hamiltonian are in the kernel of the QCM, the variance is zero and, ultimately, the Hamiltonian is a symmetry. Being elements of a matrix kernel, the symmetries form a vector space: linear combinations of symmetries are in turn symmetries. We can easily define a basis for this vector space: given a basis $n_i^{(k)}$ for the kernel of the QCM, each symmetry can be written as

$$S = \sum_k s_k S_k,$$

where $S_k := \sum_i n_i^{(k)} L_i$ are realistic Hamiltonians. Moreover, if the vectors $n_i^{(k)}$ are orthogonal for the standard scalar product, $\{S_k\}$ is an orthogonal basis for the Hilbert-Schmidt product $(A, B) \equiv \mathrm{Tr}(AB)$:

$$\mathrm{Tr}\left(S_k S_l\right) = \sum_{ij} n_i^{(k)} n_j^{(l)} \mathrm{Tr}\left(L_i L_j\right) \propto \sum_{ij} n_i^{(k)} n_j^{(l)} \delta_{ij} \propto \delta_{kl}.$$

Studying the kernel of the QCM is not the only way to proceed. For example, in Ref.[58], it has been shown how parent Hamiltonians can be recovered from the kernel of the non-connected correlations matrix $C'_{ij} := \langle\psi|H_i H_j|\psi\rangle$. This is because that authors do not look for a traceless Hamiltonian. Anyway, beyond this formal difference, the two methods are practically equivalent.

One of the most successful aspects of these kernel-based approaches is that the size of the involved matrices, depending on the number of operators in $\mathcal{L}$, is polynomial in the system size. As a consequence, also the reconstruction of kernels requires a polynomial amount of time. This makes searching for symmetries very efficient once the local correlations are known.

A non-empty kernel is a fine-tuning condition for any matrix, since a small arbitrary perturbation easily changes the eigenvalues of kernel elements. As a consequence, in practical applications, the QCM is unlikely to have a non-empty kernel. In Hamiltonian learning in-

deed, any small error in measuring correlation functions destroys the matrix kernel, while in the artificial construction of local symmetries for the preparation of an arbitrary target state the existence of this kernel is exceptional. In these cases, one can look for *optimal symmetries*, which are the local Hamiltonians associated with the minimum eigenvalue of the QCM. The meaning of this optimality depends on the context: in Hamiltonian learning, this kind of solution is optimal for some likelihood estimation, while in state preparation the obtained Hamiltonian is optimal because that it minimizes the state evolution. In both cases, the optimal solution is the one that minimizes the infidelity between $|\psi\rangle$ and the infinitesimal time evolution $|\psi + d_t\psi\rangle$ generated by the unknown Hamiltonian H.

To prove this unified point of view, we need to introduce a measure of the infinitesimal infidelity between states. This is the so-called Fubini-Study length [89] of the difference between states, defines as $l_{\text{FS}}(d_t\psi) \equiv \langle d_t\psi|d_t\psi\rangle - \langle d_t\psi|\psi\rangle\langle\psi|d_t\psi\rangle$. The Fubini-Study length and the corresponding metric have a pivotal role in quantum information theory and, as we show in the following chapters, in the inverse problem. If we relate the time derivative of the state to the Hamiltonian couplings as $|d_t\psi\rangle = -i\sum_i h_i L_i|\psi\rangle$, the Fubini-Study length becomes

$$l_{\text{FS}}(d_t\psi) = \sum_{ij} C_{ij} h_i h_j$$

Hence, minimizing this length ultimately resort to looking for the minimum eigenvalues eigenvectors of the QCM.

2.5.2 *Local symmetries from local measurements*

The previously illustrated methods are based on the knowledge of non-local expectation values. However, one could ask if there is a way to reconstruct local symmetries from the knowledge of local expectation values. A possible approach has been proposed in Ref. [59], in which one starts from the Ehrenfest equation for the evolution of the expectation values of a set of local operators $\{O_k\}$ generated by the Hamiltonian $H = \sum_i h_i L_i$:

$$\partial_t\langle\psi|O_k|\psi\rangle = i\sum_j h_j\langle\psi|[L_j, O_k]|\psi\rangle.$$

Once we define the *commutator matrix* $K_{ik} = \langle\psi| - i[L_j, O_k]|\psi\rangle$, this equation can be written as

$$\partial_t\langle\psi|O_k|\psi\rangle = \sum_i h_i K_{ik}. \tag{2.3}$$

When a state is time-independent for the Hamiltonian H, the expectation values of the local operators O_k do not evolve and the LHS of the last equation becomes zero. Therefore, the coefficients of each symmetry correspond to zero-eigenvalue eigenvectors of the matrix K and optimal solutions can be obtained by looking at the minimum-eigenvalue eigenvectors of the correlation matrix $K^T K$. However, there is a caveat: Hamiltonians that only affect non-local expectation values are in the kernel of the commutator matrix even though they are not symmetries. We call these Hamiltonians *false symmetries*. Indeed, while

the evolution generated by a symmetry does not change a quantum state, i.e., each expectation value is conserved, the evolution generated by a false symmetry does not change the state locally, i.e., local expectation values are conserved but non-local ones could change. The existence of *false symmetries* depends on the fact that the evolution of non-local expectation values generally is not a function only of the local expectation values.

However, the authors of Ref. [59] have shown for some relevant examples that, when the set of measured observables O_k is sufficiently enlarged, this approach is able to effectively distinguish real symmetries. This is equivalent to increment the number of constraints on the Hamiltonians to eliminate false symmetries from the kernel.

What happens if we enlarge the set $\{O_k\}$ until it becomes a basis of the Hermitian operator space? In this case, Eq. 2.9 is equivalent to the Schrodinger equation, where the density operator $\rho = |\psi\rangle\langle\psi|$ of the state is represented as a vector. The components of this vector on the basis $\{O_k\}$ are defined through the Hilbert-Schmidt product, hence they coincide with the expectation values $\langle\psi|O_k|\psi\rangle = \mathrm{Tr}(\rho O_k)$. In this case, the couplings in the kernel of the commutator matrix K correspond to all the Hamiltonians that exactly generate the target evolution. On the other side, the couplings in the kernel of the QCM C correspond to all the Hamiltonians having the state as an eigenstate. To show the equivalence of these two definitions we prove that, when $\{O_k\}$ is an orthonormal basis for the Hermitian operators, the matrix $K^T K$ coincides with the QCM C:

$$\begin{aligned}(K^T K)_{ij} &= \sum_k K_{ki} K_{kj} = \sum_k \langle\psi| - i[L_i, O_k]|\psi\rangle\langle\psi| - i\langle[L_i, O_k]|\psi\rangle \\ &= \sum_k \mathrm{Tr}\left(-i[\rho, L_i]O_k\right) \mathrm{Tr}\left(-i[\rho, L_j]O_k\right) = -\mathrm{Tr}\left([\rho, L_i][\rho, L_j]\right) \\ &= \langle\psi|\{L_i, L_j\}|\psi\rangle - 2\langle\psi|L_i|\psi\rangle\langle\psi|L_j|\psi\rangle = C_{ij},\end{aligned}$$

where in the second line we exploited the cyclic property of the trace and the completeness of the basis $\{O_k\}$. As a consequence of the last equality, the kernels of the QCM and the commutator matrix coincide.

We have shown that local expectation values may contain sufficient information to reconstruct symmetries. The method of Ref. [59] is a clear example in this direction. At this point, one could ask if more computationally sophisticated methods can be used to eliminate false symmetries without using non-local measurements. This was proposed and analyzed in Refs. [60, 61]. As stressed by the authors, such an approach must be possible if the marginal problem for the considered state has a unique solution. At the same time, we know that finding this solution generally is a computationally hard task, hence we can anticipate a similar behavior for the reconstruction of symmetries.

To reach their goal, authors of Refs. [60, 61] reduce the search for symmetries to the search of proper parent Hamiltonians. Indeed, if $H = \sum_i h_i L_i$ is a symmetry for $|\psi\rangle$, $|\psi\rangle$ is the ground state of the non-local Hamiltonian $\tilde{H}^2$, with

$$\tilde{H}(\vec{h}) = H - \langle\psi|H|\psi\rangle\mathbb{1} = \sum_i h_i(L_i - \langle\psi|L_i|\psi\rangle\mathbb{1}).$$

Afterwards, they attach the PPH reconstruction problem by only knowing local expectation values. For this reason, this approach is illustrated in the next section.

2.6 GROUND STATE INVERSE PROBLEM: RECONSTRUCTING PPHS

We have described the search for the local symmetries of a given quantum state. In some cases, it is more desirable to find a local proper parent Hamiltonian (PPH) such that the state $|\psi\rangle$ is its ground state. Such a Hamiltonian, when it exists, can be a precious tool in quantum state preparation. For example, t can be exploited to implement $|\psi\rangle$ by cooling down a device in which the PPH is implemented, or by adiabatically driving states by implementing the corresponding PPHs. Analogously, the reconstruction of PPH allows learning the Hamiltonian of a low-temperature system through measurements on its state.

Such as the search for symmetries, also the search for PPH does not generally have a unique solution. For an interacting spins system, a trivial example is given by the product state $|\uparrow \dots \uparrow\rangle$, whose PPH can either be the single-particle Hamiltonian $H_1 = -\sum_i \sigma_i^z$ or the ferromagnetic Ising-like Hamiltonian $H_2 = -\sum_i \sigma_i^z \sigma_{i+1}^z$. As symmetries form a vector space, we can linearly combine many solutions of the inverse problem to obtain a new solution. The question, here, is whether that can be done for PPHs. First of all, PPHs are a subset of symmetries, thus the search for PPHs can be simplified by first reconstructing the space of symmetries. In Ref. [57], the authors have identified PPH among symmetries via exact diagonalization, an approach that requires a huge computational cost for large systems. A major problem is that the set of PPH is not a vector space. As a simple example, we may notice that if H is a PPH for $|\psi\rangle$, the same does not hold for $-H$, which has $|\psi\rangle$ as the most excited eigenstate. As a consequence, we can not identify a vector basis for this set. In particular, it can be shown that the set in exam is a *convex cone*, that is if H_1 and H_2 are PPHs, also

$$H(\alpha, \beta) = \alpha[\beta H_1 + (1-\beta)H_2]$$

is a PPH for each $\alpha > 0$ and $\beta \in [0,1]$. The fact that the set of PPH is a convex cone gives an important insight into the difficulty of its reconstruction: while the identification of the space of symmetries is obtained by finding a finite number of vectors - a basis -, a convex cone is identified by its extreme points, that can be infinite even if the cone lies in a finite-dimensional space.

As briefly illustrated, the search for PPHs is harder than the search for symmetries, and, while symmetries can be easily found by looking at the kernel of the QCM, checking if a symmetry is a PPH in principle requires diagonalization. Since such an approach is impractical for large systems, alternative methods have been proposed in the last few years. In this section, we illustrate some of these methods. The first one [60, 61], designed for arbitrary states, represents the state as a low-temperature Gibbs state of the unknown Hamiltonian. This approach does not require strong assumptions on the state but can be computationally hard in most cases. The second approach [64, 65] instead is more efficient, being independent of the system size, but is based on a specific Ansatz - the applicability of the Bisognano-Wichmann theorem - that holds only in some cases. The last approach

illustrated in this section instead is based on the strong assumption that the unknown Hamiltonian is frustration-free [62]. In recent work, we present a novel approach inspired by adiabatic quantum computation, capable of finding a not frustration-free local PPH in polynomial time for generic non-critical many-body states. This method is illustrated in Chapter 5 of this thesis.

The different approaches to local PPH reconstruction share a common feature: they only require the knowledge of local expectation values. In this case indeed, unlike that for symmetry reconstruction, one can easily prove that the marginal problem has a unique solution. In particular, if some state is the non-degenerate ground state of a local Hamiltonian, it is fully determined by its local expectation values. Indeed, if $|\psi\rangle$ is the unique ground state for some local Hamiltonian $H = \sum_i h_i L_i$, it has to be the unique pure state for which the expectation values of the L_i's are $\langle\psi|L_i|\psi\rangle$, otherwise it will exist another state $|\psi'\rangle$ with the same energy, since $\langle\psi|L_i|\psi\rangle = \langle\psi'|L_i|\psi'\rangle$. We can conclude that:

- Local expectation values of non-degenerate ground state fully determine its PPHs.
- States that can not be distinguished by local measurements are degenerate ground states of the same PPHs. The GHZ states $|\mathrm{GHZ}\rangle_\pm = |\uparrow \ldots \uparrow\rangle \pm |\downarrow \ldots \downarrow\rangle$ on an N spins system are an example in this direction: one can easily check that all the m-spins observables with $m < N$ have the same expectation values for these states. As a consequence, there is no local PPH having $|\mathrm{GHZ}\rangle_+$ as the unique ground state. Note that, $|\mathrm{GHZ}\rangle_+$ and $|\mathrm{GHZ}\rangle_-$ can be degenerate ground states for the same Hamiltonian, for example the Ising Hamiltonian $\sum \sigma_i^z \sigma_{i+1}^z$.

2.6.1 *The thermodynamic approach*

The thermodynamic approach proposed in Ref. [60] is based on the fact that, if $|\psi\rangle$ is the unique ground state of some local Hamiltonian $H = \sum_i h_i L_i$, one can define a thermal density matrix that converges to $|\psi\rangle$ for a sufficiently large inverse temperature β:

$$\lim_{\beta\to\infty} \frac{e^{-\beta H}}{\mathrm{Tr}\left(e^{-\beta H}\right)} = |\psi\rangle\langle\psi|. \tag{2.4}$$

This equation relates the Hamiltonian couplings to the state. Since the free parameters of the Hamiltonian are only the coefficients h_i associated with local operators, the expectation values of local operators on $|\psi\rangle$ can be sufficient to determine H. In practice, one checks the convergence of the Gibbs state to $|\psi\rangle\langle\psi|$ through the convergence of local expectation values:

$$\lim_{\beta\to\infty} \frac{\mathrm{Tr}\left(L_i e^{-\beta \sum_i h_i L_i}\right)}{\mathrm{Tr}\left(e^{-\beta \sum_i h_i L_i}\right)} = \langle L_i\rangle. \tag{2.5}$$

This condition can be interpreted as a constraint on the PPH couplings. Therefore, authors of Ref. [60] define an optimal PPH as the minimum of the cost function

$$f_\beta(\vec{h}) \equiv \sum_i \left(\langle L_i \rangle - \frac{\mathrm{Tr}\left(L_i e^{-\beta \sum_i h_i L_i}\right)}{\mathrm{Tr}\left(e^{-\beta \sum_i h_i L_i}\right)} \right)^2 + \mathrm{Tr}\left(\frac{\sum_i h_i L_i e^{-\beta \sum_i h_i L_i}}{\mathrm{Tr}\left(e^{-\beta \sum_i h_i L_i}\right)} \right) \tag{2.6}$$

for large values of β, where the first term of f_β optimizes the condition in Eq. (2.5), while the second term, ensures that the Gibbs state is the ground state of H.

The main obstacle in finding an optimal PPH through this method comes from the evaluation of the cost function, which, depending on the exponential of the Hamiltonian, can be exponentially hard in the system size. Supervised learning with a neural network has also been adopted in Ref. [61] to improve the evaluation of the cost function. In this work, the neural network is trained with randomly chosen coefficients h_i for the PPH and with the corresponding ground states expectation values of the operators L_i. The authors show that supervised learning can be exploited to select appropriate initial points for minimization.

As anticipated in the previous section, these methods are originally implemented to search symmetries. However, as shown in Ref. [61], the more excited the initial state $|\psi\rangle$ is for its symmetry H, the more difficult it to reconstruct H from local expectation values.

2.6.2 *The Bisognano-Wichmann theorem*

A promising approach to finding PPHs has been suggested in Refs. [64, 65]. Given a family of trial Hamiltonians, the authors propose as an Ansatz the applicability of the Bisognano-Wichmann (BW) theorem. This theorem allows writing the reduced density matrix of a ground state as a function of the Hamiltonian in the corresponding reduced Hilbert space. As a consequence, the complexity of estimating the reduced density matrix only depends on the dimension of the reduced space, and not on the entire system size. At this point, an optimal PPH can be easily calculated by minimizing the distance between this matrix and the reduced density matrix of the input state $|\psi\rangle$, that only depends on local expectation values. Since the BW theorem holds in the context of relativistic quantum field theories, this approach is particularly significant for trial Hamiltonians whose low-energy physics is well described by a relativistic theory. Remarkably, some of these Hamiltonians generate physically relevant phenomena such as quantum criticality, topological matter, and quantum ferromagnets [64].

In order to exploit the BW Ansatz for spin models, local operators $\{L_i\}$ are written as $\{O_{r,\alpha}\}$, where r points to the lattice site and α labels the local spin operator - e.g. $\sigma^x_r \sigma^x_{r+1}$ or $\sigma^y_r \sigma^y_{r+1}$-. The trial Hamiltonian is written as

$$H = \sum_{r,\alpha} h_{r,\alpha} O_{r,\alpha}.$$

In short, the BW ansatz states that the reduced density matrix of the Hamiltonian H on a half space - for example, the sites with $r > 0$ in a linear lattice - is

$$\sigma_{\mathrm{BW}}(H) = \frac{e^{-H_{\mathrm{BW}}}}{\mathrm{Tr}\left(e^{-H_{\mathrm{BW}}}\right)},$$

with

$$H_{\mathrm{BW}} = \beta \sum_{r>0,\alpha} r h_{r,\alpha} O_{r,\alpha}, \tag{2.7}$$

for some value of β called inverse *entanglement temperature*. This ansatz is very similar to Gibbs representation of the state given in Eq. 2.4, where here β is an inverse entanglement temperature. However, the state σ_{BW} is a reduced density matrix and it is related to the Hamiltonian acting only on a given region of the lattice, as expressed in Eq. 2.7.

The inverse method consists in exploring the space of local Hamiltonians, defined by their couplings $h_{r,\alpha}$, in order to minimize the relative entropy

$$f(\vec{h}) = \mathrm{Tr}\left(\rho \log\left(\rho\right)\right) - \mathrm{Tr}\left(\rho \log\left(\sigma_{\mathrm{BW}}(H)\right)\right)$$

between the BW state $\sigma_{\mathrm{BW}}(H)$ and the reduced density matrix of the input state $|\psi\rangle$ on the half space. When this entropy vanishes, the reduced density matrix ρ of $|\psi\rangle$ is equal to $\sigma_{\mathrm{BW}}(H)$ and, if the BW ansatz holds, $|\psi\rangle$ is a ground state for H. The minimization of $f(\vec{h})$ can be performed via gradient descend, so one has to evaluate the derivatives $\frac{\partial f}{\partial h_{r,\alpha}}$, which only depend on the expectation values of the local operators for ρ and $\sigma_{\mathrm{BW}}(H)$.

One of the most promising aspects of this method is that in some cases [65] the BW ansatz can be used to evaluate the density matrix of a sub-lattice whose extension does not depend on the size of the entire system, instead of the density matrix of the half-space. For these cases, the difficulty of performing the gradient descend on $f(\vec{h})$ does not increases with the system size.

2.6.3 *Frustration-free PPHs*

Before concluding this section, let us briefly analyze the category of frustration-free (FF) PPHs. An Hamiltonian is FF is it can be written as a sum of terms such that the ground state of the full Hamiltonian is the ground state of each individual term. In other words, the global ground states are also local ground states. Hence, there is no frustration (energy increase) when all the terms in the Hamiltonian are combined.

A simple way to reconstruct FF PPHs is illustrated in Ref. [62]. The authors start by reconstructing local PPH H_X for the target state, such that H_X is an operator that acts non-trivially only on a finite-size subset X of the many-body lattice - for example, only on pairs of neighboring spins. As we will see, constructing these PPHs is very simple both from a conceptual and computational point of view. The main problem of the Hamiltonians H_X is that their ground states are exponentially degenerate in the system size. Since we know that a convex combination of PPHs is a PPH, at this point we can define frustration-free PPHs as the convex cone spanned by all the H_X.

The Hamiltonians H_X for the state $|\psi\rangle$ can be defined as the projectors on the null space of the reduced density matrices of $|\psi\rangle$ on X. This condition is equivalent to a system of three equations for H_X. First of all, one needs that H_X acts non-trivially only on X, in equations:

$$H_X = \mathrm{Tr}_{\overline{X}}(H_X) \otimes \mathbb{1}_{\overline{X}},$$

where $\mathrm{Tr}_{\overline{X}}$ is the partial trace with respect to the complement of X. Moreover, H_X has to be a projector, hence

$$H_X^2 = H_X.$$

In this way, we can be sure that the eigenvalues of H_X are 0 or 1. At this point, $|\psi\rangle$ is a ground state for H_X only if

$$\langle\psi|H_X|\psi\rangle = \mathrm{Tr}\left(\mathrm{Tr}_{\overline{X}}(H_X)\,\mathrm{Tr}_{\overline{X}}(|\psi\rangle\langle\psi|)\right) = 0.$$

The conditions above can be checked in polynomial time also for a large quantum system once one knows the local expectation values, which is equivalent to knowing the reduced density matrices. At this point, all the FF PPHs are easily found as convex combinations of the Hamiltonians H_X.

Despite its simplicity, this approach has two important limitations. The first one is that when a state is sufficiently entangled its reduced density matrices have all nonzero eigenvalues, so the null space of these matrices is empty and there are no FF PPHs. As a consequence, this approach is suitable only for states with small entanglement such as MPSs, for which an analogous method has been proposed [63]. The second limit is that many physically significant local Hamiltonians, for example, the Ising Hamiltonian in transverse field, are not FF proper PPHs for their ground states.

2.7 DYNAMIC INVERSE PROBLEM AND HAMILTONIAN LEARNING

The possibility of reconstructing a Hamiltonian from the evolution of the system state opens beneficial perspectives on quantum state control and Hamiltonian learning. In the first case, one wants to find an engineerable time-dependent parent Hamiltonian that can drive a quantum state along a target evolution [2], while, in the second case, one wants to know the Hamiltonian that is responsible for the dynamics of the system [70, 71, 87]. Analogously, in benchmarking quantum analog devices [25–30], a possible problem consists in verifying if the Hamiltonian that is effectively evolving the system corresponds to the Hamiltonian that we are trying to implement.

In Hamiltonian learning a time-dependent state has been actually implemented in a quantum system [70, 71, 87], hence an exact solution of the inverse problem always exists. This is not true for a generic quantum state $|\psi(t)\rangle$, whose evolution could be impossible to generate through a local Hamiltonian. When this is the case, we look for an optimal Hamiltonian, that is, a local Hamiltonian that generates an evolution as close as possible to the target state $|\psi(t)\rangle$ [2]. We focus on this problem in Chapter 3 of this thesis, while this section is devoted to reviewing Hamiltonian learning techniques.

Here, we present three different approaches aiming to reconstruct Hamiltonians from measurements in evolving systems. Indeed, results of measurements can be arranged to constrain the Hamiltonian couplings. All these methods suppose that the unknown Hamiltonian is time-independent, hence measurements at different times can be exploited as different constraints on the same Hamiltonian. Another shared feature of these approaches is the possibility of preparing, measuring, and evolving different initial states. This freedom, which characterizes the Hamiltonian learning protocol, is exploited to further increase the number of constraints on the unknown Hamiltonian.

2.7.1 *Short-time evolution*

In Ref. [70], the authors aim to learn the couplings of a time-independent Hamiltonian $H = \sum_i h_i L_i$ by measuring the short-time evolution of a set of local observables $\{O_k\}$. This approach can be seen as the time-dependent version of Ref. [59], where the authors reconstruct symmetries of a time-independent state.

Measurements are repeated for a collection $\{|\psi_\alpha\rangle\}$ of easy-to-implement initial states. For each state, the short time evolution of local expectation values is governed by Eq. 2.3, that defines a collection of constraint on the Hamiltonian corresponding to the different observables O_k. Considering all the states, we have a large set of constraints expressed by the system of equations

$$\partial_t o_{k\alpha} = \sum_j h_j K_{j,k\alpha}, \tag{2.8}$$

where $o_{k,\alpha} = \langle\psi_\alpha|O_k|\psi_\alpha\rangle$ and $K_{j,k\alpha} = \langle\psi_\alpha|i[L_j, O_k]\psi_\alpha\rangle$. In experiments, this system of constraint has never an exact solution due to the statistical error that characterizes expectation values and to the error in calculating derivatives from expectation values at times 0 and dt. Therefore, one resorts to the least square methods, considering the minimum of $\|\partial_t o_{k,\alpha} - \sum_j h_j K_{j,k\alpha}\|^2$ as the best guess for the unknown Hamiltonian.

The estimated Hamiltonian is affected by uncertainty, that depends on the system size through the number of local operators O_k that one has to measure. The scaling of the error with the system size is one of the most important figure of merit in Hamiltonian learning. About this, through this approach, the authors prove two points that are significant for the dynamical inverse problem in general. Firstly, if the initial states $|\psi_\alpha\rangle$ are separable, local expectation values and local correlations are sufficient to solve the inverse problem. Moreover, the number of initial separable states necessary to identify the Hamiltonian of the system through this approach is independent of the system size.

Since the number of local observables $\{O_k\}$ is polynomial in the system size, this is an efficient approach that works also for large systems. As previously suggested in Ref. [86], this depends on the Lieb-Robinson bounds [90] on spreading of information under local Hamiltonians. Thanks to this bound indeed, the error that comes when approximating derivatives with short-time evolutions does not depend on the Hamiltonian norm, that is a function of the system size, but only on the so called Lieb-Robinson speed, independent

on the system size. As a consequence, the time resolution dt necessary to approximate derivatives does not decrease when the number of particles is increased.

2.7.2 *Long-time evolution*

In Ref. [59], short-time evolution is exploited to generate a set of constraints for the unknown Hamiltonian that can be collected and solved in a polynomial amount of time. Even if, in principle, observing the system for a longer time would allow for a smaller uncertainty in Hamiltonian learning, this approach generally requires an exponential amount of resources. This is because the expectation value of a local observable at time t generally depends on the initial expectation values of all the non-local observables appearing in the Dyson series. This situation drastically changes when some symmetry of the Hamiltonian constraints the system evolution to a small region of the Hilbert space. In this case, the long-time evolution of local observables can be measured and exploited to infer with high precision the system Hamiltonian, as in Ref. [71].

In this paper, the authors develop a method to identify the Hamiltonian governing a Google Sycamore chip. This device consists of a two-dimensional array of nearest-neighbor coupled superconducting qubits. These physical qubits can be represented as non-linear oscillators with bosonic excitations, which, for large values of the non-linearity parameter, are well approximated by logical qubits.

The dynamics of the Google Sycamore chip can be described using the rotating-wave approximation by the Bose-Hubbard Hamiltonian

$$H^{\mathrm{BH}} = -\sum_{ij} h_{ij} a_i^\dagger a_j + \nu_i a_i^\dagger a_i^\dagger a_i a_i,$$

where $a_i^\dagger$ and a_i denote bosonic creation and annihilation operators at site i, ν_i is the non-linear one-site interaction strength, and h_{ij} is an $N * N$ Hermitian parameter matrix. Knowing the value of ν_i, the authors aim to reconstruct the unknown Hamiltonian couplings h_{ij}.

When the initial state of the system is a single particle state, the interaction term of the Hamiltonian vanishes, and ν_i can be considered to be null. The effective dynamics in this case conserves the number of particles, leading to simple equations of motion.

Specifically, the authors propose to initialize the system in the single-particle states $|\psi_n(0)\rangle \equiv \left(1 + a_n^\dagger\right)|0\rangle^{\otimes n}$, let the system evolve and estimate the local expectation values $x_{mn}(t) = \langle\psi_n(t)|a_m + a_m^\dagger|\psi_n(t)\rangle/2$ and $p_{mn}(t) = \langle\psi_n|a_m - a_m^\dagger|\psi_n(t)\rangle/(2i)$ by averaging results of the measurements of the X and Y Pauli operators. At this point, the function $a_{mn}(t) = x_{mn}(t) + iy_{mn}(t)$ depends on the unknown Hamiltonian parameters as follows:

$$a_{mn}(t) = \frac{1}{2}(e^{-ith})_{ij}.$$

Once a sufficient number of measurements have been performed on a discrete set of time steps, the function $a_{mn}(t)$ can be estimated and the couplings matrix h_{ij} can be inferred

exploiting Fourier analysis. Since the matrices involved in the last equation are $N \times N$ matrices, all these operations require a polynomial amount of resources. Thanks to this approach, the authors managed to estimate the Hamiltonian implemented on a grid of 27 qubits.

2.7.3 *Active Hamiltonian learning*

We conclude this section by briefly illustrating the active Hamiltonian learning approach proposed in Ref. [87]. Here, the freedom in the initial state preparation, evolution time, and measurements is richly exploited by the authors to search for the optimal approach that allows for a precise Hamiltonian reconstruction with the minimum possible number of experiment repetitions. Here, the authors fix the system size and consider small systems of two qubits.

The approach of Ref. [87] is paradigmatic, not only because it is an example of the prolific interplay between quantum technology and machine learning, but also because it allows for the application of an important result from quantum metrology to Hamiltonian learning.

Due to the central limit theorem, standard Hamiltonian learning techniques require $\mathcal{O}(\epsilon^{-2})$ experiment shots to reconstruct the couplings with a precision ϵ. This limit is known as *standard quantum limit*. However, using quantum resources, some techniques in quantum metrology are capable of estimating parameters of a quantum system with a number of experiment shots that scale as $\mathcal{O}(\epsilon^{-1})$. This limit is called *Heisenberg limit* and is known to be fundamental [91–95]. In Ref. [87], the authors wonder if the standard quantum limit can be overcome through active learning techniques.

Let us schematically illustrate the active Hamiltonian learning approach. Each experiment shot starts with the initialization of the system in the state $|0\dots0\rangle$, followed by some operation U from a set S_U of unitary operators. Then, the system evolves for a time t chosen in a given interval $[0, T]$, and finally, it is rotated by some other unitary operator $M \in S_M$ and measured on the computational basis obtaining some element $|y\rangle$ of this basis. Each set (U, t, M) defines a query that the experimenter executes on the system. Given a query $x = (U, t, M)$, the conditional probability $p_{y|x}$ of measuring the state $|y\rangle$ after the experiment shot is

$$p_{y|x}(y|x, \vec{h}) = |\langle y|Me^{-it\sum_i h_i L_i}U^\dagger|0\dots0\rangle|^2,$$

that is a function of the Hamiltonian parameters h_i.

At this point, we repeat the experiment, performing different queries $\{x^{(i)}\}$ and collecting the corresponding measured states $\{y^{(i)}\}$. Given a set $\{x^i, y^i\}$ of queries and corresponding measured states, the optimal guess h_i^* for the Hamiltonian can be obtained through the maximum likelihood estimator as follows:

$$h_i^* = \text{Argmin}_{h_i} \sum_i -\log p_{y|x}(y^{(i)}|x^{(i)}, \vec{h})$$

The accuracy of the Hamiltonian couplings that we learn in this way will depend on the set $\{x^i, y^i\}$, and therefore on the choice of the queries. Some collection of queries allows for Hamiltonian learning with more precision. In information theory, this feature is called informativeness and can be estimated through the inverse norm of the Fisher information matrix [96]. For a single query q this matrix is defined as

$$I(x,\vec{h})_{ij} = \sum_y \log p_{y|x}(y^{(i)}|x^{(i)},\vec{h}) \frac{\partial \log p_{y|x}(y^{(i)}|x^{(i)},\vec{h})}{\partial h_i} \frac{\partial \log p_{y|x}(y^{(i)}|x^{(i)},\vec{h})}{\partial h_j},$$

and for a collection of queries $Q = \{x\}$ it is

$$I(Q,\vec{h})_{ij} = \sum_{x\in Q} I(x,\vec{h})_{ij}.$$

The informativeness of Q is estimated through the inverse norm $\mathrm{Tr}\left[I(Q,\vec{h})^{-1}\right]$ of the Fisher matrix, and depends on the unknown Hamiltonian. In particular, the most informative collection of queries is $Q^* = \mathrm{Argmin}_Q \,\mathrm{Tr}\left[I(Q,\vec{h})^{-1}\right]$.

How can we exploit the informativeness criteria without knowing the system Hamiltonian? Active learning is an effective answer to this problem [97, 98]. An active learner starts from an arbitrary initial guess for the Hamiltonian couplings. Given this guess, it selects the most informative collection of N queries, performs these queries on the system, collects the answers, and infers a better guess for the Hamiltonian couplings through the maximum likelihood principle. Then, the whole process is repeated until a target accuracy is reached.

By applying this technique to Hamiltonian learning for learning the six parameters of a two-qubit cross-resonance Hamiltonian on different superconducting IBM Quantum devices, the authors of [87] obtain a 99.1% reduction of the number of experiment shots required over the comparable non-adaptive learning algorithm. Moreover, with access to prior information on a subset of Hamiltonian parameters, their approach can exceed the standard quantum limit and achieve Heisenberg-limited convergence rates during learning.

The main limitation of this approach is related to the system size. For a large quantum system, estimating and minimizing the Fisher information matrix is an impossible computational task, because the function $p_{y|x}(y|x,\vec{h})$ depends on the time evolution of the system state. A possible solution is to reconstruct the Hamiltonian from short-time evolutions, as in Ref. [59] and develop strategies to maximize the informativeness of this approach. We analyzed this approach in Ref. [3], which is illustrated in detail in Chapter 4 of this thesis.

2.8 AN OVERALL POINT OF VIEW

The different formulations of the many-body inverse problem that we have presented in this chapter share a similar mathematical structure. This structure also determines important features such as the existence and the number of solutions and the strategies to find

these solutions. In particular, we are going to show that the inverse problem is a constrained optimization problem, in which one has to find the minimum of a suitable cost function in a fixed space of Hermitian operators whose dimension is polynomial in the system size.

Let us consider the time-dependent state of a closed quantum system, represented by the density operator $\rho(t)$. A Hamiltonian can be the solution of the inverse problem when is compatible with the state evolution $\rho(t)$, that is, the Schrödinger equation

$$\partial_t \rho(t) = -i[H(t), \rho(t)]$$

holds, where we set $\hbar = 1$. This approach is valid both in the time-dependent and time-independent inverse problem.

If we only require that the system Hamiltonian is a generic Hermitian operator, we can choose a basis $\{O_\alpha\}$ for the Hermitian operators and write the Hamiltonian as $H = \sum_\alpha h_\alpha O_\alpha$. The Schrödinger equation becomes

$$\partial_t \rho(t) = \sum_\alpha h_\alpha(t) \left(-i[O_\alpha, \rho(t)]\right).$$

This is a liner equation for the Hamiltonian couplings $h_\alpha(t)$, whose solutions correspond to all the Hamiltonians that are compatible with the system dynamics. In the rest of this thesis and in the previously illustrated works, we focus on pure states $\rho(t) = |\psi(t)\rangle\langle\psi(t)|$. Hence, the last equation has got multiple solutions. These can be written as the sum of a generic solution, such as the Berry potential $H(t) = i|\partial_t\psi\rangle\langle\psi| + \text{h.c.}$, plus an arbitrary Hamiltonian commuting with $\rho(t)$. If the dimension of the Hilbert space is n, the dimension of the space of Hermitian operators commuting with a pure state is $(n-1)^2$. Indeed, these are indeed all the Hermitian block-matrices with an 1×1 block acting on the space spanned by $\rho(t)$ and an $(n-1) \times (n-1)$ arbitrary Hermitian block. Therefore, the solutions to the inverse Schrödinger equation form a manifold with dimension $(n-1)^2$.

As previously seen, when we consider real world many-body systems, this situation drastically changes. In this case, the dimension of the space of realistic Hamiltonians, that is spanned by some set of Hermitian operators $\mathcal{L} = \{L_i\}$, is polynomial in the number of particles N, because of physical and engineering constraints. Now, the previous equation reads:

$$\partial_t \rho(t) = \sum_\alpha h_i(t) \left(-i[L_i, \rho(t)]\right). \tag{2.9}$$

Remarkably, by projecting this equation on a set of observables $\{O_k\}$ we obtain Eq. (2.3), exploited in Sections 2.5 and 2.7 to reconstruct symmetries of a steady state and generators of a time-dependent state. Moreover, the corresponding imaginary evolution leads to the cost function introduced in 2.6 to attack the ground state inverse problem.

While the dimension of the space of Hamiltonians increases polynomially in N, the space of states with their infinitesimal evolutions increases exponentially. As a consequence, it could be impossible to find any solution to Eq. (2.9), that is a realistic solution to the

inverse problem. In practice, this restriction can be an advantage or an obstacle based on the specific problem setting. In quantum state control, we want to find which Hamiltonian has to be implemented to generate a target evolution in an engineered device. In this case, the absence of exact solutions means that we have to accept an approximate solution, that will generate the target evolution only approximately. Instead, if we want to learn the Hamiltonian from the observed evolution, knowing some restriction on the space of possible Hamiltonians allow rejecting unrealistic solutions. However, even in the latter case, we have to look for approximate solutions that take into account the experimental uncertainty on the system state.

We can conclude that, regardless of the application, the inverse problem consists in finding an approximate solution of Eq. 2.9 in a space of realistic Hamiltonians. This approximate solution is usually defined as the minimum of some suitable cost function. The computational effort needed to evaluate this function and find its minimum for the system of size N determines the computational complexity of a given approach to the inverse problem. As we have seen, in some cases such as the search for local symmetries, it is easy to define polynomially complex methods. These methods are often based on the minimization of a quadratic lower-bounded function or, equivalently, on the search for the ground states of a semi-definite positive matrix, for example the QCM. In other cases, for example in the search for PPH, the inverse problem seems to be exponentially hard for a classical computer, and it is necessary to define sophisticated approaches to efficiently generate approximate solutions.

3

OPTIMAL GENERATOR FOR TIME-DEPENDENT STATES

3.1 INTRODUCTION

The time-dependent inverse problem consists in reconstructing the local (or engineerable) Hamiltonian that generates the evolution of a given state $\rho(t)$. The interaction couplings that identify this parent Hamiltonian can be inferred from the realized state evolution and from the knowledge of the physical restrictions that characterize the system under exam. This is a dynamical approach to Hamiltonian learning, and we have presented some major contributions to this topic [70, 71, 87] in Sec. 2.7. In this chapter instead, we suppose that the state $\rho(t)$ is a target time-dependent state, which we want to implement on a device. Hypothesizing that the device Hamiltonian is time-dependent, with tunable couplings $h_i(t)$, we look for the optimal tuning capable of generating an evolution as close as possible to the target state. With two key changes, this question differs from a quantum optimal control problem [43–51]: here, the desired state is defined at each time rather than only at the end, and the Hamiltonian is constrained in a large space of local or engeenerable interactions.

As mentioned in the previous chapter, in many-body systems an exact generator for generic quantum dynamics usually does not satisfy the unavoidable constraints on the engineerable interactions. Hence, we will look for an optimal generator as the minimum of a suitable cost functional. This functional goes to zero when the fidelity between the target state and the state generated via the driving with a Hamiltonian goes to one, ensuring that a "low-cost" solution can be useful for quantum driving. We evaluated the extension of this approach to Hamiltonian learning in Ref. [3], to which the next chapter is dedicated. Remarkably, we also show that the proposed cost functional can be used to estimate if a target path of state can be accessed through realistic interactions.

A further result arising from the design of an optimal pare Hamiltonian is the connection with adiabatic and counterdiabatic quantum state driving. Adiabatic quantum state driving refers to the process of slowly changing the parameters of a quantum system in such a way that the system remains in its instantaneous eigenstate [76–79]. This is a useful technique for preparing and manipulating quantum states. Counterdiabatic quantum state driving is a method for speeding up adiabatic driving by adding a term to the system's Hamiltonian [99]. This additional term counteracts the non-adiabatic transitions that would otherwise occur during the adiabatic evolution, resulting in a faster and more effi-

cient quantum state driving process. We will show that solutions to the inverse problem have the structure of a counterdiabatic driving.

This chapter is organized as follows. Section 3.2 is devoted to the search for exact solutions to the time-dependent inverse problem. In Section 3.3, we take into account the constraints on the space of realistic Hamiltonians, and we define the optimal generator for the target evolution. In Section 3.4, we consider the cost associated with the optimal generator of a time-dependent state, as a geometric measure of our ability to generate its evolution by exploiting only the available interactions. Sections 3.5 and 3.6 are devoted to exemplifying applications of our method in some paradigmatic cases, i.e., time-dependent ground states of the Ising and p-spin models in transverse field. Through these examples, we also see how the optimal Hamiltonian can generate shortcuts to adiabaticity [100–109], similarly to the so-called counterdiabatic potential [99, 110]. The link between optimal Hamiltonian and counterdiabatic driving is analyzed in Section 3.7. The last section of the chapter summarizes our results and the related future perspectives.

3.2 EXACT DYNAMICS GENERATOR

The problem of determining the exact and realistic generator $H(t) = \sum_i h_i(t) L_i$ associated with a time-dependent quantum state can be easily posed. Given a pure time-dependent state $\rho(t) = |\psi(t)\rangle\langle\psi(t)|$ of a (possibly many-body) quantum system in the time interval $[0, T]$, the evolution of this state is related to the generator couplings $h_i(t)$ via the Schrödinger equation, that can be written as a set of constraints on these couplings:

$$\partial_t \rho(t) = \sum_i h_i(t) \left(-i[L_i, \rho(t)]\right).$$

As anticipated, in small quantum systems this equation can have many solutions, while in many-body systems the absence of solutions is very common and one looks for an optimal solution. Before focusing on the latter case, in this section, we show how Eq. (2.9) can be exactly solved. To this aim, we exploit the Schmidt scalar product $(A, B) \equiv \mathrm{Tr}(AB)$ on the space of Hermitian operators. Endowed with this product, Hermitian operators form a Euclidean vector space where some concepts and tools from Euclidean geometry, such as orthonormal basis, Euclidean distances, and projections, can be exploited.

Firstly, we can fix an orthonormal basis $\{O_\alpha\}$ for this space. As an example, an orthonormal basis for the Hermitian operators acting on an N-spins Hilbert space is given by all the tensor product operators $O_\alpha = \frac{1}{\sqrt{2^N}} \left(\sigma_1^{\mu_\alpha} \otimes \sigma_2^{\nu_\alpha} \otimes ... \otimes \sigma_N^{\tau_\alpha}\right)$, where σ_i^μ is the μ^{th} Pauli matrix describing the i^{th} spin (σ_i^0 is the identity $\mathbb{1}$ acting on the i^{th} spin). Using this basis, the quantum state ρ can be written as

$$\rho(t) = \sum_\alpha o_\alpha(t) O_\alpha,$$

where $o_\alpha(t) = \mathrm{Tr}(\rho(t) O_\alpha)$ is the expectation value of O_α.

At this point, we can project Eq. (2.9) on each element of the orthonormal basis $\{O_\alpha\}$ through the Hilbert-Schmidt scalar product, obtaining a vector representation of this equation:

$$\partial_t o_\alpha(t) = \mathrm{Tr}\left(-i\left[\sum_i h_i(t)L_i, \rho(t)\right]O_\alpha\right) = -\sum_i h_i K_{\alpha,i}(\rho(t)), \tag{3.1}$$

where

$$K_{\alpha,i}(\rho(t)) \equiv \mathrm{Tr}(-i[L_i, \rho(t)]O_\alpha) = \langle\psi(t)| - i[O_\alpha, L_i|\psi(t)\rangle$$

is the commutator matrix introduced in Ref. [59] and presented in the previous chapter.

At each time t, the exact generator couplings correspond to a solution to this system of inhomogeneous equations. The kernel $\mathrm{Ker}(K)$ of the commutator matrix contains the symmetries of the state $\rho(t)$, that is, all Hamiltonians that do not generate any evolution acting on this state. As a consequence of Eq. (3.1), the exact generators, which form a vector space, differ from each other in terms of the elements of $\mathrm{Ker}(K)$. These are solutions for the time-independent inverse problem. We will demonstrate in the next section how the behavior of the optimal generator is similarly influenced by the QCM.

Let us consider the reconstruction of the generator for a generic time-dependent spin-1/2 system as a straightforward instance of what we have covered thus far. In this case, the local operators in $\mathcal{L}$ are σ^x, σ^y and σ_z and the unknown dynamics generator is $H(t) = h_x(t)\sigma^x + h_y(t)\sigma^y + h_z(t)\sigma^z$.

In the Bloch sphere, the evolution of a pure state is expressed in the orthonormal basis defined by the Pauli operators $\{\mathbb{1}/\sqrt{2}, \sigma^x/\sqrt{2}, \sigma^y/\sqrt{2}, \sigma^z/\sqrt{2}\}$ as

$$\rho(t) = \left(\vec{v}\cdot\vec{\sigma} + \mathbb{1}\right)/2,$$

where

$$\vec{v} = \left(\sin(\theta(t))\cos(\phi(t)), \sin(\theta(t))\sin(\phi(t)), \cos(\theta(t))\right).$$

In this case, Eq. (3.1) reads

$$\begin{pmatrix} 0 \\ \frac{d}{dt}v_x/\sqrt{2} \\ \frac{d}{dt}v_y/\sqrt{2} \\ \frac{d}{dt}v_z/\sqrt{2} \end{pmatrix} = \begin{pmatrix} 0 & 0 & 0 \\ 0 & v_z & -v_y \\ -v_z & 0 & v_x \\ v_y & -v_x & 0 \end{pmatrix} \begin{pmatrix} h_x \\ h_y \\ h_z \end{pmatrix}$$

and the generator for this evolution is

$$H(t) = \frac{\left(-\dot{\vec{v}}\times\vec{v}\right)}{2}\cdot\vec{\sigma} + f(t)\vec{v}\cdot\vec{\sigma} \tag{3.2}$$

with $f(t)$ arbitrary function of time. The first term in this equation determines how the system evolves. The second term corresponds to the unique symmetry for the steady state

$\rho(t)$ at each time, it is an element of the commutator matrix's kernel and does not generate any evolution.

The above example highlights the connection between the inverse problem, the adiabatic theorem, and the search for shortcuts to adiabaticity. From this perspective, the second term $f(t)\vec{v}\cdot\vec{\sigma}$ can be interpreted as the adiabatic Hamiltonian having $\rho(t)$ as an eigenstate. Thus, the first term is the counterdiabatic potential[99] correcting the Landau-Zener transitions between different eigenstates of $f(t)\vec{v}\cdot\vec{\sigma}$. In the adiabatic limit $\dot{\lambda}\to 0$, this term vanishes and $f(t)\vec{v}\cdot\vec{\sigma}$ is the only responsible for the system evolution.

3.3 OPTIMAL DYNAMICS GENERATOR

In the previous section, we exploited Eq. (3.1) to select all the realistic Hamiltonians that generate the target evolution $\rho(t)$. Equation Eq. (3.1) represents a set of constraints on the Hamiltonian couplings, each of which expresses the evolution of an expectation value $o_k(t)$. The number of these expectation values increases exponentially with the system size. At the same time, the space of physically relevant systems is described by linear superpositions of operators in $\mathcal{L}$, which contains a polynomial number of elements. Therefore, for an arbitrary time-dependent state, we cannot expect that an exact and realistic generator exists. In this section, we resort to an optimization method to construct an approximate generator using only a limited number of physically relevant interactions.

3.3.1 *Definition of the cost functional*

A suitable cost functional $\mathcal{F}[H]$ for the optimal generator measures how far the dynamics

$$\rho'_H(t)=\left(\mathcal{T}e^{-i\int_0^t H(t')dt'}\right)\rho(0)\left(\mathcal{T}e^{-i\int_0^t H(t')dt'}\right)^\dagger$$

generated by H is from the target dynamics $\rho(t)$, whose minimum indicates that $\rho'(t)$ is the closets possible evolution to $\rho(t)$. This is implemented by the distance $\sqrt{\int_0^t dt'\,\mathrm{Tr}[(\rho(t')-\rho'_H(t'))^2]}$. However, minimizing this distance is impractical in large many-body systems, because it requires the time integration of any candidate Hamiltonian $H(t)$.

A simpler approach consists in defining a cost functional that is easy-to-minimize and upper-bounds the Frobenius distance $\|\rho(t)-\rho'_H(t)\|\equiv\sqrt{\mathrm{Tr}[(\rho(t)-\rho'_H(t))^2]}$. When the cost goes to zero also the distance goes to zero, signaling that the generated state $\rho'_H(t)$

exactly follows the target evolution $\rho(t)$. To reach this goal, we start from the chain of inequalities:

$$\begin{aligned} \|\rho(T) - \rho'_H(T)\| &= \left\| \int_0^T dt\, \partial_t \left(\rho(t) - \rho'_H(t)\right) \right\| \\ &\leq \int_0^T dt \left\| \partial_t \left(\rho(t) - \rho'_H(t)\right) \right\| \\ &\leq \int_0^T dt \left| \partial_t \|\rho(t) - \rho'_H(t)\| \right| \\ &= \int_0^T dt \frac{\left|\partial_t \|\rho(t) - \rho'_H(t)\|^2\right|}{2\|\rho(t) - \rho'_H(t)\|}, \end{aligned} \tag{3.3}$$

where, in the last line, we take into account that $\left|\partial_t \|\rho(t) - \rho'_H(t)\|^2\right| = 2\left|\partial_t \|\rho(t) - \rho'_H(t)\|\right| \|\rho(t) - \rho'_H(t)\|$.

We want to upper-bound $\left|\partial_t \|\rho(t) - \rho'_H(t)\|^2\right|$ with a simple-to-minimize quadratic function of the trial Hamiltonian $H(t)$. Exploiting the Leibniz rule and considering that $\partial_t \rho'_H = -i[H, \rho'_H]$, the derivative in exam can be simplified as

$$\begin{aligned} \partial_t \|\rho - \rho'_H\|^2 &= 2\,\mathrm{Tr}\left[(\rho - \rho'_H)\partial_t(\rho - \rho'_H)\right] \\ &= 2\,\mathrm{Tr}\left[(\rho - \rho'_H)(\partial_t \rho + i[H, \rho] - i[H, \rho - \rho'_H])\right] \\ &= 2\,\mathrm{Tr}\left[(\rho - \rho'_H)(\partial_t \rho + i[H, \rho])\right], \end{aligned}$$

where, in the last line, we have taken into account that $\mathrm{Tr}(A, [A, B]) = 0$ for any A and B.

Finally, we apply the Cauchy-Schwartz inequality to obtain

$$\left|\partial_t \|\rho - \rho'_H\|^2\right| \leq 2\|\rho - \rho'_H\| \|\partial_t \rho + i[H, \rho]\|,$$

and, replacing the latter in Eq. (3.3), we derive the bound

$$\|\rho(T) - \rho'_H(T)\| \leq \mathcal{F}[H] \tag{3.4}$$

where

$$\mathcal{F}[H] \equiv \int_0^T dt f(H, t) = \int_0^T dt \|\partial_t \rho(t) + i[H(t), \rho(t)]\| \,. \tag{3.5}$$

Remarkably, the argument of the last integral is the Frobenius norm of the difference between the RHS and the LHS of the Schrödinger equation. Hence, this is a measure of the error done in approximating the exact infinitesimal evolution $\partial_t \rho(t)$ of the state with the evolution $-i[H(t), \rho(t)]$ generated by the candidate Hamiltonian $H(t)$.

As illustrated in Figure 3.1, inequality (3.4) means that the state $\rho'_H(t)$, during its evolution, remains in a sphere of radius $\mathcal{F}[H, t] = \int_0^t f(H_{\mathrm{opt}}, t')dt'$ with center in $\rho(t)$. The Hamiltonian

$$H(t)_{\mathrm{opt}} = \mathrm{Argmin}_{H=\sum_i h_i(t) L_i} \mathcal{F}[H]$$

is optimal because, minimizing the functional $\mathcal{F}$, it constrains the evolution near to the target state $\rho(t)$.

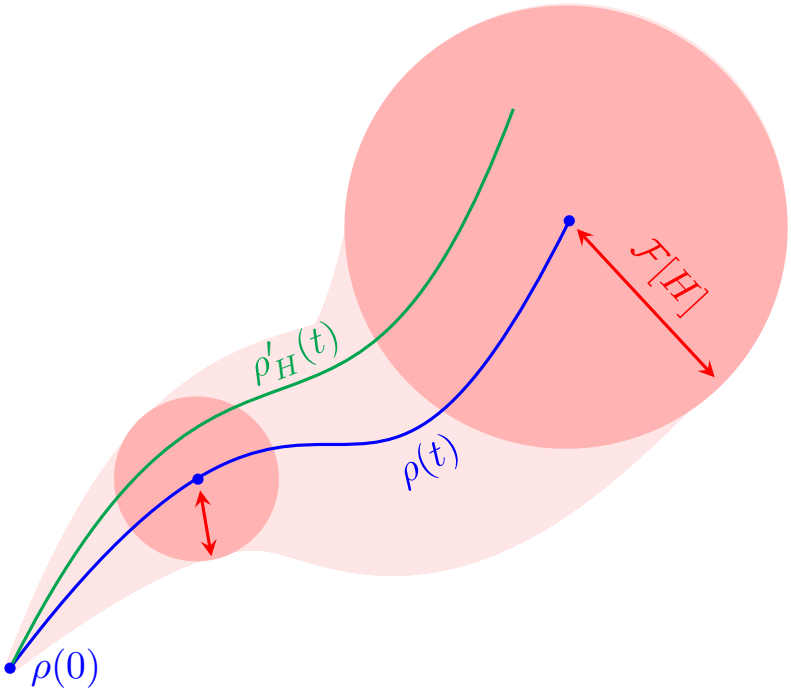

Figure 3.1: At each time t, the state $\rho(t)$ generated by the Hamiltonian $H(t)$ lies inside a sphere of radius $\mathcal{F}[H,t]$ centered on the target state $\rho(t)$.

In the context of quantum control, a figure of merit of the optimal Hamiltonian is the squared fidelity $F \equiv \left(\mathrm{Tr}\sqrt{\sqrt{\rho(t)}\rho'_H(t)\sqrt{\rho(t)}}\right)^2$ between the generated evolution and the target evolution, which measures how much the state $\rho'_H(t)$ is experimentally indistinguishable from the state $\rho(t)$. To write inequality (3.4) as a function of the fidelity, we consider that, for pure states, $\|\rho(T) - \rho'_H(T)\| = 2(1 - F(\rho(T), \rho'_H(T)))$, and we obtain

$$1 \geq F(\rho(T), \rho'_H(T)) \geq 1 - \frac{1}{2}\mathcal{F}[H,T]^2. \tag{3.6}$$

While Eq. (3.5) assures that the cost functional $\mathcal{F}[H]$ is minimized when $H(t)$ generates an infinitesimal evolution as close as possible to $\partial_t\rho(t)$, this last inequality only implies that a sufficiently low-cost minimum of $\mathcal{F}$ generates a high-fidelity driving of the initial state. However, that does not imply that the minimum of $\mathcal{F}$ also maximizes the fidelity with the target evolution: it is possible that certain Hamiltonians exist with a higher cost but also higher fidelity. This is the price that we pay to use an easy-to-minimize cost functional.

3.3.2 *Minimizing the cost functional*

We have defined the optimal generator as the minimum of the functional $\mathcal{F}[H]$ in Eq. (3.5). The integrand $f(H,t)$ in this functional does not depend on the derivative of the Hamiltonian, therefore a minimum for $\mathcal{F}[H]$ can be obtained as the time-dependent minimum of $f(H,t)$, recasting our problem from a global to a local form. In this way, as in an adiabatic

system, the Hamiltonian evolves with time while remaining in the minimum of a time-dependent potential. This potential depends on the target state $\rho(t)$ and its derivative.

The cost $f(H,t)$ has a direct geometric meaning, which is illustrated in Figure 3.2. The time-derivative $\partial_t\rho$ of the state $\rho(t)$ is a vector in the tangent space $T_{\rho(t)}$ for the state $\rho(t)$. This is the space of all the infinitesimal unitary evolutions and is spanned by the vectors $\{-i[O_\alpha,\rho(t)]\}$. Also the operator $i[H,\rho(t)]$ is a vector of this tangent space, but, since H is spanned only by the engineerable interactions in $\mathcal{L}$, it is constrained in the subspace of $TL_{\rho(t)}$, spanned by the vectors $l_i(t) = -i[L_i,\rho(t)]$. We call $TL_{\rho(t)}$ *engineerable tangent space*, since this is the space of infinitesimal evolutions that can be generated by engineerable operators. $f(H,t)$ is the therefore the distance between the vectors $\partial_t\rho(t) \in T_{\rho(t)}$ an arbitrary vector $\sum_i h_i(t)l_i(t) \in TL_{\rho(t)}$.

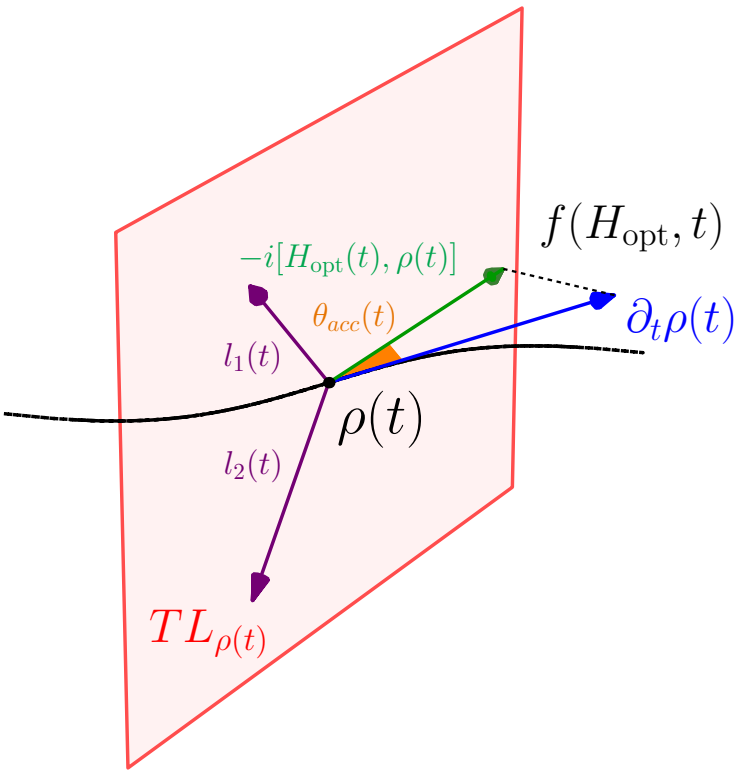

Figure 3.2: The commutator $-i[H_{\text{opt}}(t),\rho(t)]$ has to be the projection of $\partial_t\rho(t)$ on the space spanned by the vectors $l_i(t)$.

The minimization of this distance results in an "inverse" time-deponent variational principle [111, 112], and is obtained by imposing that $-i[H_{\text{opt}}(t),\rho(t)]$ is the Euclidean projection of $\partial_t\rho(t)$ on $TL_{\rho(t)}$. In equations, we have

$$\text{Tr}(l_i(t)\partial_t\rho(t)) = -i\,\text{Tr}(l_i(t)[H_{\text{opt}}(t),\rho(t)]) \tag{3.7}$$

for each l_i. If we replace the expression $H_{\text{opt}}(t) = \sum_i h_{\text{opt},i}(t)L_i$ of the optimal generator in terms of the couplings in Eq. (3.7), it becomes

$$\text{Tr}(l_j(t)\partial_t\rho(t)) = \sum_i \text{Tr}(l_i(t)l_j(t))h_{\text{opt},j}(t) \tag{3.8}$$

where the Gram matrix $\mathrm{Tr}(l_i(t)l_j(t))$ corresponds to the QCM

$$V_{ij}(t) = \langle\psi(t)|\{L_i, L_j\}|\psi(t)\rangle - 2\langle\psi(t)|L_i|\psi(t)\rangle\langle\psi(t)|L_j|\psi(t)\rangle$$

introduced in [57]. Typically, this is a singular matrix because the vectors l_i are linearly dependent. The kernel of this matrix, as demonstrated in Section 2.5, contains all the symmetries of the quantum state at a particular time.

Eq. (3.8) defines a linear inhomogeneous system with several solutions, that are the minima of the cost function $f(H,t)$ at time t. The temporal evolution produced by each of these solutions generates a different fidelity between the evolved state and the target state, even if they all have the same cost f. In the rest of this chapter, we will focus our attention on the solution that does not include the instantaneous symmetries from the kernel of the QCM. Since this solution minimizes the norm $\sqrt{\sum_i h_i^2}$, this approach reduces the number and the magnitude of non-null coupling exploited to drive the state. Moreover, with this particular choice of the optimal generator, the fidelity between $\rho(t)$ and $\rho'_H(t)$ does not depend on the schedule of the evolution: evolving the state $\rho(0)$ with the Hamiltonian $\dot{\tau}(t)H_{\mathrm{opt}}(t(\tau))$, where $\tau(t)$ is an arbitrary monotonous function, we will obtain $\rho'_H(\tau)$, that is the same evolution but with different velocity. This is because the solution to Eq. (3.8) that does not include the instantaneous symmetries is proportional to the time derivative of the state: $H_{\mathrm{opt}}(t) = \dot{\lambda}(t)A(\lambda)$ for some Hermitian operator $A(\lambda)$. As a consequence, the generated unitary evolution

$$U(t) = \mathcal{T}\exp\left(-i\int_0^t \dot{\lambda}(t')A(\lambda)dt'\right)$$

only depends on $\lambda(0)$ and $\lambda(t)$. This is no more the case if we include an element of the kernel of the QCM in the optimal Hamiltonian.

The selection of other solutions to Eq. (3.8), which includes components from the QCM kernel, can produce some intriguing perspectives. To make the experimental implementation of the Hamiltonian simpler, one may, for instance, use kernel components to reduce the time fluctuations of the couplings. Furthermore, it may be possible to use the final fidelity's dependence on evolution's rate to improve driving precision by increasing the total evolution time. Finally, one may look into how an evolution produced by a solution with an intriguing spectrum, such level repulsion [113], behaves.

3.4 ACCESSIBILITY OF THE STATES

The cost $\mathcal{F}[H_{\mathrm{opt}}(t)]$ associated with the optimal generator H_{opt} measures how accurately we can follow the state $\rho(t)$ through the engineerable interactions in $\mathcal{L}$.

Here, we show that $\mathcal{F}[H_{\text{opt}}(t)]$ only depends on the path of states $|\psi(\vec{\lambda}(t))\rangle$ defined by $\rho(t) = |\psi(\vec{\lambda}(t)\rangle\langle\psi(\vec{\lambda}(t))|$, where $\vec{\lambda}$ are coordinates in the space of states. As a consequence, we define the *accessibility* $\mathcal{A}[\psi(\vec{\lambda})]$ of $|\psi(\vec{\lambda}(t))\rangle$ through the optimal cost as follows:

$$\mathcal{A}[\psi(\vec{\lambda})] \equiv -\mathcal{F}[H_{\text{opt}}(t)].$$

The accessibility of a path of states, that estimates the error committed while trying to generate the path with limited available resources, can be an important figure of merit in the context of quantum state control. Indeed, one could select the most suitable path of states to prepare a given final quantum state by maximizing the accessibility over all the possible paths. Moreover, the time necessary to prepare a quantum state with a finite amount of resources, i.e., its quantum complexity, could be related to the accessibility of the paths towards the state. Therefore, we believe that accessibility may play a key role in the geometrization of quantum complexity [114–116].

To reach our goal, firstly we note that the optimal cost is proportional to the Frobenius length of the infinitesimal evolution $\partial_t\rho$ through the sine of the *accessibility angle* θ_{acc} between the vectors $\partial_t\rho$ and its projection on the engineerable tangent space, as illustrated in Figure 3.2. This angle does not depend on the schedule of the evolution, but only on the path of states. Analogously, the Frobenius length $\|\partial_t\rho\|$ depends on the Hilbert-Schmidt metric $V_{\mu\nu} \equiv \text{Tr}\left(\frac{\partial\rho}{\partial\lambda_\mu}\frac{\partial\rho}{\partial\lambda_\nu}\right)$ as $\|\partial_t\rho\| = \sqrt{\sum_{\mu\nu} V_{\mu\nu}\dot{\lambda}_\mu\dot{\lambda}_\nu}$. We can therefore write:

$$\mathcal{A}[\psi(\vec{\lambda})] \equiv -\mathcal{F}[H_{\text{opt}}(t)] = -\int_0^T dt \sqrt{\sum_{\mu\nu} V_{\mu\nu}(\vec{\lambda})\dot{\lambda}_\mu\dot{\lambda}_\nu}\,\sin(\theta(|\psi(\lambda)\rangle, \sum_\mu \dot{\lambda}_\mu\nabla_\mu|\psi(\lambda)\rangle)),$$

that is invariant for any reparametrization $t \to \tau(t)$.

As shown in Appendix A, the Hilbert-Schmidt metric for pure states is equal to twice the Fubini-Study metric $g_{\mu\nu} = \text{Re}(\langle\partial_\mu\psi|\partial_\nu\psi\rangle - \langle\psi|\partial_\mu\psi\rangle\langle\partial_\nu\psi|\psi\rangle)$, whose key role in quantum information and many-body theory has been deeply investigated [6, 89, 117–120]. Therefore, we can write

$$\mathcal{A}[\psi(\vec{\lambda})] = -\int_0^T dt \sqrt{2\sum_{\mu\nu} g_{\mu\nu}(\vec{\lambda})\dot{\lambda}_\mu\dot{\lambda}_\nu}\,\sin(\theta(|\psi(\lambda)\rangle, \sum_\mu \dot{\lambda}_\mu\nabla_\mu|\psi(\lambda)\rangle)). \tag{3.9}$$

As can be seen, only the accessibility angle depends on the available interactions. As a consequence, this angle controls how well the available interactions can generate the desired evolution. The closer the accessibility angle is to $\pi/2$ during the evolution, the harder it is to access the goal, resulting in a larger cost of the optimal solution.

The other contribution to Eq. 3.9, i.e., Fubini-Study metric on the path, does not depend on the interactions, hence it is an absolute measure of how difficult is to follow the path. Considering that the sine is bounded by one, the Fubini-Study length of the path of states determines the minimum possible values for the accessibility. When the fluctuations of the accessibility angle are negligible, the maximization of this $\mathcal{A}$ is reduced to the search for the Fubini-Study geodesic. These features help us understand to what extent it is possible to exploit the geodesics of this metric in the context of quantum state preparation, as shown in

Refs. [121, 122]. Moreover, considering the critical scaling of this metric at quantum phase transitions [117–120], Eq. 3.9 also explains the drop of fidelity that affects adiabatic [123] and local counterdiabatic [110] state driving at phase transitions.

3.5 DRIVING THE GROUND STATE OF THE ISING MODEL IN TIME-DEPENDENT TRANSVERSE FIELD

3.5.1 *Exact generator*

As a first example of the methods depicted in the previous sections, we want to find an exact generator and an optimal local generator for the time evolution $\rho(t) = |\psi(t)\rangle\langle\psi(t)|$, where $|\psi(t)\rangle$ is the instantaneous ground state of the one-dimensional Ising model in a time-dependent transverse field, i.e.,

$$H_{\mathrm{I}}(\lambda(t)) = -J\sum_{i=1}^{L}\sigma_i^x\sigma_{i+1}^x - \lambda(t)J\sum_{i=1}^{L}\sigma_i^z\,. \tag{3.10}$$

Here, $J > 0$ is an arbitrary energy scale that we set $J = 1$. We consider periodic boundary conditions $\sigma_{L+1,\mu} = \sigma_{1,\mu}$ and even number of sites L. Here, as well as in the following examples, $\lambda(t)$ is a monotonous smooth function of time. It is crucial to note that the Hamiltonian H_{I} is not involved in the definition of the time-dependent generator; rather, it merely sets the state $\rho(t)$ for which we will solve the inverse problem.

Firstly, we represent the Hamiltonian $H_{\mathrm{I}}(\lambda)$ as a system of non-interacting particles [124]. As illustrated in Appendix D, this representation is possible for a large class of spin systems. Indeed, several many-spin interactions on one-dimensional lattices can be represented as free-fermions Hamiltonians through the Jordan-Wigner transformations [125, 126]. Moreover, in presence of a lattice reflection and rotation symmetry, all the resulting interactions can be rearranged into operators that obey the algebra of Pauli matrices $\tilde{\sigma}_k^{\mu}$ acting on different sites, each of them is labeled by a momentum index k. We call these operators pseudo-spins.

Before proceeding, we remark that the free-fermions Hamiltonians obtained through the Jordan-Wigner transformations act differently on the two eigenspaces of the symmetry operator $Q = \prod_{i=1}^{L}\sigma_{i,z}$. Since the ground states in exams lie in the even parity sector for Q [124], from now on we will refer to H_I as the action of the Ising Hamiltonian on this sector. Analogously, we will represent only the action on the even parity sector of the Pauli strings involved in the following discussions. The Hamiltonian acting on the odd parity sector, only differs for a boundary term [80].

In the pseudo-spin formalism, the Ising Hamiltonian in transverse field reads (see Appendix D for details):

$$H_{\mathrm{I}} = -\sum_{k\in\mathcal{K}^+}\epsilon_k\left(v_k^x\tilde{\sigma}_k^x + v_k^y\tilde{\sigma}_k^y + v_k^z\tilde{\sigma}_k^z\right), \tag{3.11}$$

where

$$\mathcal{K}^+ \equiv \left\{ k = \frac{(2n+1)\pi}{L}, \text{ with } n \in \{0, \dots, L/2-1\} \right\}, \tag{3.12}$$

and

$$\begin{aligned} \epsilon_k &= 2\sqrt{\sin^2(k) + (\cos(k) - \lambda)^2} \\ v_k^x &= \sin(k)/\epsilon_k \\ v_k^y &= 0 \\ v_k^z &= (\cos(k) - \lambda)/\epsilon_k. \end{aligned} \tag{3.13}$$

The pseudo-spin operators $\{\tilde{\sigma}_k^\mu\}$ can be written as superpositions of Pauli strings, and vice-versa, as follows:

$$\tilde{\sigma}_k^\mu = \frac{2}{L} \sum_{0 \le m \le L/2} F^\mu(mk) S_m^\mu \qquad\qquad S_m^\mu = 2 \sum_{k \in \mathcal{K}^+} F^\mu(mk) \tilde{\sigma}_k^\mu \tag{3.14}$$

where $F^\mu(x) \equiv (\sin(x), \sin(x), \cos(x))$ and

$$\begin{aligned} S_0^Z &= -\sum_n^L \sigma_n^z \\ S_m^X &= \frac{1}{2} \sum_n^L \left(\sigma_n^x \sigma_{n+1}^z \dots \sigma_{n+m-1}^z \sigma_{n+m}^x - \sigma_n^y \sigma_{n+1}^z \dots \sigma_{n+m-1}^z \sigma_{n+m}^y \right) \\ S_m^Y &= -\frac{1}{2} \sum_n^L \left(\sigma_n^x \sigma_{n+1}^z \dots \sigma_{n+m-1}^z \sigma_{n+m}^y + \sigma_n^y \sigma_{n+1}^z \dots \sigma_{n+m-1}^z \sigma_{n+m}^x \right) \\ S_m^Z &= \frac{1}{2} \sum_n^L \left(\sigma_n^x \sigma_{n+1}^z \dots \sigma_{n+m-1}^z \sigma_{n+m}^x + \sigma_n^y \sigma_{n+1}^z \dots \sigma_{n+m-1}^z \sigma_{n+m}^y \right). \end{aligned}$$

Here the dots represent a string of σ_i^z operators.

In this representation, ground states are factorized as follows:

$$\rho(\lambda(t)) = \bigotimes_{k \in \mathcal{K}^+} \left(v_k^x \tilde{\sigma}_k^x + v_k^y \tilde{\sigma}_k^y + v_k^z \tilde{\sigma}_k^z + \mathbb{1} \right)/2. \tag{3.15}$$

In Eq. (3.2), we have shown how to apply our method to reconstruct the exact generator for a single spin. We can generalize that result to $\rho(\lambda(t))$, finding the exact generator for the dynamics in exam:

$$H_{\mathrm{E}}(t) = \frac{1}{2}\dot{\lambda} \sum_{k \in \mathcal{K}^+} (\partial_\lambda \theta_k)\, \tilde{\sigma}_k^y + f(t) \sum_{k \in \mathcal{K}^+} \epsilon_k \left(\cos(\theta_k) \tilde{\sigma}_k^z + \sin(\theta_k) \tilde{\sigma}_k^x \right). \tag{3.16}$$

In terms of spin strings, this reads

$$\begin{aligned} H_{\mathrm{E}}(t) = &-\frac{\dot{\lambda}}{2L} \sum_n^L \sum_{k \in \mathcal{K}^+} \sum_{1 \le m \le L/2} (\partial_\lambda \theta_k) \sin(mk) \left(\sigma_n^x \sigma_{n+1}^z \dots \sigma_{n+m-1}^z \sigma_{n+m}^y + \sigma_n^y \sigma_{n+1}^z \dots \sigma_{n+m-1}^z \sigma_{n+m}^x \right) \\ &+ f(t) H_{\mathrm{I}}(\lambda(t)). \end{aligned}$$

This generator coincides with the Ising Hamiltonian plus the related Berry counterdiabatic potential [127]. This remarks the connection between optimal generator and shortcuts to adiabaticity. We can also observe that the exact generator is non-local, involving interactions whose weight and magnitude scale linearly with the system size.

3.5.2 *Optimal local generator*

So far, our approach allows for an exact solution in terms of arbitrary long strings of spin operators. Now, we look for an approximate local solution to the inverse problem. In particular, we look for an optimal generator for $\rho(t)$ spanned by one- and two-spin translationally invariant interactions of the set $\mathcal{L} = \{S_0^Z, S_1^X, S_1^Y, S_1^Z\}$.

To reach our goal, we replace the derivative of the state $\partial_t\rho$ in Eq. (3.8) with $-i[H_{\mathrm{E}}, \rho]$, obtaining:

$$\mathrm{Tr}\left[\left(-i[H_E,\rho]\right)\left(-i[S_m^\mu,\rho]\right)\right] = \sum_{l\nu} h_{l,\nu}\,\mathrm{Tr}\left[\left(-i[S_m^\mu,\rho]\right)\left(-i[S_l^\nu,\rho]\right)\right],$$

with $S_m^\mu \in \mathcal{L}$. This equation can be easily solved in the pseudo-spin representation, where the system state ρ is separable. In this representation, the involved commutators read:

$$\begin{aligned}
-i[S_m^\mu,\rho] &= 2\sum_{k\in\mathcal{K}^+} f^\mu(mk)\left(\bigotimes_{k'\neq k}\rho_{k'}\right)\otimes\left(-i[\tilde{\sigma}_k^\mu,\rho_k]\right)\\
-i[H_E,\rho] &= \frac{\dot{\lambda}}{2}\sum_{k\in\mathcal{K}^+}(\partial_\lambda\theta_k)\left(\bigotimes_{k'\neq k}\rho_{k'}\right)\otimes\left(-i[\tilde{\sigma}_k^y,\rho_k]\right),
\end{aligned}$$

and, exploiting the cyclic property and the Kronecker's product property, traces can be simplified as follows:

$$\begin{aligned}
\mathrm{Tr}\left[\left(-i[H_E,\rho]\right)\left(-i[S_m^\mu,\rho]\right)\right] &= \dot{\lambda}\sum_{k\in\mathcal{K}^+}(\partial_\lambda\theta_k)f^\mu(mk)\left(\delta_{y\nu}-2v_k^y v_k^\nu\right)\\
\mathrm{Tr}\left[\left(-i[S_m^\mu,\rho]\right)\left(-i[S_l^\nu,\rho]\right)\right] &= 4\sum_{k\in\mathcal{K}^+} f^\mu(mk)f^\nu(lk)\left(\delta_{\mu\nu}-2v_k^\mu v_k^\nu\right),
\end{aligned}$$

where we have taken into account that $\mathrm{Tr}\left[\left(-i[\tilde{\sigma}_k^\mu,\rho_k]\right)\left(-i[\tilde{\sigma}_k^\nu,\rho_k]\right)\right] = \delta_{\mu\nu} - 2v_k^\mu v_k^\nu$.

Now, since $v_k^y = 0$ for each moment k, Eq. (3.8) assumes a simple block-matrix representation:

$$\begin{pmatrix}\vec{0}\\ \dot{\lambda}\sum_{k\in\mathcal{K}^+}(\partial_\lambda\theta_k)\sin(k)\\ \vec{0}\end{pmatrix} = \begin{pmatrix}\mathbf{A} & 0 & \mathbf{B}\\ 0 & 4\sum_{k\in\mathcal{K}^+}\sin(k)^2 & 0\\ \mathbf{B}^T & 0 & \mathbf{C}\end{pmatrix}\begin{pmatrix}\vec{h}_a\\ h_{1,Y}\\ \vec{h}_c\end{pmatrix},$$

where the matrices $\mathbf{A}$, $\mathbf{B}$, and $\mathbf{C}$ does not determine the solution with zero projection on the kernel.

The last equation has multiple solutions, however, the unique solution that has a null projection on the kernel is:

$$H_{\rm opt}(t) = h_{1,Y}(t) S_1^Y = h(t) \sum_n^L \left(\sigma_n^x \sigma_{n+1}^y + \sigma_n^y \sigma_{n+1}^x\right)$$

where explicit expression of the optimal coupling $h(t)$ is

$$h(t) \equiv -\frac{1}{2} h_{1,Y} = -\dot{\lambda} \frac{\sum_{k\in\mathcal{K}^+} (\partial_\lambda \theta_k) \sin(k)}{8 \sum_{k\in\mathcal{K}^+} \sin(k)^2}$$

As anticipated, this coupling depends on the time schedule only through $\lambda(t)$ and its time derivative.

Figure 3.3 illustrates the behavior of the renormalized coupling $h(t)/\dot{\lambda}$ for various system sizes L. As we can see, in synthetic quantum systems the optimal Hamiltonian can be implemented in a scalable manner because the amplitude of the couplings does not depend on L.

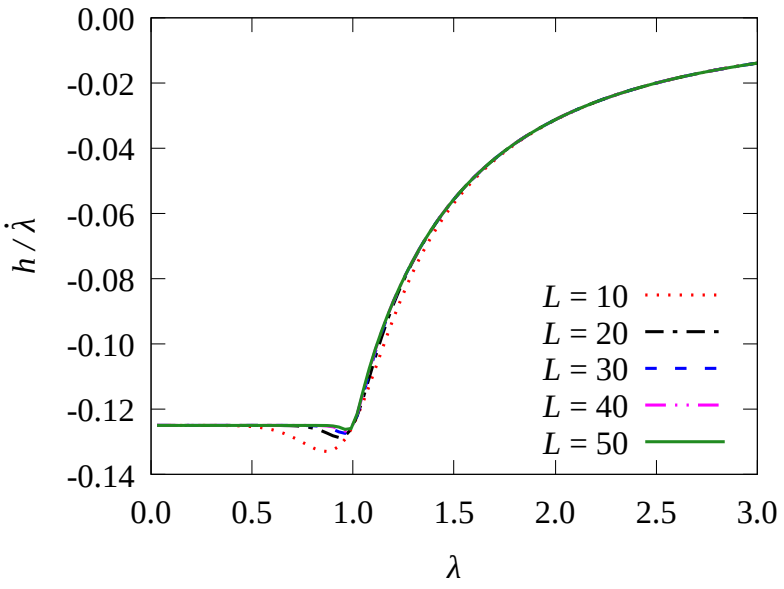

Figure 3.3: Evolution of the (rescaled) optimal coupling $h/\dot{\lambda}$ for different system sizes.

In Figure 3.4 we show the rescaled local cost $f(H_{\rm opt}, t)/(\sqrt{L}\dot{\lambda})$ of the optimal solution, which determines the accessibility of $\rho(t)$ thought local interactions. For noncritical states, the different curves converge for a sufficiently large system, signaling that $f(H_{\rm opt}, t)$ scales with $\sqrt{L}$. For the critical states, instead, the rescaled cost diverges and finding a local optimal generator becomes very hard. This scaling behavior is analogous to the Fubini-Study metric on the target path of states [89, 117–120], as we argued in the previous section.

The fidelity $F(t) = \mathrm{Tr}(\rho(t)\rho_{\rm opt}(t))$ between $\rho(t)$ and the state $\rho_{\rm opt}(t)$ driven by the optimal Hamiltonian assumes a simple form in the pseudo-spin representation of the

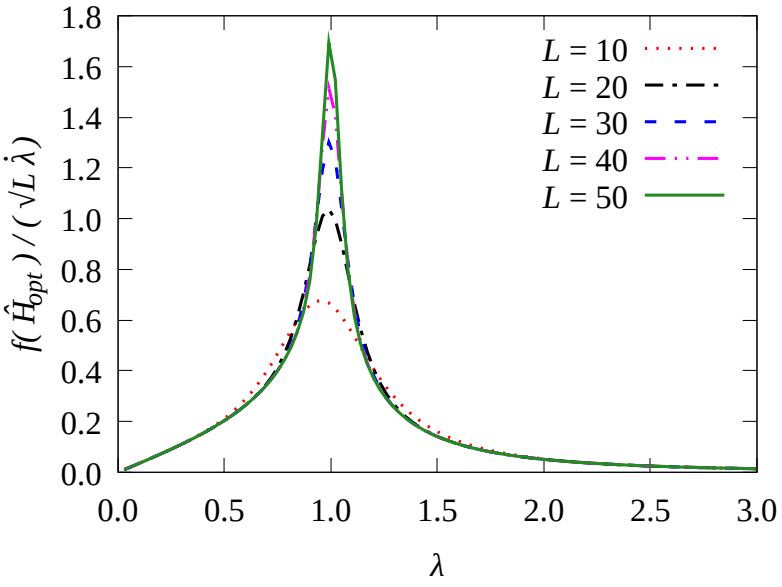

Figure 3.4: Evolution of the (rescaled) optimal cost $f(H_{\text{opt}})/(\sqrt{L}\dot{\lambda})$ for different system sizes.

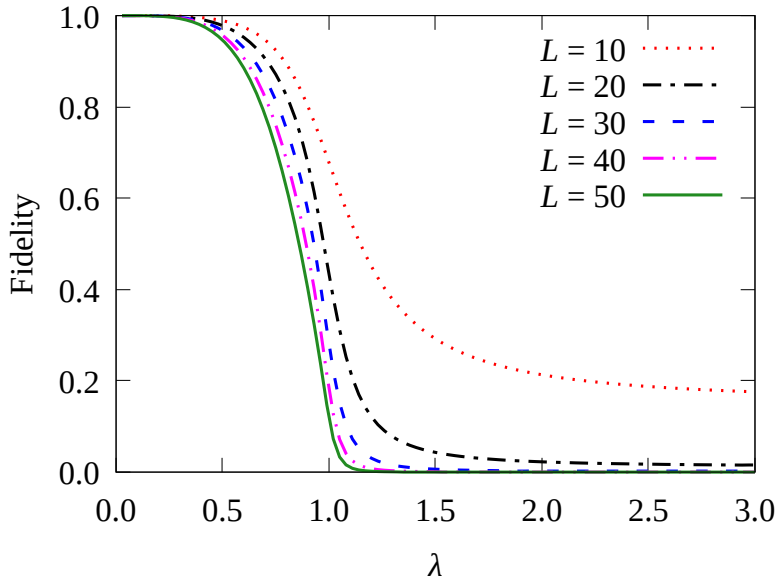

Figure 3.5: Evolution of the fidelity between the target state and the state evolved through the optimal generator for different system sizes.

Hilbert space, where defining the time-dependent angle $\alpha_k(t) = 4\sin(k)\int_{t_0}^{t} h(t')dt' + \frac{\theta_k(\lambda(t))-\theta_k(\lambda(t_0))}{2}$, we obtain

$$F(t) = \prod_{k\in\mathcal{K}^+} \cos(\alpha_k(t))^2.$$

$F(t)$ depends on time through λ but does not depend on the schedule. As we can see in Figure 3.5, where F is shown for different system sizes, away from the critical coupling $\lambda_c = 1$ the optimal generator drives the state with high fidelity. In correspondence to λ_c, instead, a significant amount of fidelity is irreversibly lost. By the inequality (3.6), the cost function's shape in Figure 3.4 allows for the prediction of this behavior.

Remarkably, the Lieb-Robinson bounds [90] can be used to explain the sharp drop of the in fidelity in correspondence with the critical state. According to these bounds, the correlation length grows under the influence of a local Hamiltonian at a velocity that does not depend on the system size. As a result, if we want the correlation length to diverge in the thermodynamic limit, as it does for critical states, we also require a diverging magnitude of the couplings. This is because the Lieb-Robinson speed is proportional to the magnitude of the interactions involved in the Hamiltonian. According to Figure 3.3, the couplings do not grow with the size of the system in this case, making it impossible to attain the critical state. This results in a drastic drop in fidelity.

3.6 DRIVING THE GROUND STATES OF THE p-SPIN MODEL IN TIME-DEPENDENT TRANSVERSE FIELD

The time-dependent inverse problem for the ground state a p-spin Hamiltonian is another paradigmatic example of the potential of our method. This Hamiltonian, which was presented in Ref. [128] to model spin glasses [129–131], consists in a spin system in which the elementary interactions connect each set of p spins regardless of their distance. According to a computational perspective, the non-local interactions in the p-spin Hamiltonian are involved in the solution of several computationally challenging problems such as Grover's search [132]. Consequently, the ability to produce the dynamics generated by this type of Hamiltonians by utilizing actual resources can provide an intriguing advance for the implementation of quantum algorithms. Because of this, several studies have been published recently that offer methods for implementing the p-spin Hamiltonian's ground states, with an emphasis on methods that involve shortcuts to adiabaticity [108, 109, 133–138]. The search for an optimal generator can furnish a novel contribution to the debate on this topic.

Let us consider the p-spin Hamiltonian in transverse field

$$H_{p\text{-spin}}(\lambda) = -\Gamma(1-\lambda)\Sigma_x - \lambda\frac{J}{n^{p-1}}(\Sigma_z)^p \tag{3.17}$$

where $\lambda(t)$ is the time-dependent parameter and

$$\Sigma_\mu = \sum_i \sigma_i^\mu.$$

Setting $J = \Gamma = 1$ and $p = 3$ in $H_{p\text{-spin}}$, the system exhibits a first-order phase transition [134]. The non-locality of the model comes from the interactions in the term $(\Sigma_z)^p$, which connect sites regardless of their mutual distance in the spin chain.

The p-spin Hamiltonian only involves the total spin of the system and its projection along the z-axis, and its ground state is located in the space of maximum total spin Σ^2. For this reason, we can represent our target time-dependent state in the maximum spin subspace, with dimension $L+1$ [134]. We also look for the optimal generator in a space spanned by operators that conserve the total spin, and can therefore be represented in the

same subspace. This approach allow us to attack the inverse problem of Eq. (3.8) also for a large number of spins.

In this section, we consider two time-dependent states $\rho(t)$. In the first subsection, $\rho(t)$ is defined as the path of ground states for $H_{p\text{-spin}}(\lambda(t))$. Instead, in the second subsection $\rho(t)$ connects the ground states of $H_{p\text{-spin}}(0)$ and $H_{p\text{-spin}}(1)$ through a linear interpolation. In both cases, since $H_{p\text{-spin}}$ involves all-to-all interactions, we look for a non-local optimal generator. However, we ask that the elementary interactions in $\mathcal{L}$ have maximum weight equal to weight one, two, and three alternatively. Because of the symmetries inherited by the state $\rho(t)$, $\mathcal{L}$ contains only interactions that are invariant for an arbitrary permutation of the chain sites and are the product of an odd number of Σ_y operators. Therefore, we consider the following sets of Hermitian operators

$$\begin{aligned}
\mathcal{L}_1 &= \{\Sigma_y\}, \\
\mathcal{L}_2 &= \mathcal{L}_1 \cup \{\Sigma_{xy}, \Sigma_{yz}\}, \\
\mathcal{L}_3 &= \mathcal{L}_2 \cup \{\Sigma_{yyy}, \Sigma_{xyx}, \Sigma_{zyz}, \Sigma_{xxy}, \Sigma_{yzz}, \Gamma_{xxy}, \Gamma_{yzz}, \Sigma_{xyz}, \Sigma_{xzy}, \Sigma_{yxz}, \Gamma_{xyz}, \Gamma_{xzy}, \Gamma_{yxz}\},
\end{aligned}$$

where $\Sigma_{\mu_1,..,\mu_n} \equiv (\Sigma_{\mu_1} \dots \Sigma_{\mu_n} + \text{h. c.})/2$ and $\Gamma_{\mu_1,..,\mu_n} \equiv i(\Sigma_{\mu_1} \dots \Sigma_{\mu_n} - \text{h. c.})/2$.

By numerically solving Eq. (3.8) for $\mathcal{L}_1$, $\mathcal{L}_2$ and $\mathcal{L}_3$, we find the optimal generator for the evolution with weight equal to one, two, and three respectively.

3.6.1 *Generating a path of ground states*

Here, we consider the optimal generator for the non-degenerate ground state $\rho(t)$ of $H_{p\text{-spin}}(\lambda(t))$. If we consider weight $w = 2$ interactions, it is

$$H(t) = \dot{\lambda}\left(\lambda_Y(t)\Sigma_y + \lambda_{XY}(t)\Sigma_{xy} + \lambda_{YZ}(t)\Sigma_{yz}\right),$$

where the normalized couplings $h_Y/\dot{\lambda}$, $h_{XY}/\dot{\lambda}$, and $h_{YZ}/\dot{\lambda}$ are depicted in Figure 3.6 for different system sizes. In correspondence of noncritical states, optimal couplings converge in the thermodynamic limit, this allows for a scalable implementation of Hamiltonian $H(t)$. Instead, the critical state is characterized by a coupling magnitude that increases with the system size.

In Figure 3.7, we represent the local cost associated to the optimal solution $f(H_{\text{opt}}, t)$ of weight $w = 2$, which determines the accessibility of the state. This cost decreases and converges to a minimum value for noncritical states when the system size is increased. This feature determines the fidelity between the target state and the driven one in Figure 3.8 (a) : larger p-spin noncritical states are easier to be driven. In contrast, in correspondence of the critical states, when the cost of the optimal solution sharply rises with system size, there is a rapid decline in fidelity. In conclusion, the optimal generator fails to generate a quantum phase transition, as it happens in the Ising model. An analogous behavior characterizes the cost function and the fidelity obtained through weight one and three Hamiltonians.

Let us consider now the fidelity for the final state of the evolution, for example for $\lambda(t) = 1$ after the phase transition. This is shown in Figure 3.8 (b) for different system

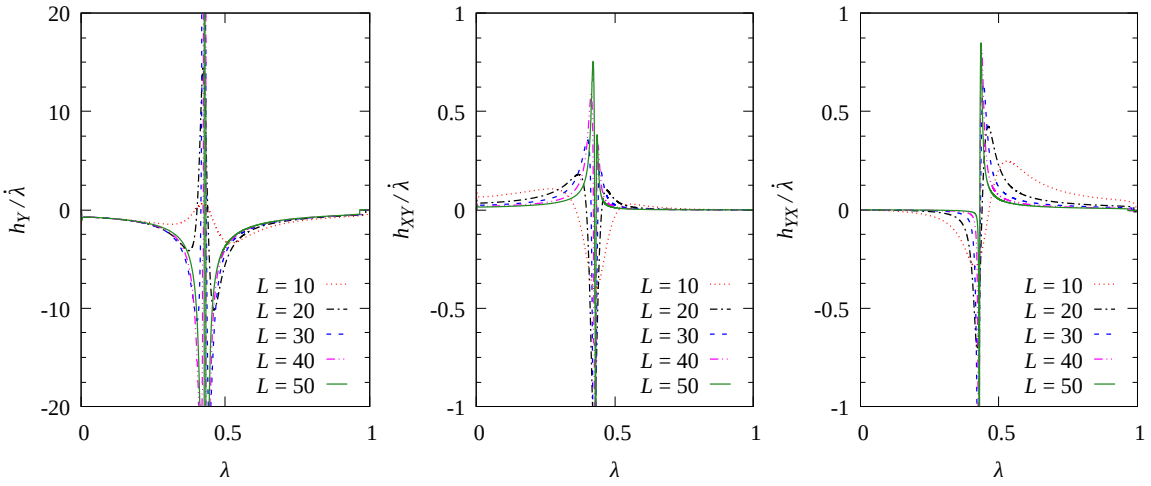

Figure 3.6: Evolution of the (rescaled) optimal coupling $h_i/\dot{\lambda}$ for different system sizes when the available interactions have weight $w = 2$. The couplings shown in the figure respectively correspond to the interactions Σ_y, Σ_{xy} and Σ_{yz}.

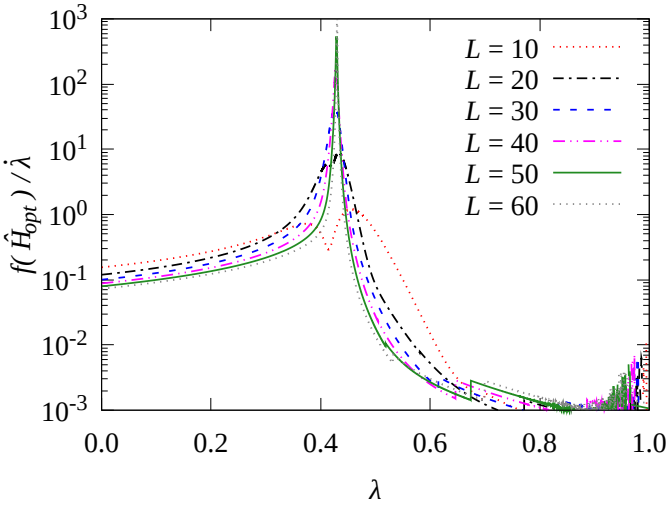

Figure 3.7: Evolution of the (rescaled) optimal local cost $f(H_{\text{opt}})/\dot{\lambda}$ for different system sizes when the available Hamiltonians have weight $w = 2$.

sizes weights of the Hamiltonian. Remarkably, we observe a drastic improvement of the driving fidelity in correspondence of larger Hamiltonian weights.

As explained in Section 3.4, the accessibility angle measures the capability of the available interactions of generating the target evolution. This angle is plotted in Figure 3.9 for different system sizes and operator weights $w = 1$ and $w = 3$. A peak in correspondence with the critical states signals the impossibility of generating these states through finite weight Hamiltonians. By contrasting the two panels in this figure, we can see how the accessibility can be significantly improved through weight three interactions, especially prior to the phase transition.

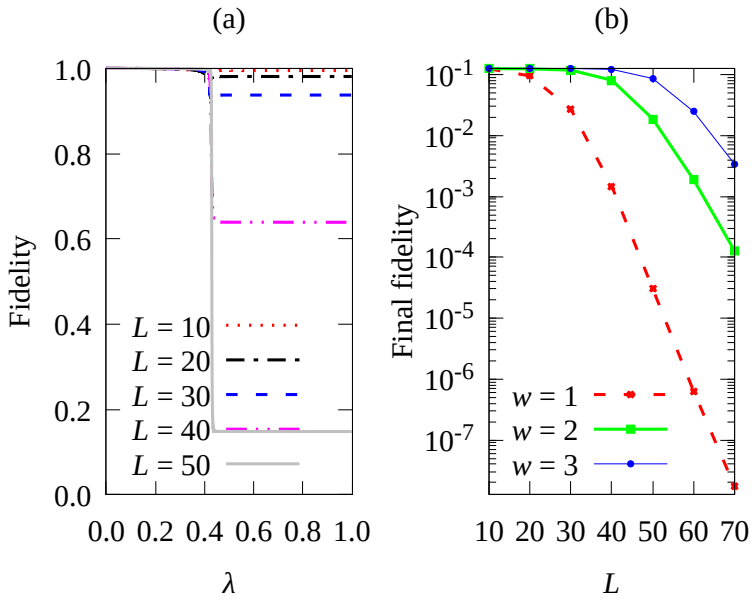

Figure 3.8: In panel (a) evolution of the fidelity between the target state and the state evolved through the optimal generator of weight $w = 2$. In panel (b), fidelity between the target state and the state generated by the optimal generator at $\lambda = 1$ as a function of the system size and for different weights of the available interactions.

3.6.2 *Generating interpolations of ground states*

The inverse problem for a time-dependent state that follows the ground states of a certain time-dependent Hamiltonian has been addressed in the preceding examples. However, our strategy is appropriate for determining the optimal generator of arbitrary time-dependent states. Here we consider a time-dependent linear interpolation of a pair of states. The initial and final states are ground states of the p-spin Hamiltonian $H_{p\text{-spin}}(\lambda)$ at $\lambda = 0$ and $\lambda = 1$. This allows us to evaluate how well our strategy performs for various evolutions having the same extremal points.

The target time-dependent state is

$$|\psi(t)\rangle = Z(t)\left[\cos\left(\lambda(t)\pi/2\right)|\psi_0\rangle + \sin\left(\lambda(t)\pi/2\right)|\psi_1\rangle\right]$$

where $|\psi_0\rangle$ and $|\psi_1\rangle$ are the ground states of the Hamiltonian in Eq. (3.17) with $\lambda = 0, 1$, respectively, and $Z(t)$ is a normalization factor. $\lambda(t)$ goes from 0 to 1 during the time evolution. We construct an optimal generator with the operators of weight one, two and three, respectively in $\mathcal{L}_1$, $\mathcal{L}_2$ and $\mathcal{L}_3$.

The solution to Eq. (3.8) in the space spanned by the operators of weight two leads to the optimal couplings shown in Figure 3.10. Here, we can see that the coupling's strength declines with the size of the system and is greatest at the start and end of the evolution. A similar behavior is shared by the local cost associated to the optimal Hamiltonian, in Figure 3.11: it increases with the system size and is maximized at the initial and final times. It is evident from the coupling and total cost behavior at extre times how challenging it is to interpolate ground states with the available interactions.

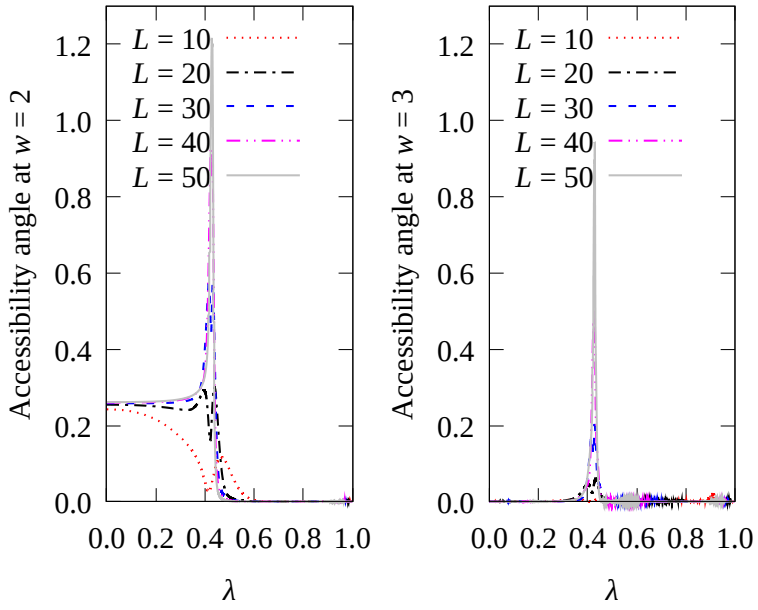

Figure 3.9: Evolution of accessibility angle associated to the optimal generator of weight $w = 2$ and $w = 3$ for different system sizes.

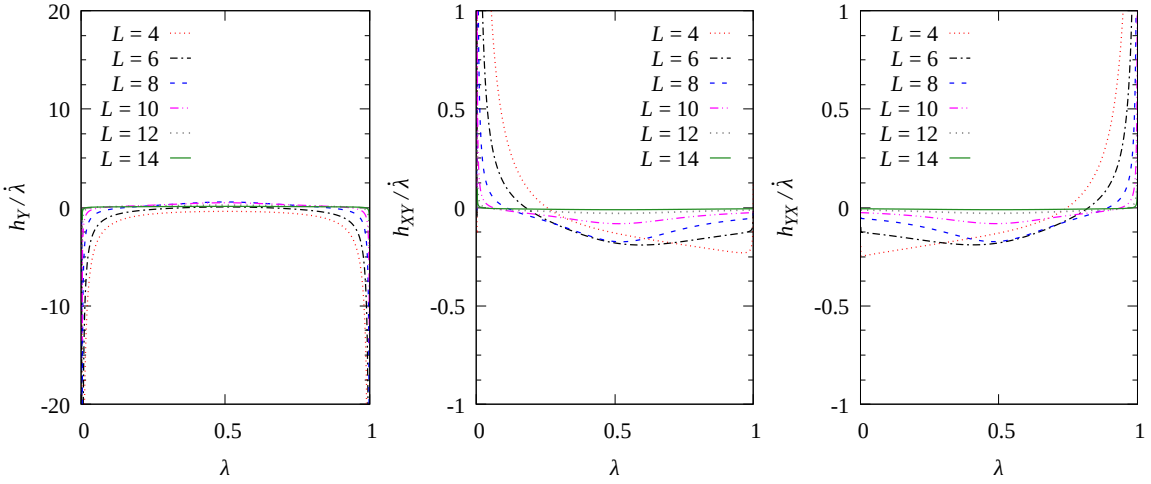

Figure 3.10: Evolution of the (rescaled) optimal coupling $h_i/\dot{\lambda}$ for different system sizes when the available interactions have maximum weight $w = 2$. The couplings shown in the figure respectively correspond to the interactions Σ_y, Σ_{xy} and Σ_{yz}.

Figure 3.12 (a) shows the fidelity between the target state and the evolution generated by the optimal Hamiltonian, reflecting the behavior of the optimal cost function: larger values of the local cost function are linked with a higher drop of the fidelity.

In Figure 3.12 (b), we represent the final fidelity between the target state and the driven one at $\lambda = 1$, for different system sizes and interactions weights. As anticipated, it is clear that a higher weight results in a larger final fidelity.

Both the time evolution examined here and the one examined in the previous subsection begin at and terminate at the same state. However, for a fixed number of spins, the cost function associated to the second evolution is greater, and the final fidelity is noticeably lower. We can state that the path of states of the previous section is more accessible with the

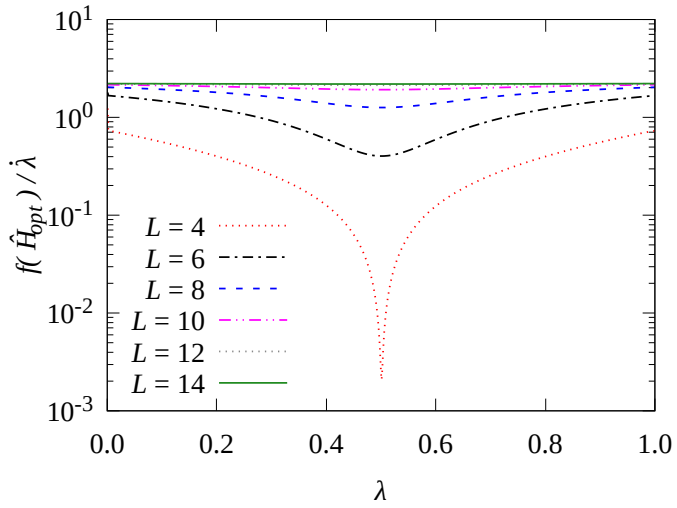

Figure 3.11: Evolution of the (rescaled) optimal local cost $f(H_{\text{opt}})/\dot{\lambda}$ for different system sizes when the available interactions have weight $w = 2$.

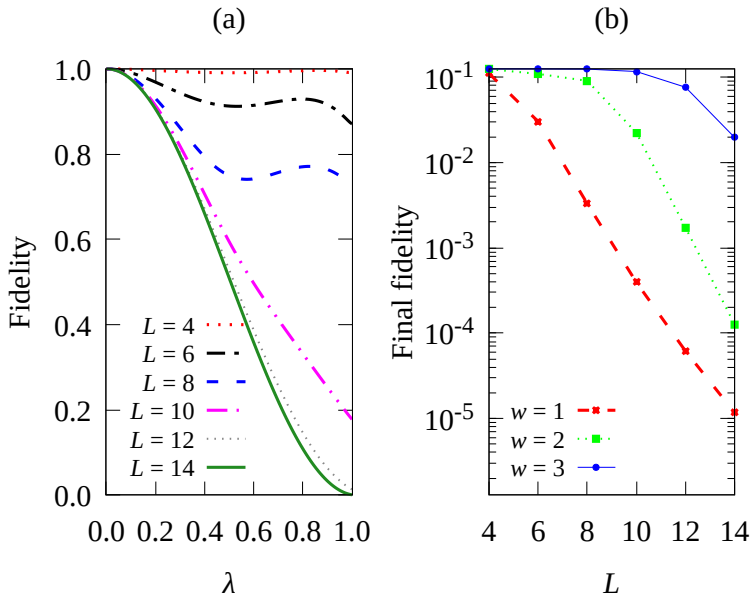

Figure 3.12: Panel (a): evolution of the fidelity between the target state and the state evolved through the optimal generator of weight $w = 2$. Panel (b): fidelity between the target state and the state generated by the optimal generator at $\lambda = 1$ for different sizes of the system and for different weights of the available interactions.

interactions in exam. Since creating interpolations of states appears to be more challenging than creating ground states, we can hypothesize a correlation between the evolution of the entanglement and the accessibility of the time-dependent state.

3.7 OPTIMAL HAMILTONIAN VS COUNTERDIABATIC DRIVING

Two examples from the previous sections have been devoted to the search for an optimal generator for the time-dependent ground state of a Hamiltonian $H_{\text{a}}(\lambda(t))$. In this form,

the inverse problem can be seen as a method to drive the ground state of $H_a(\lambda(t))$ in a shorter time than that required by an adiabatic process.

The attempt to accelerate adiabatic processes, i.e., the search for shortcuts to adiabaticity [100–109], is very common in the adiabatic quantum computation, where the long time required for the validity of the adiabatic theorem is in contrast with the short coherence time of actual quantum devices. To obtain such a shortcut, one can suppress Landau-Zener transitions to the excited eigenstates, which naturally arise when the control parameters of the system rapidly change. This can be done through an additional Hamiltonian, the so-called counterdiabatic potential [99], associated with $H_a(\lambda(t))$. Unfortunately, this Hamiltonian involves a range of interactions that are extremely challenging to produce in an experiment, thus one searches for an optimal potential that only includes a specific set of interactions. Sels and Polkovnikov [110] proposed to approximate the counterdiabatic potential as a local Hamiltonian by minimizing a cost functional. The obtained local Hamiltonian could be exploited in real experiments to accelerate the adiabatic quantum computation suppressing, in part, the Landau-Zener transitions. For example, recent works have been devoted to the search for a counterdiabatic potential for the p-spin ground states through the minimization of this cost functional [134, 135].

The conceptual difference between local counterdiabatic potential and the local generator of a time-dependent ground state is immediately evident, and it regards the inputs and the goal of these two methods. The counterdiabatic potential, indeed, is a function of the adiabatic Hamiltonian and helps generate its unknown ground state. Instead, the optimal generator is a function of a known state and can be exploited to prepare that state.

In this section, we want to clarify the relationship between the local counterdiabatic potential and the local generator of a time-dependent ground state in terms of the related cost functionals. In particular, we want to show that, while the first is suited to simultaneously drive all the eigenstates of H_a, the second one exploits all the available resources to drive only its ground state.

The optimal counterdiabatic potential in Ref. [110] is defined as the minimum $A(t)^*$ of the functional

$$S_{H_a}[A(t)] = \int_0^T \mathrm{Tr}\left[(\partial_t H_a + i[A, H_a])^2\right] dt,$$

where $H_a(t)$ is the adiabatic Hamiltonian and $A(t)$ is an engineerable time-dependent Hamiltonian. As shown by in Ref. [110], the minima of the latter potential are also the minima of

$$S'_{H_a}[A(t)] = \int_0^T \mathrm{Tr}\left[\left(\sum_i E_i\left(\partial_t \rho_i + i[A, \rho_i]\right)\right)^2\right] dt.$$

where the E_i and the ρ_i are the eigenvalues and the eigenvectors of H_a respectively.

This functional does not depend on the derivative of the potential, hence its minimum is the minimum of the integrand function at each time. Moreover, since the square is a

monotonic function, here we can replace the integrand with its square root, obtaining another equivalent functional

$$S''_{H_a}[A(t)] = \int_0^T \left\| \sum_i E_i \left(\partial_t \rho_i + i[A, \rho_i] \right) \right\| dt.$$

This last cost is related to cost $\mathcal{F}_{\rho_i}[A(t)]$ associated to the inverse problems for the eigenstates $\rho_i(t)$ of H_a:

$$S''_{H_a}[A(t)] \leq \sum_i |E_i| \mathcal{F}_{\rho_i}[A(t)] \tag{3.18}$$

Therefore, the minimum of S_{H_a} is suited to simultaneously driving all the eigenstates of the adiabatic Hamiltonian. Indeed, the driving of each of these states ρ_i is obtained by minimizing the inverse problem cost functional $\mathcal{F}_{\rho_i}$. When the $\mathcal{F}_{\rho_i}$ have different minima, the optimal solution is a compromise between the best driving of the different states, where the optimization of states with higher energy is the favorite. As a consequence, a minimum for the potential S_{H_a} is generally different from a minimum of $\mathcal{F}$.

As an example, let us consider the transformation $H_a \to H_a + dH_a$ for the Hamiltonian H_a, where $H_a = \mathrm{diag}(E_1, E_2, E_3)$ and

$$dH_a = dt\dot{\lambda} \begin{pmatrix} 0 & (E_2 - E_1) & 0 \\ (E_1 - E_2) & 0 & 2(E_3 - E_2) \\ 0 & 2(E_2 - E_3) & 0 \end{pmatrix} i,$$

in which i is the imaginary unit. If we look for the minimum of the cost function S_{H_a} in the space spanned by the operator

$$P = \begin{pmatrix} 0 & 1 & 0 \\ 1 & 0 & 1 \\ 0 & 1 & 0 \end{pmatrix},$$

we obtain the counterdiabatic potential

$$H_{\mathrm{CD}} = -\dot{\lambda} \frac{(E_1 - E_2)^2 + 2(E_3 - E_2)^2}{(E_1 - E_2)^2 + (E_3 - E_2)^2} P.$$

The optimal generator for the ground state of H_a instead corresponds to the minimum of the associated cost functional $\mathcal{F}$. This can be obtained by replacing E_2 and E_3 with zero in the last expression. Now, the minimization leads to:

$$H_{\mathrm{opt}} = -\dot{\lambda} P.$$

As we can see, the optimal counterdiabatic potential is different from the optimal generator for the target evolution.

3.8 SUMMARY

In this chapter, we have shown how the parent Hamiltonian generating the system evolution can be determined thourgh system of linear equations. By restricting the space of Hamiltonians to a subset of realistic interactions, we have also defined an optimal solution that can be engineered in a realistic device. This optimal solution not only allows us to reconstruct the time-dependent generator, but also causes the initial state to evolve towards the target state with high fidelity. Hence, our techniques can be used for manipulating quantum states and, as we show in the following chapter, extended to Hamiltonian learning. A significant aspect of our analysis is the geometric significance of the proposed cost functional, which captures the geometry induced on the space of states by a set of permitted interactions. By interpreting the cost function as a geometric object, we have obtained an analytical expression for the optimal generator at each time as a function of the state and its time derivative. The leading role of the QCM in this expression also highlights the connection between symmetry reconstruction and optimization techniques in optimal control. We have demonstrated that our method can drive the time-dependent ground state of the Ising model and of the p-spin model in a transverse field. Finally, we have investigated connections and differences between the optimal generator for a time-dependent ground state and the counterdiabatic shortcut to adiabaticity.

In Section 3.4, we have also defined a geometric measure of the difficulty of creating a desired time-dependent state using local interactions, the *accessibility* functional. This geometric notion can be used to identify the most efficient path to connect quantum states by searching for geodesics of a related metric. Additionally, the physical meaning of this object bears a close resemblance to the concept of a geometry of quantum complexity [114–116] and the questions surrounding the accessibility of the Hilbert space [53]. In the future, further investigation of these connections could have significant implications for quantum state control and quantum information theory.

4

LEARNING THE HAMILTONIAN OF A TIME-DEPENDENT STATE

4.1 INTRODUCTION

In the previous chapter, we showed how to reconstruct the time-dependent Hamiltonian capable of generating a given temporal evolution. This was possible through Eq. (3.1), which relates the coefficients of the Hamiltonian at a given instant to the infinitesimal evolution of the expectation values. In this chapter, we show how to extend the same approach to Hamiltonian learning, which consists of the inference of a realistic Hamiltonian model from experimental data. This process has been essential for validating theoretical models over the years, where the observation of the system's evolution aims to characterize the unknown model parameters and determine their plausibility. It is now gaining significant attention in the scientific community due to its importance for the verification and benchmarking of quantum technologies.

Beyond the design of a specific algorithm for Hamiltonian learning, depicted in Section 4.2, and the estimation of its performances in terms of uncertainty, that is illustrated in Section 4.3, the main result of this chapter regards quantum resource theory. We want to figure out what feature of a time evolution determines the learnability of the Hamiltonian, understood as the rate at which the accuracy of our reconstruction increases with the number of experiment iterations. After introducing the inverse participation ratio (IPR) [139–141] as a measure of delocalization of the initial state in the Hamiltonian eigenstates, in Section 4.5 we demonstrate through analytical arguments that effectiveness of the proposed learning method depends on the state delocalization. Specifically, we prove that there is an analytical relationship between the IPR of the initial state and the information matrix, which reflects the amount of information gained during the learning process. States that are equally weighted superpositions of the Hamiltonian eigenstates, and therefore delocalized, provide the maximal information about the system Hamiltonian, as shown in Figure 4.1. As a proof of concepts, in Section 4.6, we apply our method to learn the Hamiltonian of systems of few superconducting qubits, highlighting its relevance to gate-based quantum computation and confirming our predictions about the relationship between IPR and accuracy. We conclude that delocalization can be considered a resource for Hamiltonian learning. Remarkably, this offers a new perspective on the use of quantum information theory in the study of out-of-equilibrium quantum systems [139, 142]. The last section is devoted to summarize our results and the future perspectives.

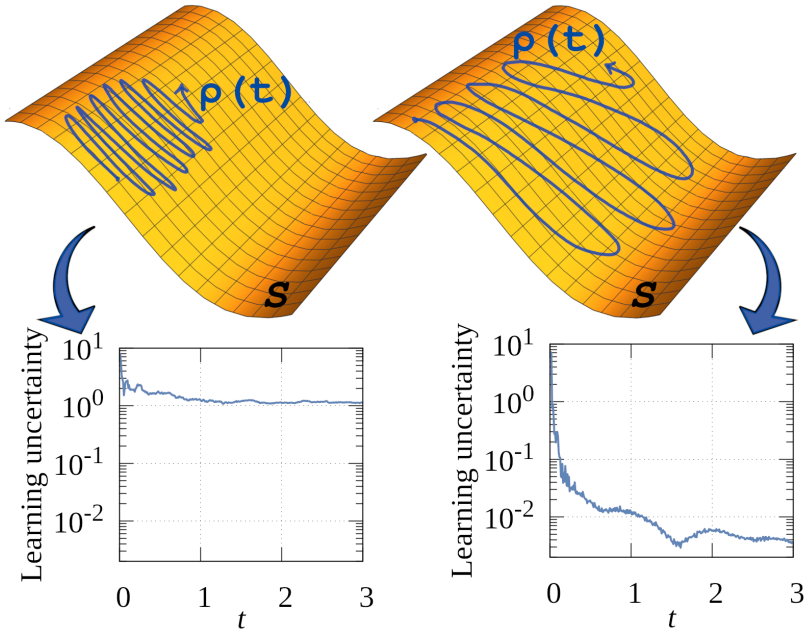

Figure 4.1: The larger is the capability of the state $\rho(t)$ to explore the space of states S, the larger is the amount of information obtained through the learning process, and, consequently, the smaller is the uncertainty in reconstructing the Hamiltonian.

4.2 HAMILTONIAN LEARNING ALGORITHM

Every Hamiltonian learning algorithm infers the system Hamiltonian from a collection of measurements. As illustrated in Chapter 2, there are several proposals in recent literature about how to optimize the choice of these measurements in many situations [70, 87]. Here, we focus our attention on the investigation of the feature of a quantum state that makes high-accuracy Hamiltonian learning possible. For this reason, we base our method on the entire reconstruction of a quantum state at different times, obtained through a simple approach to quantum tomography. More sophisticated approaches to tomography, as well as other efficiency improvements that come with an accurate selection of the observables to measure, are possible but would represent an unwanted complication in our analytical investigation.

We collect information about the system evolution by performing tomographies of the state at a collection of N_T times $\{t_n\} \equiv \{0, \delta t, \ldots, (N_T - 1)\delta t\}$. Hence, we need to estimate how many resources, in terms of the number of experiment shots N_S, are exploited in this process. Each shot starts with the preparation of the initial state, then the system evolves for a time t_n with the unknown Hamiltonian, and finally, a set of commuting observables is measured. As in section 3.2, we define an orthonormal basis $\mathcal{B} = \{O_\alpha\}$ for the space of Hermitian operators endowed with the Hilbert-Schmidt product. In this basis, the system density matrix $\rho(t)$ can be expanded as $\rho(t) = \sum_\alpha o_\alpha(t) O_\alpha$ where $o_\alpha(t) \equiv \mathrm{Tr}(O_\alpha \rho(t))$, the components of $\rho(t)$ over $\mathcal{B}$, are the expectation values of the observables O_α over the state $\rho(t)$. At each time t_n, the state is completely reconstructed by measuring all the observables in the set $\mathcal{B} = \{O_\alpha\}$, grouped in subsets of commuting operators. Finally, we have to take into account that each expectation value $o_\alpha(t_n)$ that contributes to the definition of $\rho(t_n)$ is

affected by statistical uncertainty. This is $\sigma(o_\alpha(t_n)) = \sqrt{\mathrm{Tr}(O_\alpha^2 \rho(t_n))/N_M}$, where N_M is the number of repeated measurements of O_α at time t_n.

We consider superconducting quantum processing units of N_Q qubits, where measurements are always performed in the computational basis, i. e., in the basis of simultaneous eigenstates of the single-qubit operators σ_i^z. Measuring any operator in basis $\mathcal{B}$ of all the Pauli strings can be done by independently rotating any qubit around the axis x ($\sigma_z \to \sigma_y$), y ($\sigma_z \to \sigma_x$) or z ($\sigma_z \to \sigma_z$). With 3 rotations per qubit, we measure any possible observable and we have full information about the system state. Indeed, in a single experiment shot, a large set of Pauli strings is simultaneously measured. For example, after rotating each qubit along the x axis, we simultaneously measure all the many-spins correlations of σ_i^y. As a consequence, in a system of N_q qubits, the number of experiment shots needed for the state tomography in this simple approach is $N_S = 3^{N_q} N_T N_M$.

The time-independent Hamiltonian of the system is $H = \sum_i h_i L_i$, where the $L_i \in \mathcal{L}$ are Hermitian traceless operators that represent the relevant interactions between the constituents of the system. We exploit the information collected in the tomography of the time-dependent state of the system to learn the Hamiltonian couplings h_i.

In the spirit of equation Eq. (3.1) we constrain the Hamiltonian couplings through the short-time evolution of the state. However, in Hamiltonian learning, we need to take into account the approximations due to the finite time-step δt: the system state at a time t_{n+1} is related to $\rho(t_n)$ via the equation

$$\frac{\rho(t_{n+1}) - \rho(t_n)}{\delta t} + i \sum_i h_i [L_i, \rho(t_n)] = R_n \delta t, \tag{4.1}$$

where $R_n = \frac{-[H,[H,\rho(t^*)]]}{2}$ is the remainder of the Taylor expansion at the first order of $\rho(t_{n+1})$, for some $t^* \in [t_n, t_{n+1}]$.

The best optimal guest $h_i^{(\mathrm{opt})}$ for the Hamiltonian couplings can be calculated taking into account an ideal experiment, where δt could be made arbitrarily small and the statistical uncertainty on the state tomography would vanish as well. In this case, the optimal couplings are the ones that minimize the Frobenius norm of the LHS of Eq. (4.1) at each time, that is:

$$f(\vec{h}) = C - 2 \sum_i h_i B_i + \sum_{ij} V_{ij} h_i h_j,$$

where

$$V_{ij} = -\sum_n \mathrm{Tr}\left([L_i, \rho(t_n)][L_j, \rho(t_n)] \right) , \tag{4.2}$$

$B_j = \sum_n \mathrm{Tr}\left(-i[L_j, \rho(t_n)](\rho(t_{n+1}) - \rho(t_n))/\delta t \right)$, and $C = \sum_n \mathrm{Tr}\left((\rho(t_{n+1}) - \rho(t_n))^2/\delta t^2 \right)$. We call the matrix V_{ij} the Total Quantum Covariance Matrix (TQCM).

The optimal couplings correspond to the argument that minimizes $f(\vec{h})$, and, since this is a quadratic function, these can be found by imposing the nullity of the gradient

$$\partial_{h_i} f(\vec{h}) = -2B_i + 2 \sum_j V_{ij} h_j.$$

When the TQCM is invertible, this leads to a unique solution:

$$h_i^{(\mathrm{opt})} = \sum_j (V^{-1})_{ij} B_j. \tag{4.3}$$

Eq. (4.3) can serve our goal if the kernel of V_{ij} is empty, otherwise, the experimental data are insufficient to specify the system Hamiltonian, meaning that different Hamiltonians can produce the same evolution. As we show in the next chapter, in this case, the uncertainty on the Hamiltonian coupling diverges.

4.3 UNCERTAINTY ESTIMATION

The performance of a Hamiltonian learning algorithm is determined by the scaling of the relative uncertainty of the reconstructed Hamiltonian as a function of the computational effort required, here estimated in terms of the number N_S of shots. The goal of this section is to investigate this uncertainty, highlighting its dependence on the initial state in which the system is prepared.

In our approach, the two main sources of uncertainty are the statistical uncertainty $\sigma(a_\gamma(t_m))$ that affects the expectation values $o_\alpha(t_n)$ due to the finite number of measurements M_N, and the impossibility to reduce the time step δt to zero. The first one determines a discrepancy between the real system state and the state reconstructed in tomography, while the second one, expressed by the reminder R_n, is a systematic source of error for the derivatives $(\rho(t_{n+1}) - \rho(t_n))/\delta t$. These contributions determine a total uncertainty δB_i on the vector B_i:

$$\delta B_i = \sqrt{\sum_{\gamma,m} \left(\frac{\partial B_i}{\partial a_\gamma(t_m)} \sigma(a_\gamma(t_m)) \right)^2} + \sum_m |\mathrm{Tr}\left(-i[L_i, \rho(t_m)] R_m\right)|,$$

where the first term on the RHS is the statistical uncertainty and the second one is the systematic uncertainty. Remarkably, since we perform tomography even at the initial time, state preparation errors do not directly affect the uncertainty of the reconstructed Hamiltonian.

In Appendix B, we show that δB_i is upper-bounded by a function that does not depend on the specific evolution of the system, but only on the Hamiltonian and L_i operator norms, the total number of repetitions N_M, time steps N_T and the number of qubits N_q:

$$\delta B_i \leq \frac{16 \|H\|_{\mathrm{op}} \|L\|_{\mathrm{op}}}{\sqrt{2^{N_q} N_M}} \sqrt{N_T} + 4\delta t \|L\|_{\mathrm{op}} \|H\|_{\mathrm{op}}^2 N_T.$$

The uncertainty on B_i is propagated to the Hamiltonian couplings h_i, which are known up to an uncertainty δh_i. In other words, any Hamiltonian $H = \sum_i h_i L_i$ with $|h_i - h_i^{(\mathrm{opt})}| < \delta h_i$ is compatible with the dynamics reconstructed by the tomography.

Relating the uncertainty δB_i to the uncertainty δh_i through Eq. (4.3) and considering the relationship between the vector norm of the exact couplings $\|\vec{h}\|$ and the operator norm $\|H\|_{\text{op}}$, in Appendix B we obtain a bound for the relative error

$$\varepsilon \equiv \|\vec{h}^{(\text{opt})} - \vec{h}\| / \|\vec{h}\|$$

on the reconstructed Hamiltonian:

$$\varepsilon \leq \sqrt{l \operatorname{Tr}\left[\left(\frac{V_{ij}}{\|L\|_{\text{op}}^2 N_T}\right)^{-2}\right]} \left(16 \frac{(3/2)^{\frac{N_q}{2}}}{\sqrt{N_S}} + 4\|H\|_{\text{op}} \delta t\right), \tag{4.4}$$

where l is the number of couplings of the Hamiltonian and, without loss of generality, we suppose that $\|L_i\|_{\text{op}} = \|L\|_{\text{op}}$.

In the RHS of inequality (4.4) we can individuate three main factors that determine the final accuracy. The first factor in round parentheses represents the effect of statistical uncertainty, which can be recognized since it scales as $\sqrt{N_S}^{-1}$. The second factor in round parentheses is the systematic source of error, related to the finite time steps δt. It is important to note that this error, that here scales with the system size through the Hamiltonian norm, can be shown to be independent of this size for local Hamiltonians through the Lieb-Robinson bounds [53]. These first two factors are independent of the state. Hence, the upper bound on the relative error only depends on the system evolution through the inverse norm $\sqrt{\operatorname{Tr}(V^{-2})}$ of the TQCM, determined by the eigenvalues. Indeed, the more information about the system Hamiltonian we learn through studying the state evolution, the greater these eigenvalues are. Conversely, when a given TQCM eigenvalue reaches zero and the matrix cannot be inverted, the uncertainty diverges, indicating that there is insufficient data from the experiment to sustain Hamiltonian learning. Hence, Eq. (4.4) is analogous to a Cramer-Rao bound [87, 143] on the Hamiltonian uncertainty, where the TQCM takes the role of an information matrix.

At any given fixed time, the spectrum of the QCM

$$V_{ij,n} \equiv -\operatorname{Tr}\left([L_i, \rho(t_n)][L_j, \rho(t_n)]\right) \tag{4.5}$$

determines the amount of information about the Hamiltonian gained by observing the short-time evolution, whereas the spectrum of the TQCM determines the total amount of information about the Hamiltonian that we have learned from the state evolution. The preparation of the starting state and the subsequent evolution affect both the QCM and the TQCM. As a result, the choice of the initial quantum state is essential for the algorithm to succeed, and the best initial states are those that maximize the amount of information learned, reducing uncertainty in the reconstructed Hamiltonian.

4.4 THE IPR AS A MEASURE OF ERGODICITY

In the previous section, we have shown how the accuracy of the reconstruction is influenced by the system time-dependent state through the inverse norm of TQCM. In the followings, we are going to identify the property of a quantum state that determines this norm. We will focus our attention on pure states.

First of all, let us note that the TQCM is the sum over the different time steps of the QCMs $V_{ij,n}$. Following the definition of Eq. (4.5), eigenvalues of this matrix are either positive or null. During the time evolution, the more the system state changes, the more its symmetries change. These are represented by the zero eigenvalues of the QCM, which rotate during the evolution. As a consequence, the minimum eigenvalues of TQCM resulting from this process rapidly increase. Contrarily, if the system state is stationary, symmetries does not change in time and form a non-empty kernel for the TQCM. Based on this argument, we are going to show that the property of the evolution that determines the learning accuracy is the ergodicity of the state evolution, understood as its capability of visiting all possible states with equal probability.

To this aim, we need to introduce some measure of ergodicity. The inverse participation ratio (IPR) is a good estimator of this property [139–141]. It is defined as the inverse of the sum of the squares of the wave function amplitudes. In systems where the IPR is high, the wave function is highly localized, and the system is less likely to visit all possible states. This can lead to a lack of ergodicity, as the system may become stuck in a particular region of state space. On the other hand, systems with low IPR tend to be more delocalized and are more likely to visit a wider range of states, leading to a higher degree of ergodicity.

In our chase of study, where it is convenient for the state to explore the entire Hilbert space, we consider the IPR of the initial state in the Hamiltonian eigenstates. If the system Hamiltonian is $H = \sum_\alpha E_\alpha |\alpha\rangle\langle\alpha|$ and the initial state of the system is $|\psi\rangle = \sum_\alpha a_\alpha |\alpha\rangle$, the wave function amplitudes are $|a_\alpha|^2$. Therefore, the IPR is defined as

$$\mathrm{IPR}(\psi, H) = \sum_\alpha |a_\alpha|^4.$$

Therefore, the IPR measures the spreading of the initial state in the Hamiltonian eigenstates: the lower is the IPR, the more the initial state spreads out. To better understand the link between IPR and the ergodic hypothesis, we can look at time average of observables. Indeed, the long-time average of an observable A converges to

$$\bar{A} = \mathrm{Tr}(\bar{\rho} A), \tag{4.6}$$

where $\bar{\rho} = \sum |a_\alpha|^2 |\alpha\rangle\langle\alpha|$ is the so-called *dephased state*. This happens for any not-fine tuned Hamiltonians because of the vanishing oscillating terms in time evolution. When the IPR, that can be written as the purity of the dephased state, is minimum ($\mathrm{IPR}_{\min} = 1/2^{N_q}$), all the populations of $\bar{\rho}$ are equal. Thus, the time average coincides with the equal weights average on the energy eigenstates.

4.5 INFORMATION AND IPR

In this section, our aim is to show that states with a small IPR are associated with large eigenvalues of the TQCM and, due to Eq. (4.4), with a small error of the reconstructed Hamiltonian.

We consider a system in a pure state, represented by the density matrix $\rho(t) = |\psi(t)\rangle\langle\psi(t)|$. At time zero, the expansion of the system state on the Hamiltonian eigensates $|\alpha\rangle$ is $|\psi(0)\rangle = \sum_\alpha a_\alpha|\alpha\rangle$. We study the behavior of the eigenvalues ω_i of the TQCM. Given a basis $a_j^{(i)}$ of normalized eigenvectors for this matrix, the ω_i can be written as $\omega_i = \sum_{jj'} V_{jj'} a_j^{(i)} a_{j'}^{(i)}$. Defining the local operators $A_i \equiv \sum_j a_j^{(i)} L_j$ and exploiting the definition of the TQCM in Eq. (4.2), we can see that these eigenvalues are the sum of local connected correlation functions:

$$\omega_i = -\sum_n^{N_T} \mathrm{Tr}\left([A_i,\rho(t_n)][A_i,\rho(t_n)]\right) = 2\sum_n^{N_T}\left(\langle\psi(t_n)|A_i^2|\psi(t_n)\rangle - \langle\psi(t_n)|A_i|\psi(t_n)\rangle^2\right).$$

We approximate this sum to an integral by considering a small time-step δt, and we make explicit the oscillating terms by writing the system state evolution in terms of the Hamiltonian energy levels:

$$\omega_i \approx= \frac{2N_T}{T}\int_0^T dt\Big(\sum_{\alpha\beta} a_\alpha a_\beta^* \langle\alpha|A_i^2|\beta\rangle e^{-it(E_\alpha-E_\beta)} - \sum_{\alpha\beta\gamma\delta} a_\alpha a_\beta^* a_\gamma a_\delta^* \langle\alpha|A_i|\beta\rangle\langle\gamma|A_j|\delta\rangle e^{-it(E_\alpha-E_\beta+E_\gamma-E_\delta)}\Big).$$

If we exclude fine-tuning situations, for the unknown Hamiltonian H we can assume that $E_\alpha = E_\beta$ if and only if $\alpha = \beta$, and $E_\alpha - E_\beta + E_\gamma - E_\delta = 0$ if and only if $E_\alpha = E_\beta$ and $E_\gamma = E_\delta$ or $E_\beta = E_\gamma$ and $E_\alpha - E_\delta$. These two conditions, which are also involved in the prof of Eq. (4.6) as well as in important results about equilibration of quantum systems [144–146], are respectively called *non-degeneracy* and *non-resonance* condition. Under these conditions, after an equilibration time T_e that scales as the inverse of the minimum energy gap or the inverse of the minimum difference between energy gaps, the oscillating terms vanish and the previous equation becomes

$$\omega_i \approx 2N_T\Big[\sum_\alpha |a_\alpha|^2\langle\alpha|A_i^2|\alpha\rangle - \sum_{\alpha\beta}|a_\alpha|^2|a_\beta|^2\Big(\langle\alpha|A_i|\alpha\rangle\langle\beta|A_i|\beta\rangle + |\langle\alpha|A_i|\beta\rangle|^2\Big)\Big],$$

or, equivalently,

$$\omega_i \approx 2N_T[\mathrm{Tr}(\bar\rho A_i^2) - (\mathrm{Tr}^2(\bar\rho A_i) + \mathrm{Tr}(\bar\rho^2 A_i^2))]. \tag{4.7}$$

We can see that after the equilibration transient, the TQCM eigenvalues become linear in the number of time steps, with a coefficient $k_i \equiv [\mathrm{Tr}(\bar\rho A_i^2) - (\mathrm{Tr}^2(\bar\rho A_i) + \mathrm{Tr}(\bar\rho^2 A_i^2))]$. Hence, the uncertainty bound in Eq. (4.4) can be written as:

$$\varepsilon \leq \|L\|_{\mathrm{op}}^2\sqrt{l\sum_i k_i^{-2}}\left(16\frac{(3/2)^{\frac{N_q}{2}}}{\sqrt{N_S}} + 4\|H\|_{\mathrm{op}}\delta t\right), \tag{4.8}$$

The k_i measure the variance of the local operators A_i in the dephased state $\bar{\rho}$. The positive contribution to this variance comes from the term $\mathrm{Tr}(\bar{\rho}A_i^2)$, while the negative contributions come from $\mathrm{Tr}^2(\bar{\rho}A_i)$ and $\mathrm{Tr}(\bar{\rho}^2A_i^2)$. When the IPR of the system state is minimized, the dephased state is the totally mixed state and, since the L_i's are traceless, the term $\mathrm{Tr}^2(\bar{\rho}A_i)$ vanishes. The remaining negative contribution also decreases in magnitude with the IPR, that can be written as the purity $\mathrm{Tr}(\bar{\rho}^2)$ of the dephased state. As a consequence, minimizing the IPR is a good strategy to generate larger eigenvalues ω_i of the TQCM.

Now, we can understand inequality (4.8) as follows. In the initial transient, the state explores a region of the Hilbert space whose extension is measured by the k_i's. The larger are these values, the larger is the amount of information collected. After, the state evolves near to its previous orbits, providing redundant constraints to the Hamiltonian: the error depends on the number of time steps only through the number of experiment shots.

Before concluding this section, two remarks are in order. The first one regards the choice of optimal initial states, minimizing the IPR and therefore optimizing the learning process. The states can be written in terms of the Hamiltonian eigenstates as

$$|\psi_{\mathrm{opt}}\rangle = \sqrt{2^{-N_q}} \sum_{\alpha} e^{i\phi_\alpha} |\alpha\rangle \tag{4.9}$$

where the ϕ_α's are arbitrary phases. It is important to note that, in order to define these states, one needs to know the system Hamiltonian. This may sound odd, as the reconstruction of the Hamiltonian is the goal of the learning process, while the knowledge of optimal states should be exploited to accelerate this process. However, for practical applications, this problem could be addressed resorting to adaptive learning approaches as in Ref. [87]. Starting from the optimal states associated to a guessed Hamiltonian, one can obtain a better estimate of the target Hamiltonian and iterate this process until the result converges.

The second remark regards the beneficial effect of delocalization. Since we have shown that this is a resource for Hamiltonian learning, one could wonder if mixed states can also be exploited to improve accuracy. At a first analysis, this seems not to be the case. Indeed, the TQCM in Eq. (4.2) is related to the trace of ρ^2, therefore states with small purity also have a small TQCM.

4.6 SIMULATIONS

To test our hypotheses about the error scaling in Eq. (4.4) and the connection between the TQCM and IPR in Eq. (4.7), in this section we perform Hamiltonian learning on small quantum systems with a few qubits. We start by examining a basic two-qubit problem, then move on to a three-qubit model with randomly chosen couplings. Finally, we exploit Qiskit [147] to demonstrate how to use our method on a real quantum computer.

To simulate our learning method, we first select a Hamiltonian H and compute the evolution of the expectation values of the basis elements $\{O_\alpha\}$ by numerically solving the Schrödinger equation. This process is repeated for a set of initial states that cor-

respond to different initial configurations for the experiment, each with a different IPR. To simulate the impact of statistical error, we add uniform random noise with an amplitude $1/\sqrt{2^{N_q} N_M}$ to each expectation value. Next, we infer the optimal Hamiltonian $H^{(\mathrm{opt})} = \sum_i h_i^{(\mathrm{opt})} L_i$ from our simulated evolutions.

We verify the effectiveness of the learning procedure by comparing H with $H^{(\mathrm{opt})}$. Specifically, we examine how the relative error ε and the TQCM behave for each initial state and for different total observation times. We also investigate the relationship between the IPR and the information content of the experiment, as measured by the eigenvalues of the TQCM. Finally, we calculate the optimal initial state $|\psi_{\mathrm{opt}}\rangle$ for each Hamiltonian and use it to achieve optimal learning.

4.6.1 *Cross-resonance gate*

As a paradigmatic example, here we simulate the learning of the Hamiltonian that governs a cross-resonance (CR) gate developed by IBM [148–151]. This gate is often used in quantum computation to entangle two qubits and perform operations on them simultaneously. Moreover, it can be used to perform a controlled-NOT (CNOT) operation on one qubit, with the other qubit as the control qubit. For this reason, implementing this gate with high accuracy is a fundamental step toward universal quantum computation. In the computational basis $\{|\downarrow\downarrow\rangle, |\downarrow\uparrow\rangle, |\uparrow\downarrow\rangle, |\uparrow\uparrow\rangle\}$, the CR gate is represented by the matrix

$$CR = \begin{pmatrix} 0 & 1 & 0 & 0 \\ 1 & 0 & 0 & 0 \\ 0 & 0 & 1 & 0 \\ 0 & 0 & 0 & 1 \end{pmatrix}.$$

In the device under exam, the gate is approximately realized by coupling two superconducting quantum circuits, called transmons, by a resonator. Each transmon acts like an anharmonic oscillator, coupled with the other transmon and the environment through an electromagnetic field. Thanks to the anharmonicity, under suitable conditions on the external electromagnetic signal the whole system behaves as a pair of interacting qubits governed by the effective Hamiltonian:

$$\begin{aligned} H = &-1.548\, \mathbb{1} \otimes \sigma_x - 0.004\, \mathbb{1} \otimes \sigma_y + 0.006\, \mathbb{1} \otimes \sigma_z + 9.578\, \sigma_z \otimes \mathbb{1} \\ &+ 5.316\, \sigma_z \otimes \sigma_x - 0.225\, \sigma_z \otimes \sigma_y - 0.340\, \sigma_z \otimes \sigma_z, \end{aligned} \tag{4.10}$$

where the couplings are taken from Ref. [152] and the energies are expressed in MHz.

After simulating the system evolution, we aim to learn the Hamiltonian coupling, with the hypotheses that the involved interactions are $\{L_i\} = \{\mathbb{1} \otimes \sigma_x, \mathbb{1} \otimes \sigma_y, \mathbb{1} \otimes \sigma_x, \sigma_z \otimes \mathbb{1}, \sigma_z \otimes \sigma_x, \sigma_z \otimes \sigma_y, \sigma_z \otimes \sigma_z\}$. This choice of the set $\{L_i\}$ is supported by first-principles studies [150]. To perform the Hamiltonian learning algorithm, we set the time step to $\delta t = 0.01$ and

conduct a total of $N_M = 1000$ measurement repetitions with $N_S = 3 \times 10^6$ shots. The algorithm is run on several initial states that have varying IPRs.

The reconstructed Hamiltonian couplings after $N_S = 3 \times 10^6$ shots are shown in Table 4.1 for the following states: $|\uparrow\uparrow\rangle$ with IPR $= 0.503$, $|\rightarrow\rightarrow\rangle \equiv (|\uparrow\rangle + |\downarrow\rangle) \otimes (|\uparrow\rangle + |\downarrow\rangle)/2$ with IPR $= 0.498$, $|\psi^+_{\text{Bell}}\rangle \equiv (|\uparrow\uparrow\rangle + |\downarrow\downarrow\rangle)/\sqrt{2}$ with IPR $= 0.251$, and the optimal state $|\psi_{\text{opt}}\rangle$ corresponding to the minimum IPR $= 0.25$. We can see that better results are obtained when the initial state has a small IPR.

In Fig. 4.2 (a), we plot the relative error ε of the reconstructed couplings as a function of the experiment shots N_S. Since both the time step δt and the number of measurements N_M are fixed, N_S is proportional to the total evolution time of the system. The curves in the plot represent states with various IPR values. Our predictions are confirmed by the numerical simulations: after an initial period in which the error decreases exponentially with the number of time steps, the final error tends towards smaller values for states with a smaller IPR. The optimal results are achieved when the initial state is $|\psi_{\text{opt}}\rangle$.

To prove that this behavior is driven by the evolution of the eigenvalues of the TQCM, in Fig. 4.2 (b), we plot the Frobenius norm of the inverse TQCM times the number of time steps. We observe that this norm exponentially decreases during an initial equilibration transient and eventually approaches the equilibrium behavior that is predicted in Section 4.5. Specifically, the norm becomes linear in the evolution time, with the proportionality coefficient decreasing as the IPR increases.

In Fig. 4.2 (c), repeating the learning simulation with a large set of the randomly chosen initial state, we directly show the relationship between the IPR of the initial state and the long-time inverse norm of the TQCM (for $N_T = 300$). To obtain states with a sufficiently uniform distribution of IPRs, random states are sampled as follows. In a basis $\{|\alpha\rangle\}$ of Hamiltonian eigenstates, we randomly choose the probability p_1 of being in the first eigenstate $|1\rangle$ from the uniform distribution in the interval $[0, 1]$. Then the probability p_2 of being in $|2\rangle$ is randomly chosen in the interval $[0, 1 - p_1]$, and so on. Finally, the random state is $|\psi\rangle = \sum \sqrt{p_\alpha}|\alpha\rangle$. Looking at the figure under the exam, we can confirm the predictions of the previous section: the IPR and the inverse norm of the TQCM are positively

Table 4.1: Estimated Hamiltonian coupling for different initial states with the corresponding IPR in parentheses, with $\delta t = 0.01$, $N_M = 1000$ and $N_S = 3 \times 10^6$.

Term	Target	$\|\uparrow\uparrow\rangle$ (IPR $= 0.503$)	$\|\rightarrow\rightarrow\rangle$ (IPR $= 0.498$)	$\|\psi^+_{\text{Bell}}\rangle$ (IPR $= 0.251$)	$\|\psi_{\text{opt}}\rangle$ (IPR $= 0.25$)
$\mathbb{1} \otimes \sigma_x$	-1.548	2.142	-1.143	-1.543	-1.542
$\mathbb{1} \otimes \sigma_y$	-0.004	1.021	-0.024	-0.011	0.000
$\mathbb{1} \otimes \sigma_z$	0.006	1.073	-0.017	-0.009	0.023
$\sigma_z \otimes \mathbb{1}$	9.578	-1.418	9.748	9.556	9.553
$\sigma_z \otimes \sigma_x$	5.316	1.627	5.089	5.301	5.295
$\sigma_z \otimes \sigma_y$	-0.225	-1.254	-0.218	-0.216	-0.237
$\sigma_z \otimes \sigma_z$	-0.340	-1.409	-0.328	-0.324	-0.357

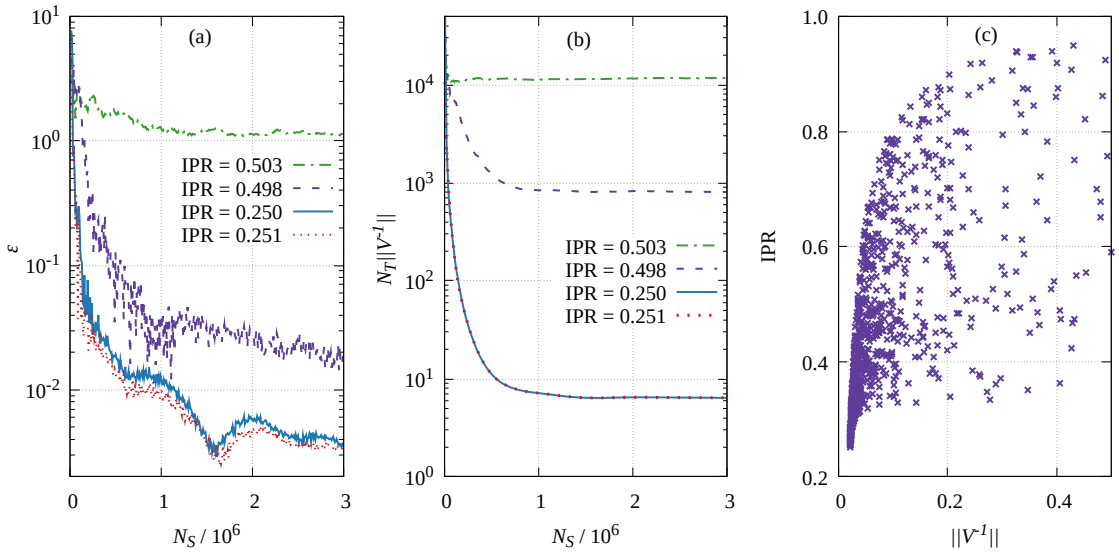

Figure 4.2: (a) relative reconstruction error and (b) Frobenius norm of the inverse TQCM multiplied by N_T, as a function of N_S for the cross-resonance gate Hamiltonian in Eq. (4.10), with $\delta t = 0.01$, $N_M = 1000$ and $N_S = 9 \times N_M \times N_S$, for different initial states with different IPR. (c) IPR and Frobenius norm of the inverse TQCM for a collection of random states at a large final time for the cross-resonance gate Hamiltonian, with $N_T = 300$.

correlated for small values of the TQCM. In particular, the best learning performance in terms of the information matrix corresponds to the states that minimize the IPR.

4.6.2 *Random 2-body Hamiltonian*

In this example, we seek to evaluate the effectiveness of our learning algorithm when applied to a system governed by a randomly generated Hamiltonian of the form:

$$H = \sum_i h_i L_i,$$

where couplings h_i range from -5 to 5, and the L_i represent all of the two-spin interactions acting on a three-spin system. These interactions can be represented as tensor products of two Pauli operators and the identity operator. In order to test the algorithm, we use a time step of $\delta t = 0.01$, conduct $N_M = 1000$ measurement repetitions, and run the algorithm for a maximum of 370 time steps.

The relative error of the reconstruction and the behavior of the TQCM are depicted in Figure 4.3, panels (a) and (b). In panel (c) of the same figure, we display the IPR (inverse participation ratio) and the Frobenius norm of the inverse TQCM for a collection of random states at a large final time. The validity of our theoretical predictions about the optimality of low IPR states is particularly apparent in panels (b) and (c), where we have not taken into account statistical and systematic contributions to uncertainty.

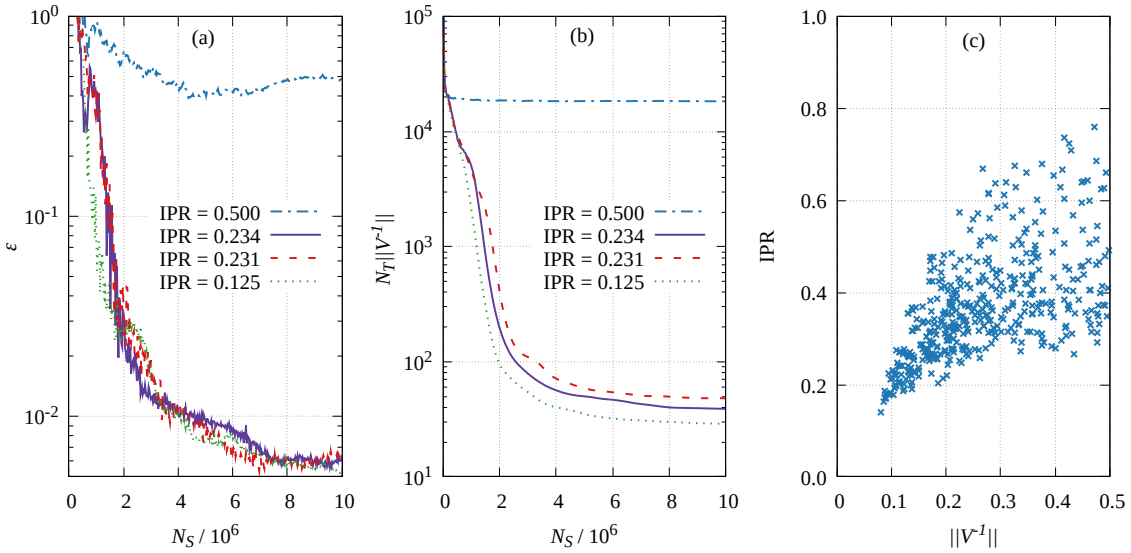

Figure 4.3: (a) relative reconstruction error and (b) Frobenius norm of the inverse TQCM multiplied by N_T, as a function of N_S, with $\delta t = 0.01$, $N_M = 1000$. The initial states are: an equal weighted superposition of two Hamiltonian eigenstates with IPR $= 0.5$, the GHZ state with IPR ≈ 0.231, $|\uparrow\uparrow\uparrow\rangle$ with IPR ≈ 0.234, and $|\psi_{\text{opt}}\rangle$ with IPR $= 0.125$. (c) IPR and Frobenius norm of the inverse TQCM for a collection of random states at large final time, $N_T = 370$.

4.6.3 *IBM Q FakeAthens processor*

In this subsection, we examine the performance of our learning algorithm on a simulated quantum processor, the *FakeAthens* processor, using the Qiskit software [147]. This approach, which encompasses everything from state preparation to final measurements, can be easily adapted to any quantum processor. The current simulator considers a two-qubit system and takes into account errors in state preparation and measurements. It is worth noting that due to preparation errors, the starting state is not a pure state; however, our method can still be applied in this scenario.

To test the algorithm, we execute a time-dependent unitary gate that can be represented in the computational basis as follows:

$$U(t) = \begin{pmatrix} \cos(4\pi t) & -i\sin(4\pi t) & 0 & 0 \\ -i\sin(4\pi t) & \cos(4\pi t) & 0 & 0 \\ 0 & 0 & 1 & 0 \\ 0 & 0 & 0 & 1 \end{pmatrix}.$$

We are aware that this gate is produced through the cross-resonance mechanism demonstrated in our first example. As such, we consider a parent Hamiltonian that is spanned by the same operators:

$$\{L_i\} = \{\mathbb{1}\otimes\sigma_x, \mathbb{1}\otimes\sigma_y, \mathbb{1}\otimes\sigma_x, \sigma_z\otimes\mathbb{1}, \sigma_z\otimes\sigma_x, \sigma_z\otimes\sigma_y, \sigma_z\otimes\sigma_z\}. \tag{4.11}$$

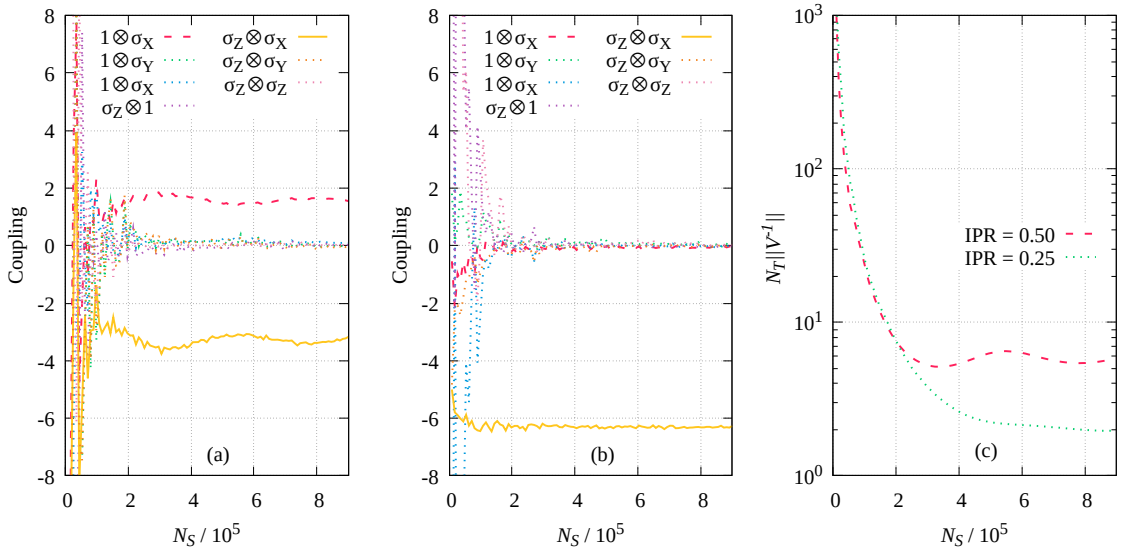

Figure 4.4: Panels (a) and (b): reconstructed Hamiltonian couplings at increasing number of shots, corresponding to longer observation time, for $N_M = 1000$, $\delta t = 0.01$. Panel (a): initial state $|\downarrow\downarrow\rangle$, Panel (b): initial state $|\psi^+_{\text{Bell}}\rangle$. Panel (c): Frobenius norm of the inverse TQCM multiplied by N_T, as a function of N_S for the two initial states.

In Figure 4.4 panels (a) and (b) we show the Hamiltonian couplings learned with different initial states as the total observation time increases with the number of experiment shots. These initial states are $|\downarrow\downarrow\rangle$ and the Bell state $|\psi^+_{\text{Bell}}\rangle$, respectively. Since we do not know the real system Hamiltonian in advance, in this case, we can not estimate the learning error directly. To select the most reliable Hamiltonian reconstruction, we can look again at the inverse norm of the TQCM. By examining panel 4.4(c), we can see that this norm is minimized when the initial state is the Bell state, which, as expected, has a smaller IPR. We can conclude that the most accurate reconstruction for the couplings corresponds to panel (b).

4.7 SUMMARY

In this chapter, we have investigated the possibility of reconstructing the Hamiltonian of a system from a single time-dependent state. To this aim, we have defined a simple learning algorithm based on time-dependent state tomography. This has allowed us to study which characteristics of a temporal evolution determine the ability to reconstruct the Hamiltonian that generated it. We have shown that the information matrix that determines the learning uncertainty is related to the IPR of the state in the eigenbasis of the Hamiltonian. Ultimately, this demonstrates that the most ergodic evolutions are those that lead to the best learning performance. To illustrate our findings, we reconstructed the Hamiltonians of systems consisting of a small number of superconducting qubits, highlighting the significance of our approach in the context of gate-based quantum computation. In these examples, as our analytical investigation predicted, the reconstruction error exponentially decreases during the initial equilibration transient. Afterward, the final accuracy improves

as the IPR decreases. Our results show that delocalization can significantly enhance the efficiency of Hamiltonian learning algorithms.

In this chapter, data have been collected through quantum state tomography, which requires an exponential number of measures in the system size. In our case, the number of required shots is scaled with 3^{N_Q}. This great effort in collecting expectation values is partially rewarded if we look at the scaling of the reconstruction error in Eq. (4.4), where the statistical contribution exponentially decreases in the system size. However, collecting data through state tomography generally is not efficient, even if it allowed for the simple uncertainty analysis of this chapter. This inefficiency can be understood by looking at Eq. (4.3) as a system of constraints for the unknown Hamiltonian couplings, each of which depends on the expected value of certain observables and their derivatives. In a quantum state, expectation values are not independent and the evolution of some observables is less influenced by the system Hamiltonian. For these reasons, some of these constraints are redundant or less significant in determining the Hamiltonian. In other words, some measurements are more informative than others. From the perspective of improving the algorithm performance, one has to measure only the expectation values of a set of observables that optimizes the accuracy. These observables could be selected through adaptive learning strategies, in analogy with Ref. [87], where the role of the TQCM is taken by the Fisher Information Matrix.

Results of this work also open an interesting perspective on the interplay between information and learning theory and quantum many-body systems: the amount of information contained in the system evolution, expressed by the TQCM, is related to the ergodic behavior. Inspired by this situation, one could investigate other emerging features of a many-body system that could influence the learning process, such as the strong sensitivity to the control parameter that characterizes critical states [6, 117–120] and chaotic systems [153, 154].

5

INVERSE QUANTUM ANNEALING

5.1 INTRODUCTION

In the previous chapters, we have studied the time-dependent inverse problem. We have proposed an exact solution to the problem, and found an optimal local solution for many-body systems. Finally, we have applied our results to the Hamiltonian learning, showing their effectiveness in the case of ergodic evolutions. This chapter is dedicated to the reconstruction of local proper parent Hamiltonians (PPHs) for many-body states. This is a fundamental step for many problems, such as inferring the high-energy behavior of a physical system from the knowledge of its low-energy behavior [52]. The search for PPHs has great impact in the realm of quantum technologies, where it could be used to prepare target many-body states [66–69] or reconstruct the couplings of the system Hamiltonian from low-temperature measurements.

As shown in Chapter 2, while symmetries can be exactly reconstructed from the knowledge of correlation functions [56–58], or approximately from local expectation values [59–61], selecting the PPHs among symmetries is unfeasible for generic large systems. Indeed, it requires Hamiltonian diagonalization to verify that the target state is a ground state for each candidate PH [57]. More sophisticated methods proposed in the literature are based on the minimization of a function that, in general, is exponentially complicated to evaluate [60, 61]; or on some very stringent Ansatz on the system state [64, 65]. Ultimately, the search for PPH is most of the times an exponentially hard task.

The search for approximate solutions for hard problems is not a novelty in many-body physics. A common example is the search for the ground state of a given Hamiltonian. In this context, several algorithms have been developed that give a good approximation of the ground state. Some of these algorithms can be efficiently executed on a classical computer, for example, simulated annealing [155–157] or algorithms based on the density matrix renormalization group [158–161], while other ones need to be implemented on a quantum computer, for example, QAOA [162–164] or quantum annealing [76–79]. This latter exploits the adiabatic theorem: the ground state of a simple Hamiltonian is prepared on a quantum device, then this Hamiltonian is slowly changed towards the target Hamiltonian. In this way, the initial state adiabatically evolves towards the ground state of the target Hamiltonian.

In this chapter, we explore the possibility of inverting quantum annealing to reconstruct a PH: in other words, we propose a novel method to efficiently generate PPHs, called *inverse quantum annealing* (IQA), that mimics quantum annealing but swaps the role of

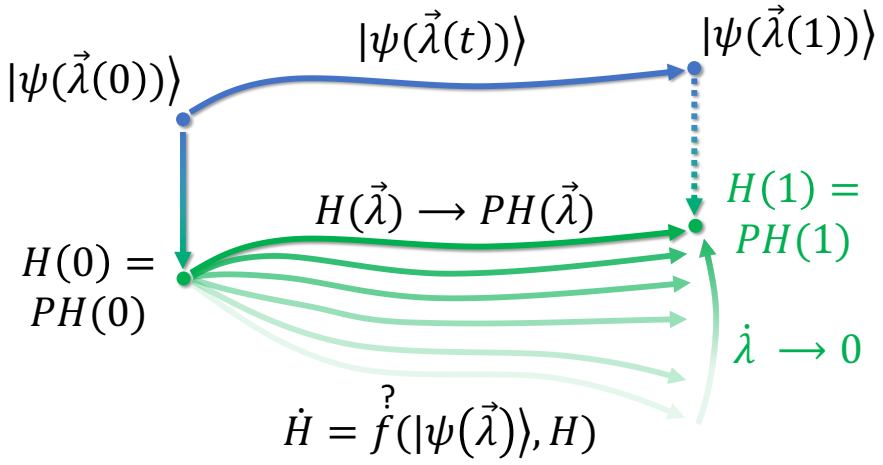

Figure 5.1: IQA consists in a dynamics for the Hamiltonian H, depending on a target path of states $|\psi(\vec{\lambda})\rangle$, that in the adiabatic limit converges to a path of proper parent Hamiltonians $PH(\lambda)$ for the target states.

Hamiltonians and states (Figure 5.1). Initializing the system with a simple many-body state with a known PPH, the procedure consists of slowly deforming the state towards the target state. The PPH correspondingly evolves according to artificial dynamics, which becomes adiabatic if the deformation is slow enough. We design these dynamics in a way such that, in the adiabatic limit, the generated Hamiltonian is a local PPH for the target state. Remarkably, the computational cost of our algorithm is polynomial in the system size. Moreover, it allows finding local PPHs starting from the knowledge of only local expectation values of the path that connects the initial state with the target state.

The chapter is structured as follows. Section 5.2 is devoted to briefly introducing the (standard) quantum annealing, and then to defining the IQA technique in general. In Section 5.3 we propose a possible artificial dynamics to realize this technique. An efficient implementation of these dynamics on a classical computer is possible through a time-dependent variational principle, illustrated in Section. 5.4. In Section 5.5 we exemplify our method by reconstructing PPHs for a path of Gaussian states. Finally, Section 5.6 is devoted to summarizing this chapter and further possible developments of the proposed technique.

5.2 FROM QUANTUM ANNEALING TO INVERSE QUANTUM ANNEALING

Before introducing our technique, we briefly explain what is quantum annealing and how it works. Computational techniques based on annealing are useful to optimize functions in large spaces, for example minimizing the energy in the space of states of a many-body systems [80] or solving a combinatorial optimization problem such as the traveling salesman problem [80] or set covering problems [73].

These methods are inspired by thermal annealing, a metallurgical technique used to improve a material's structural purity and decrease imperfections. It is accomplished by

first rapidly heating the material to a high temperature and then cooling it slowly. In this way, atoms have time to reorganize themselves to more ordered, low-energy states for each value of the temperature, until the low target temperature is reached. The high and intermediate temperature state defines a privileged path that drives the state towards the global minimum of energy, avoiding false minima.

A first example of an annealing-based computational technique is the simulated annealing, which mimics this process to find an approximate global optimum for a function with numerous variables. The algorithm works by randomly generating a starting solution and then iteratively making small changes to it, accepting the changes if they improve the solution or rejecting them if they make the solution worse. The probability of accepting a worse solution is controlled by a fictitious temperature parameter, which is gradually decreased during the optimization process. This allows the algorithm to explore a larger space of possible solutions at the beginning and gradually focus on the most promising ones as the temperature decreases.

Quantum annealing [76–80] is a variant of annealing that uses quantum mechanics to search for the global minimum of a function. It is based on the idea that a quantum system can simultaneously explore multiple states and can tunnel through energy barriers, which allows it to escape local minima and find the global minimum more efficiently than classical annealing algorithms. Quantum annealing can be implemented using synthetic quantum systems called *quantum annealers*. These devices are initialized in the non-generate ground state of an easy-to-minimize Hamiltonian H_0. Then the system Hamiltonian $H(t)$ is slowly changed from H_0 to a target Hamiltonian H_1 in the time interval $[0, T]$ as follows:

$$H(t) = \frac{T-t}{T} H_0 + \frac{t}{T} H_1.$$

If the ground state of $H(t)$ remains a non-degenerate eigenstate, the adiabatic theorem [165] ensures that for a sufficiently large annealing time T the final state of the system well approximates the ground state of the Hamiltonian H_1. More precisely, the error generated through this approximation scales as $\mathcal{O}\left(1/(\Delta_{\text{Min}} \cdot T)\right)$, where T is the total annealing time and Δ_{Min} is the minimum first energy gap of $H(t)$. This statement also clarifies the main limit of quantum annealing: if the gap Δ_{Min} becomes exponentially small with the system size, this approach becomes inefficient. As a consequence, quantum phase transitions represent a major difficulty in implementing quantum annealing [123].

As a last step before introducing inverse annealing, let us analyze the degenerate case for the adiabatic theorem [166–168]. This will have a central role in our technique. The adiabatic theorem ensures that, for a sufficiently slow evolution of the Hamiltonian $H(t)$, if the manifold $\mathcal{M}_i(t)$ of degenerate eigenstates associated with the energy level $E_i(t)$ is slowly deformed, an initial state of $\mathcal{M}_i(t)$ will evolve remaining in $\mathcal{M}_i(t)$. Moreover, as predicted by Wilczek and Zee, for a large time the final system state converges to a well-defined adiabatic limit, which generally depends on the path $H(t)$ that connects H_0 to H_1. This dependence is encoded in a non-Abelian phase called Wilczek-Zee phase [166].

We can finally introduce the scheme of IQA, described in Figure 5.1. It consists in swapping the role of the state and the Hamiltonian in quantum annealing. Firstly, we select

a path of quantum states $|\psi(\vec{\lambda}(t))\rangle$, where $\vec{\lambda}$ is a vector of parameters. The initial state $|\psi(\vec{\lambda}(0))\rangle$ is chosen so that its (local) PPH is known. Then, we artificially define inverse dynamics, in which the state of the system determines the evolution of the Hamiltonian. These dynamics are chosen so that in the adiabatic limit, the initial PPH of $|\psi(\vec{\lambda}(0))\rangle$ evolves, remaining the instantaneous PPH of the state $|\psi(\vec{\lambda}(t))\rangle$. Thanks to IQA, one can start from an easy-to-compute PPH for $|\psi(\vec{\lambda}(0))\rangle$ and generate a hard-to-compute PPH for the states of the path $|\psi(\vec{\lambda})\rangle$, in analogy to the conventional quantum annealing. In the next sections, for the sake of simplicity, we choose a dynamics in which λ is a scalar function of time.

5.3 THE INVERSE DYNAMICS

Since there are no real-world dynamics in which the evolution of local Hamiltonians depends on the system state, in this section we are going to invent the inverse dynamics involved in the QIA process. We will search for l-local PPHs, intended as Hamiltonians with finite range l. Given a path of states, we will try to solve the inverse problem using different values of this range, to check if the range l of the obtained Hamiltonian is independent of the system size N. If this is the case, we have found a local PPH, and our method works. To this aim, we introduce the sets $\mathcal{L}^{(l)}$ of l-local interactions $L_i^{(l)}$. Clearly, if $l < l'$ then $\mathcal{L}^{(l)} \subset \mathcal{L}^{(l')}$. For example, in a spin system $\mathcal{L}^{(l)}$ can be defined as the set of all the l-spins Pauli strings.

In Section 3.2, we have shown that it is possible to reconstruct the couplings of a time-dependent l-local Hamiltonian by measuring the evolution of a set of l-local observables. This is done by solving a system of linear equations:

$$\partial_t \langle \psi(\lambda(t)))|L_i^{(l)}|\psi(\lambda(t)))\rangle = \sum_j K_{ij}^{(l)} h_j(t),$$

where

$$K_{ij}(\rho(t)) = \langle \psi(t)| - i[L_j^{(l)}, L_i^{(l)}|\psi(t)\rangle. \tag{5.1}$$

is the *commutator matrix* introduced in Refs. [2, 59, 70]. At this point, it is natural to ask whether the IQA can be obtained by taking the adiabatic limit of this system of equations. Unfortunately, this approach is impossible, as the previous equation is not a differential equation for the evolution of the Hamiltonian. If we consider the adiabatic limit $\dot{\vec{\lambda}} \to 0$ of the previous equation, we only obtain an arbitrary element from the kernel of the commutator matrix for each time t. As illustrated in Chapters 2 and 3, these elements correspond to the coupling of generic local symmetries, having the state $|\psi(t)\rangle$ as an eigenstate [59], but not as a ground state.

To perform the IQA, one has to artificially define a differential equation for the evolution of local Hamiltonians depending on the state $|\psi(\lambda(t)))\rangle$, with $t \in [0, T]$. This equation must satisfy the following condition: if $h_i(0)$ define a PPH for $|\psi(\lambda(0))\rangle$, in the adiabatic limit $T \to \infty$ $h_i(\lambda)$ must be the couplings of a PPH for $|\psi(\lambda)\rangle$. Any equation that satisfies these requests is suitable for IQA.

We propose the following evolution:

$$\partial_t H = -i[|\psi(\lambda(t))\rangle\langle\psi(\lambda(t))|, H]. \tag{5.2}$$

This is a Schrodinger-like equation where the role of the Hamiltonian and the state density matrix have been swapped. This equation does not represent any physically realized evolution, hence we can use dimensionless energy and time. We to study the adiabatic regime of Eq. 5.2, showing that, if the initial Hamiltonian is a PPH for $|\psi(\lambda(0))\rangle$, this dynamics generates a Hermitian operator $H(\lambda)$ having $|\psi(\lambda)\rangle$ as a ground state. Moreover, when $|\psi(\lambda)\rangle$ has a correlation length that does not depend on the system size, $H(\lambda)$ is a local Hamiltonian.

The adiabatic solution of Eq, (5.2) also is stationary, implying that $\partial_t H$ has to be null. The stationary solutions of Eq. (5.2) form a degenerate vector space, which contains all the Hermitian operators having $|\psi(\lambda)\rangle$ as an eigenstate. The space of stationary solutions also is the degenerate kernel of the linear super-operator $H \to -i[|\psi(\lambda(t))\rangle\langle\psi(\lambda(t))|, H]$ that generates the evolution, therefore we must refer to the degenerate adiabatic theory. In this setting, the existence of a well-defined adiabatic limit is ensured by the Wilczek-Zee theory [166], which also shows that this limit depends on the path $|\psi(\lambda)\rangle$.

Now, we investigate the adiabatic solution of Eq. (5.2) and its dependence on the chosen path $|\psi(\lambda)\rangle$. As prescribed by the IQA procedure, the initial Hamiltonian is chosen to have $|\psi(0)\rangle$ as the ground state. The evolution under exam is unitary, therefore $H(t)$ is isospectral to $H(0)$, and each eigenstate $|\psi_i(t)\rangle$ of $H(t)$ changes in time evolved by the "Hamiltonian"

$$\Pi(\lambda(t)) \equiv |\psi(\lambda(t))\rangle\langle\psi(\lambda(t))|.$$

Consequently, the time-dependent Hamiltonian is

$$H(t) = \sum_i E_i \mathcal{T}(e^{-i\int_0^t dt' \Pi(\lambda(t'))})|\psi_i(t)\rangle\langle\psi_i(t)|\mathcal{T}(e^{-i\int_0^t dt' \Pi(\lambda(t'))})^\dagger,$$

where the E_i's are the eigenvalues of $H(0)$ and $|\psi_0(0)\rangle = |\psi(\lambda(0))\rangle$. Hence, the ground state of $H(t)$ is $\mathcal{T}(e^{-i\int_0^t dt' \Pi(\lambda(t'))})|\psi(\lambda(0))\rangle$, and $|\psi(\lambda(t))\rangle$ is a gapped eigenstate for $\Pi(\lambda(t))$ with energy gap $\Delta = 1$. Therefore, for the adiabatic theorem, when λ changes slowly in time,

$$\mathcal{T}(e^{-i\int_0^t dt' \Pi(\lambda(t'))})|\psi(\lambda(0))\rangle = e^{i\omega(t)}|\psi(\lambda)\rangle + \mathcal{O}(\dot{\lambda}/\Delta), \tag{5.3}$$

where $\omega(t)$ is a phase factor. In words, in the adiabatic regime, the ground state of the Hermitian operator $H(t)$ approximates the target state $|\psi(\lambda)\rangle$ with an error that becomes negligible when $T >> \Delta = 1$. This happens independently of the specific path of states because $|\psi(\lambda)\rangle$ is a non-degenerate eigenstate for $\Pi(\lambda)$. Differently, since the other eigenstates of $\Pi(\lambda)$ are degenerate, the excited states of $H(\lambda)$ depend on the adiabatic path. This dependence comes from the degeneracy of the kernel of the super-operator $H \to -i[|\psi(\lambda(t))\rangle\langle\psi(\lambda(t))|, H]$, and reflects the non-Abelian behavior of the Wilczek-Zee phase.

We have shown that, in the adiabatic limit, $H(t)$ has $|\psi(\lambda(t))\rangle$ as a ground state. However, for $H(t)$ to be a PPH, the adiabatic evolution generated by Eq. (5.2) has to preserve locality. We are going to show that this request is satisfied depending on the correlation length r of the states $|\psi(\lambda(t))\rangle$. This is defined as the value such that any connected correlation function of local observables $\langle\psi(\lambda(t))|AB|\psi(\lambda(t))\rangle - \langle\psi(\lambda(t))|A|\psi(\lambda(t))\rangle\langle\psi(\lambda(t))|B|\psi(\lambda(t))\rangle$ decays exponentially as $e^{-d(AB)/r}$, where $d(AB)$ is the distance between the sites on which A and B act. The key fact here is that, excluding fine-tuned exceptions [169–172], the ground state correlation length of an effectively l-local Hamiltonian is expected to be larger to or equal than l. We call *effectively* l-local a Hamiltonian whose interactions decay as faster than or equal to $e^{-|i-j|/l}$, and therefore is well approximated by a l-local Hamiltonian. As $|\psi(\lambda)\rangle$ is the ground state of the adiabatic solution $H(\lambda)$ of Eq. (5.2), the latter has to be a local Hamiltonian when $|\psi(\lambda)\rangle$ has finite correlation length. We can conclude that Eq. (5.2) is suitable for IQA, since it generates a local PPH in the adiabatic limit, at least for states with finite correlation length.

5.4 IMPLEMENTING THE IQA

To implement IQA, we need to solve Eq. (5.2) in the adiabatic limit. This equation is a quantum evolution, involving operators on the Hilbert space that can be represented using an exponentially large amount of (classical) memory. As a consequence, we are not capable of exactly integrating it for large systems with a classical computer.

We propose a possible implementation of the IQA, which consists of approximating the adiabatic solution of Eq. (5.2) through a time-dependent variational principle (TDVP) [111, 112]. Indeed, when $|\psi(\lambda)\rangle$ does not include critical states, $H(t)$ is local at each time t in the adiabatic limit, and we can project the evolution on the space of l-local Hamiltonians. This yields a negligible error until the range r of the non-projected evolution is less than l.

The TDVP consists of a dynamics for the couplings of the l-local Hamiltonian, obtained by projecting the RSH of Eq. (5.2) on this space through the Hilbert-Schmidt product. This is the natural Euclidean structure in the space of Hermitian operators, and allows defining a notion of *nearest approximation*. In particular, we approximate Eq. (5.2) by projecting the generated infinitesimal evolution on the closest infinitesimal evolution that preserves locality. The latter is spanned by the elements of $\mathcal{L}^{(l)} = \{L_i^{(l)}\}$, and we exploit the trace distance $d(A,B) \equiv \sqrt{\mathrm{Tr}\left[(A-B)^2\right]}$ to define the closest vector.

The resulting evolution is

$$\partial_t H = P(-i[|\psi(\lambda(t))\rangle\langle\psi(\lambda(t))|, H]), \tag{5.4}$$

where the projector $P(dH)$ is defined as

$$P(dH) = \mathrm{Argmin}_{dX=\sum_i d_i L_i^{(l)}} \mathrm{Tr}\left[(dX - dH)^2\right].$$

The explicit form of $P(dH)$ can be can be found imposing the nullity of derivatives:

$$\begin{aligned}\frac{\partial}{\partial d_i}\operatorname{Tr}\left[(dX-dH)^2\right] &= \frac{\partial}{\partial d_i}\left[\sum_{ij} d_i d_j \operatorname{Tr}(L_i^{(l)}L_j^{(l)}) - 2\sum_i d_i \operatorname{Tr}(L_i^{(l)}dH) + \operatorname{Tr}(dH^2)\right] \\ &= 2\sum_j d_j \operatorname{Tr}(L_i^{(l)}L_j^{(l)}) - 2\operatorname{Tr}(L_i^{(l)}dH) \\ &= 0.\end{aligned}$$

This leads to $d_i^{\text{Min}} = \sum_{ij}[(\operatorname{Tr}(L_j^{(l)}L_i^{(l)})]^{-1}\operatorname{Tr}(L_j^{(l)}dH)$ and, therefore,

$$P(dH) = \sum_{ij} d_i^{\text{Min}} L_i^{(l)} = \sum_i \left(\operatorname{Tr}(L_j^{(l)}L_i^{(l)})\right)^{-1}\operatorname{Tr}(L_j^{(l)}dH)L_i^{(l)}.$$

At this point, we impose without loss of generality that $\mathcal{L}^{(l)}$ is an orthogonal basis normalized to some constant Z, that is, $\operatorname{Tr}(L_i^{(l)}L_j^{(l)}) = Z\delta_{ij}$. Under this condition, the last equation becomes

$$P(dH) = \sum_i \frac{\operatorname{Tr}(dHL_i^{(l)})}{Z}L_i^{(l)}. \tag{5.5}$$

Replacing Eq. (5.5) in Eq. (5.4), we obtain

$$\partial_t H = \sum_i \frac{\operatorname{Tr}(-i[|\psi(\lambda(t))\rangle\langle\psi(\lambda(t))|, H]L_i^{(l)})}{Z}L_i^{(l)},$$

and, considering $H(t) = \sum_i h_i(t)L_i^{(l)}$, the corresponding equation for the Hamiltonian couplings is

$$\begin{aligned}\partial_t h_i(t) &= \sum_j \frac{\operatorname{Tr}(-i[|\psi(\lambda(t))\rangle\langle\psi(\lambda(t))|, L_j^{(l)}]L_i^{(l)})}{Z}h_j(t) \\ &= \sum_j \frac{\langle\psi(\lambda(t))| - i[L_j^{(l)}, L_i^{(l)}]|\psi(\lambda(t))\rangle}{Z}h_j(t).\end{aligned}$$

We are interested only in the adiabatic behavior of this equation. If we rescale the RHS by removing the factor Z at the denominator, this limit does not change. Therefore, the last equation is adiabatically equivalent to the following dynamics for the Hamiltonian couplings:

$$\partial_t h_i(t) = \sum_j K_{ij}\left(\psi(\lambda(t))\right)h_j(t), \tag{5.6}$$

where, remarkably, $K_{ij}^{(l)}$ is the *commutators matrix* in Eq. (5.1). We call the adiabatic solution of this equation *adiabatic Hamiltonian*.

Eq. (5.1) defines a suitable implementation of the inverse annealing. Indeed, when the path of states $|\psi(\lambda)\rangle$ does not cross any phase transition, the computational effort required to integrate Eq. (5.6) does not depend on the system size. This is because the entries of the commutator matrix are the expectation values of local observables, showing non-

analyticities only at phase transitions and converging for large systems. Remarkably, this also implies that the IQA allows to reconstruct a local PPH by knowing only the local expectation values.

As shown in Chapter 2 of this thesis, the kernel of the commutator matrix has been exploited in previous literature to reconstruct local Hamiltonians from their eigenstates [59]. Indeed, it contains all the local symmetries of a state. The IQA, when implemented through Eq. (5.6), selects an element from this kernel, whose features depend on the correlation length r of the states of the path $|\psi(\lambda)\rangle$. When the interaction range l is larger than r, the TDVP provides a good approximation of Eq. (5.2) and the dynamics generated by $K_{ij}^{(l)}$ adiabatically converges to a l-local PH. In other words, finding the adiabatic limit of Eq. (5.6) is a way to select a PPH among the symmetries without explicit diagonalization. This is no more the case if, for some values of $\lambda = \lambda_c$, l is smaller than r. In this case the TDVP fails in approximating Eq. (5.2), and for any $\lambda > \lambda_c$ we have a pathological regime in which there is no guarantee of the adiabatic solution of being a PH.

5.5 IQA WITH GAUSSIAN STATES

In this section, we test the IQA through a practical example. To this aim, we select a path of target states $|\Psi(\lambda)\rangle$ and integrate Eq. 5.6 to the adiabatic limit to find the adiabatic Hamiltonian $H(\lambda)$. Then, we verify that the ground state of the adiabatic Hamiltonian $H(\lambda)$ well approximates the state $|\Psi(\lambda)\rangle$. This verification requires the diagonalization of $H(\lambda)$. As a result, even if Eq. 5.6 can be integrated efficiently, in general verifying the IQA is impractical for large systems. To overcome this obstacle, here we work with quadratic Hamiltonians. Indeed, quadratic Hamiltonians can be efficiently represented and diagonalized, and their ground states are Gaussian states. In a Gaussian state, all the expectation values can be calculated from 2-bodies correlation functions thanks to the Wick theorem, allowing for an efficient representation.

We indicate as $c_n^{(\dagger)}$ the creation operator of a spinless fermion on the lattice site n. For simplicity, we consider a translationally invariant fermions chain with anti-periodic boundary conditions. Imposing this constraint, a basis $\mathcal{L}^{(l)}$ of l-local quadratic fermions interactions is

$$\mathcal{L}^{(l<N/2)} \equiv \{\Sigma_0^Z/\sqrt{2}, \Sigma_1^X, \Sigma_1^Y, \Sigma_1^Z, \ldots, \Sigma_{l-1}^X, \Sigma_{l-1}^Y, \Sigma_{l-1}^Z\},$$

and

$$\mathcal{L}^{(N/2)} \equiv \mathcal{L}^{(N/2-1)} \cup \{\Sigma_{N/2}^X/\sqrt{2}, \Sigma_{N/2}^Y/\sqrt{2}\},$$

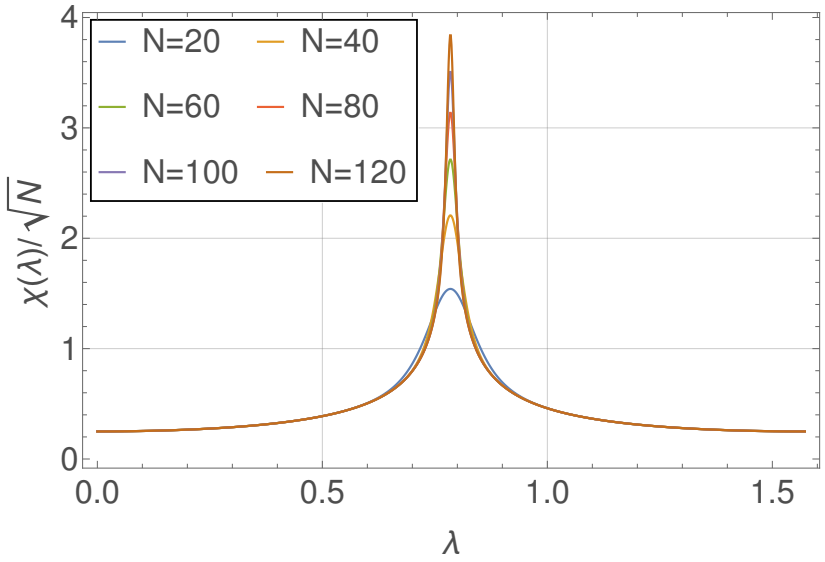

Figure 5.2: Scaling of the rescaled susceptibility $\chi(\lambda)/\sqrt{N}$ on the states $|\Psi(\lambda)\rangle$.

where

$$\Sigma_m^X = \frac{1}{2}\sum_{n=1}^{N}\left(c_n^\dagger c_{n+m}^\dagger - c_n c_{n+m}\right)$$
$$\Sigma_m^Y = \frac{i}{2}\sum_{n=1}^{N}\left(c_n^\dagger c_{n+m}^\dagger + c_n c_{n+m}\right)$$
$$\Sigma_m^Z = \frac{1}{2}\sum_{n=1}^{N}\left(c_n^\dagger c_{n+m} - c_n c_{n+m}^\dagger\right)$$

where the anti-periodic boundary conditions imply $c_{N+m} \equiv -c_m$. This is an orthogonal and normalized basis, as shown in Appendix C. Note that the basis $\mathcal{L}^{(N/2)}$ spans over the space of all translation-invariant quadratic fermionic Hamiltonians with anti-periodic boundary conditions. In this way, the evolution generated by Eq. (5.6) for $l = N/2$ is equivalent to the non-projected evolution in Eq. (5.2). Given an interaction range l, the commutator matrix that generates the IQA is explicitly calculated in Appendix C for an arbitrary Gaussian state. In Appendix D we show that, thanks to the Jordan-Wigner transformations [124], all the operators in $\mathcal{L}^{(l)}$ are equivalent to a large set of spin strings, that spans over a large space of Hamiltonians containing several important physical models such as the Ising model in transverse field [125], the XY model [126] and some cluster Hamiltonians [173]. As a consequence, the approach and the results of this section can be extended identically to a large class of spins systems.

As a paradigmatic example, here we consider the path of states $|\Psi(\lambda)\rangle$ defined as the ground states of the 1D Kiteav model [174].

$$H^{\mathrm{K}}(\lambda) = J\Big[\sin(\lambda)\sum_{n=1}^{N}\left(c_n^\dagger c_{n+1}^\dagger + c_n^\dagger c_{n+1} + \mathrm{h.c.}\right) + \cos(\lambda)\sum_{n=1}^{N}\left(c_n^\dagger c_n - c_n c_n^\dagger\right)\Big], \tag{5.7}$$

with anti-periodic boundary conditions $c_{N+1} = -c_1$, where J is an energy unit. The Kitaev model has a quantum phase transition from a topologically trivial phase to a topologically non-trivial phase at $\lambda = \lambda_c = \pi/4$. The topological phase is characterized by the presence of Majorana zero modes, which are a type of quasiparticles that are their anti-particles. It has potential applications in quantum computation: because of the presence of Majorana zero modes in the topological phase of the Kitaev model, it has been proposed as a platform for topological quantum computation, in which the Majorana zero modes can be used as a basis for a fault-tolerant quantum-bit. It is important to note that the Kitaev model is equivalent to the Ising model in transverse field, introduced in Chapter 3, through the Jordan-Wigner transformations [80].

We choose the path of states described by $|\Psi(\lambda)\rangle$ built as ground states of $H^K(\lambda)$ to be sure that we know that (at least) a 2-local PPH for these states exists (i.e. the one given by Eq. (5.7)). However, to perform the IQA we don't keep any information about the Kitaev Hamiltonian $H^{\mathrm{K}}(\lambda)$, but we only consider its ground states, whose density matrix is calculated in Appendix C in terms of the operators Σ^μ_m:

$$\Psi(\lambda) \equiv \bigotimes_{k\in\mathcal{K}^+} \left(v^x_k\tilde{\sigma}^x_k + v^y_k\tilde{\sigma}^y_k + v^z_k\tilde{\sigma}^z_k + \mathbb{1}\right)/2, \tag{5.8}$$

where

$$\begin{aligned}
\mathcal{K}^+ &\equiv \left\{k = \frac{(2n+1)\pi}{N},\ \text{with } n \in \{0, N-1\}\right\} \\
v^x_k &= -\sin(\lambda)\sin(k)/\sqrt{1+2\sin(\lambda)\cos(\lambda)\cos(k)} \\
v^y_k &= 0 \\
v^z_k &= -\left(\cos(\lambda)+\sin(\lambda)\cos(k)\right)/\sqrt{1+2\sin(\lambda)\cos(\lambda)\cos(k)} \\
\tilde{\sigma}^\mu_k &= \sum_{0\le m\le N/2} F^\mu(mk)\Sigma^\mu_m \\
F^\mu(x) &\equiv 2(\sin(x), \sin(x), \cos(x))/N,
\end{aligned}$$

and the $\tilde{\sigma}^\mu_k$ are the pseudo-spin operators introduced in Chapter 3.

We perform the IQA by numerically integrating Eq. 5.6 on the path $|\Psi(\lambda)\rangle$ to generate l-local PPHs. The annealing schedule is

$$\lambda(t) = \frac{t}{T}\frac{\pi}{2},$$

where T is the final time so that the state interpolates between $|\Psi(0)\rangle$ and $|\Psi(\pi/2)\rangle$. These are the initial and final state of the annealing process and belong respectively to two different quantum phases. We consider different annealing times T to study the convergence to the adiabatic limit, and we analyze different ranges l of the interactions in $\mathcal{L}^{(l)}$, and different system sizes N.

As anticipated, the path $|\Psi(\lambda)\rangle$ passes through a critical point at $\lambda_c = \pi/4$. Without any reference to the spectral behavior of the Kitaev Hamiltonian, we can detect this phase

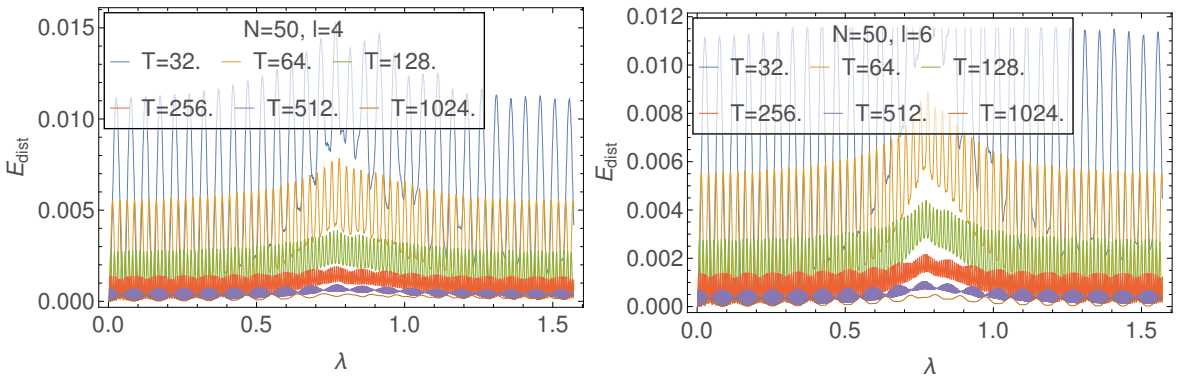

(a) (b)

Figure 5.3: Relative distance $E_{\text{dist}} = \|H_{(n)}(\lambda) - H_{(n-1)}(\lambda)\| / \|H_{(n)}(\lambda)\|$ between solutions of Eq. (5.6) with different annealing times, for a system of $N = 50$ sites and interaction range of the Hamiltonian $l = 4$ in Panel (a), $l = 6$ in Panel (b).

transition from the scaling of the infinitesimal Fubini–Study metric along the path $|\Psi(\lambda)\rangle$. This metric, that for a single parameter λ reduces to a scalar called susceptibility:

$$\chi(\lambda) = \lim_{d\lambda \to 0} \frac{|\langle \psi(\lambda) | \psi(\lambda + d\lambda) \rangle|}{d\lambda}$$

It encodes the reaction of the system to a small variation of the control parameters. It has been shown that for non-critical states, $\chi(\lambda)$ scales as $\sqrt{N}$, while for critical states it scales linearly in the system size N due to the diverging correlation length [117, 118]. This scaling captures the intuitive idea that, during a phase transition, a dramatic change occurs in the system with a very small change in the control parameters.

The scaling behavior of the susceptibility is depicted in Figure 5.2 for the states $|\Psi(\lambda)\rangle$, where the Fubini-Study length can be easily calculated thanks to the pseudo-spin representation in Eq. (C.22). Since at the critical point λ_c the correlation length of the state diverges, we can test our previous statement about the interaction range of the adiabatic Hamiltonian generated by Eq. 5.2 and about the regime in which the TDVP is a good approximation.

5.5.1 *Transition to the adiabatic regime*

Increasing the final time T, it is always possible to find an adiabatic solution for Eq. 5.6. If the approximations induced by the TDVP are negligible, the convergence to the adiabatic Hamiltonian implies the convergence to a PH. We expect that, for the path $|\Psi(\lambda)\rangle$, this is the case when $\lambda < \lambda_c$. In this subsection, we investigate the convergence to the adiabatic Hamiltonian, while the next subsection is devoted to highlighting the conditions in which this Hamiltonian is a PH.

In non-degenerate quantum annealing, the convergence to the adiabatic limit is usually investigated by looking at the fidelity between the evolved state and the ground state as a function of the annealing time. However, the IQA is based on degenerate quantum annealing. In this case, looking at the fidelity between the generated Hamiltonian and the

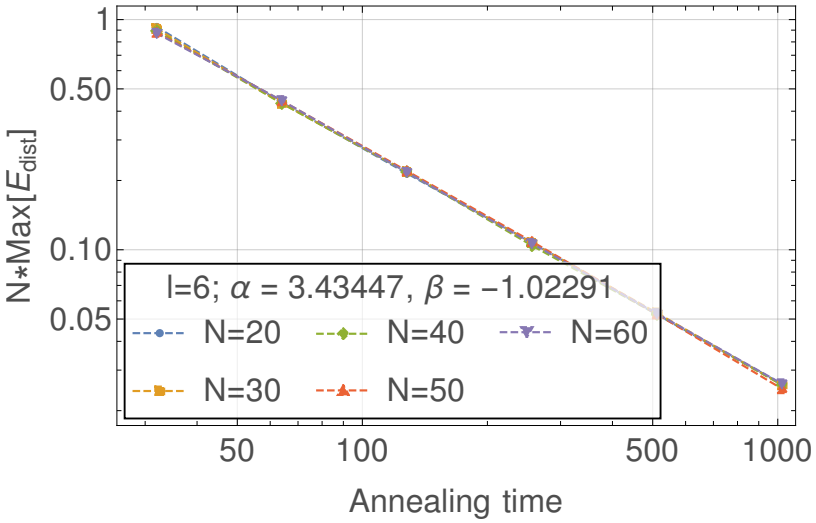

Figure 5.4: Maximum value of $N\mathrm{Max}_\lambda\,(E_{\mathrm{dist}})$, with interaction range of the Hamiltonian $l = 6$; α and β coefficients refer to the fit $\ln(N\mathrm{Max}(E_{\mathrm{dist}})) = \alpha + \beta \ln(T)$.

Kernel of the matrix $K_{ij}^{(l)}$ does not ensure the convergence, since this kernel is degenerate. Therefore, to assess the adiabaticity of the process, we calculate the distance between Hamiltonians $H_n(\lambda)$ found by IQA, at different final times T_n, where the T_n increase exponentially: $T_n = 2T_{n-1}$. In particular, we calculate the relative distance

$$E_{\mathrm{dist}} = \|H_{(n)}(\lambda) - H_{(n-1)}(\lambda)\| / \|H_{(n)}(\lambda)\|.$$

When the annealing time T_n is sufficiently large, the couplings $\{h_i\}$ converge to those of the adiabatic solution Hamiltonian, and E_{dist} goes to zero.

In Figure 5.3 (a) and (b), we show E_{dist} as a function of λ for different annealing times T_n for $l = 4$ and $l = 6$, respectively. We can see that the errors decrease by increasing T_n, however, for all T_n's a clear peak at the critical value of $\lambda = \lambda_c$ occurs. This peak is more pronounced for larger interaction range l.

In Figure 5.4 (c), we show the maximum value of E_{dist} rescaled by the system size, for different annealing times and system sizes. The functions $N \cdot \mathrm{Max}(E_{\mathrm{dist}})$ for different values of N overlap and fit to

$$\mathrm{Max}(E_{\mathrm{dist}}) \propto T^\beta / N,$$

where $\beta \approx -1$: the error is inversely proportional to the annealing time, as we expect from Eq. 5.3. The dependence on the system size is a consequence of the fact that the expectation values corresponding to the entries of the matrix $K_{ij}^{(l)}$ are linear N. This is not a significant physical effect, since it only depends on the definition of the basis $\mathcal{L}^{(l)}$, which contains extensive observables.

5.5.2 *Adiabatic Hamiltonian*

In this section, we analyze the adiabatic Hamiltonian obtained integrating Eq. (5.6) for different interaction ranges l. Our goal is to demonstrate the effectiveness of this approach

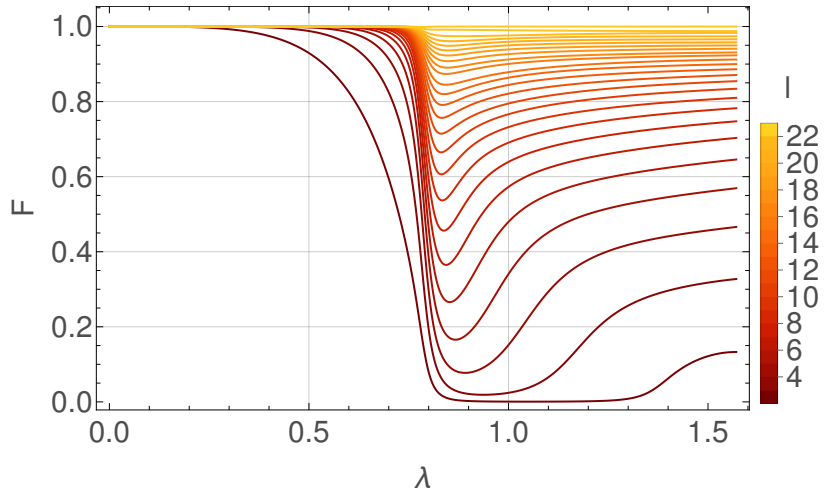

Figure 5.5: Fidelity between the target state $|\Psi(\lambda)\rangle$ and the ground state of the adiabatic l-local Hamiltonian, for a system of 50 sites.

in generating local PPHs. To ensure the adiabatic regime, we fix the annealing time at $T_{\text{adiab}} = 1024$. From Figure 5.4, we see that this choice satisfies the empirical criterion $\text{Max}(E_{\text{dist}}) << 1$.

In Figure 5.5, we plot the fidelity $F(\lambda) = |\langle\psi_{\text{GS}}(\lambda)|\Psi(\lambda)\rangle|^2$ between the target state $|\Psi(\lambda)\rangle$ and the unique ground state $|\psi_{\text{GS}}(\lambda)\rangle$ of the adiabatic l-local Hamiltonian $H(\lambda)$ obtained by IQA. We can observe two qualitatively different behaviors in the different ranges of λ. When $\lambda < \lambda_c = \pi/4$, before crossing the phase transition, the fidelity $F(\lambda)$ is close to one also for small values of l. This means that our algorithm finds an optimal l-local PPH for the target state.

The scenario drastically changes after the phase transition, when $\lambda > \lambda_c$. In this case, the long-range correlations of the critical point λ_c are hardly grasped by the adiabatic Hamiltonian, unless we include highly non-local interactions (corresponding to large values of l). As a consequence, for small values of l the fidelity $F(\lambda)$ drops down, and in order to recover a sizable fidelity, one has to resort to very large values of l. This happens despite the fact that the Kitaev Hamiltonian is 2-local. This behavior is reminiscent to the scaling of conventional quantum annealing that, as argued in Section 5.2, fails when a phase transition emerges at large system sizes [123].

A more quantitative analysis is obtained by looking at the fidelity as a function of l for different system sizes. If we restrict our target state to non-critical regions (i.e., $\lambda < \lambda_c$) the fidelity is quite large, even at small values of l, and almost independent of l. This can be clearly seen in Figure 5.6 (a), where the fidelity is calculated for a target state $|\psi(\lambda^-)\rangle$ close (but approaching the critical state from the left) to the critical state $|\psi(\lambda_c)\rangle$. By contrast, in Figure 5.6 (b), the fidelity is shown for a target state $|\psi\rangle(\lambda^+)$ close (but traversing the critical state). In this case, the larger is l the better is the fidelity as expected.

Given target accuracy ϵ, we can say that the l-local adiabatic Hamiltonian $H_l(\lambda)$ is an optimal PPH for $|\psi(\lambda)\rangle$ when the fidelity between $|\psi(\lambda)\rangle$ and the ground state $|\psi^{(l)}_{\text{GS}}(\lambda)\rangle$ of $H_l(\lambda)$, $F_l(\lambda) = |\langle\psi(\lambda)|\psi^{(l)}_{\text{GS}}(\lambda)\rangle|^2$ is larger than $1-\epsilon$. This automatically defines a minimal interaction range l_ϵ required to adiabatically find the PPH within the required accuracy ϵ.

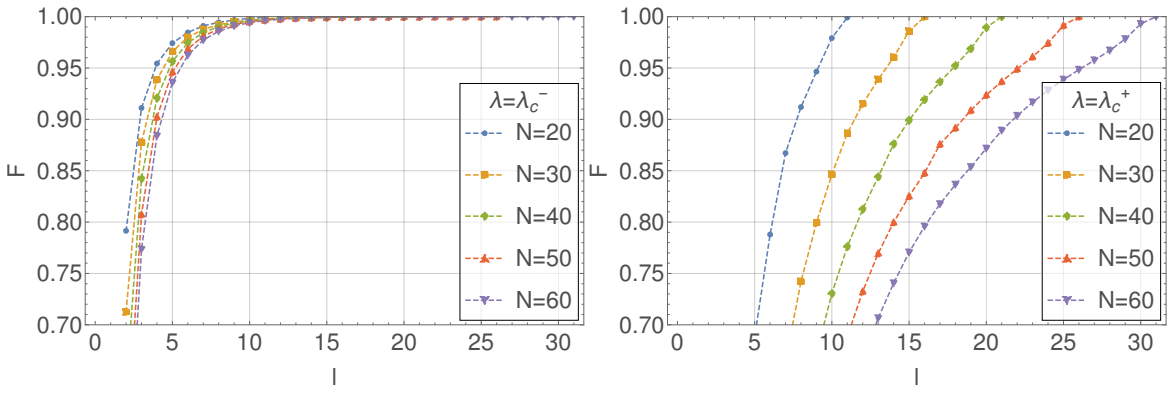

(a) (b)

Figure 5.6: Fidelity as a function of the interaction range l, for different system sizes N; in Panel a) at $\lambda^- = \lambda_c - \lambda_c/10$, in Panel b) at $\lambda^+ = \lambda_c + \lambda_c/10$.

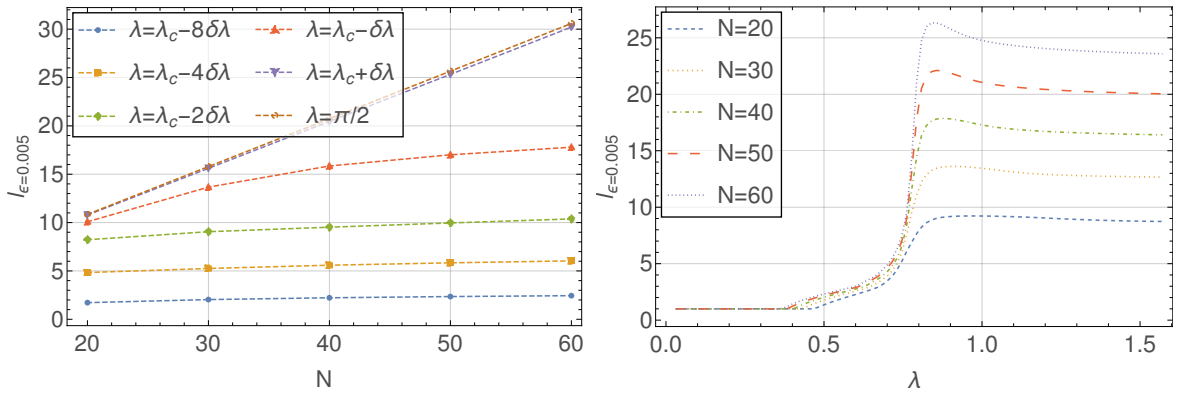

(a) (b)

Figure 5.7: Panel (a): l_ϵ as a function of the system size, for different values of λ. Panel (b): l_ϵ as a function of λ, for different system sizes.

In other words, for any given ϵ we can perform the IQA with larger and larger interaction range l, until we find the value l_ϵ of l such that the fidelity is

$$F_l(\lambda) \geq 1 - \epsilon \qquad \forall l \geq l_\epsilon \,.$$

The length l_ϵ is represented in Figure 5.7 (a) for $\epsilon = 0.005$ and different values of λ, before and after λ_c. In the first panel, for $\lambda < \lambda_c$, l_ϵ weakly depends on the system size: IQA is an efficient way to find a local PH. By contrast, after the critical point $\lambda > \lambda_c$, l_ϵ scales almost linearly in the system size. In other words, even if it is possible to find an adiabatic PPH, it is non-local and IQA fails in the thermodynamic limit. In Panel (b), we can observe how l_ϵ becomes definitely linear in the system size when approaching the critical point, in analogy with the correlation length of the states $|\Psi(\lambda)\rangle$.

The behavior observed in this section is a direct consequence of the TDVP: as previously argued, this approximation generates a negligible error until $|\Psi(\lambda)\rangle$ has a finite correlation length. In this case, the evolution in Eq. (5.2) preserves locality, as we show in the next section.

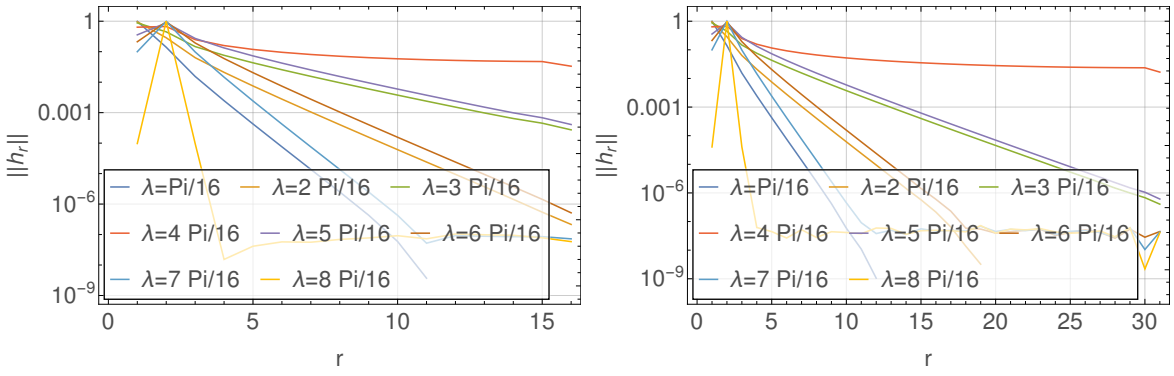

(a) (b)

Figure 5.8: Norm of the adiabatic Hamiltonian couplings of different ranges r, for various values of λ. In Panel (a) for $N = 30$ sites, and in Panel (b) for $N = 60$ sites.

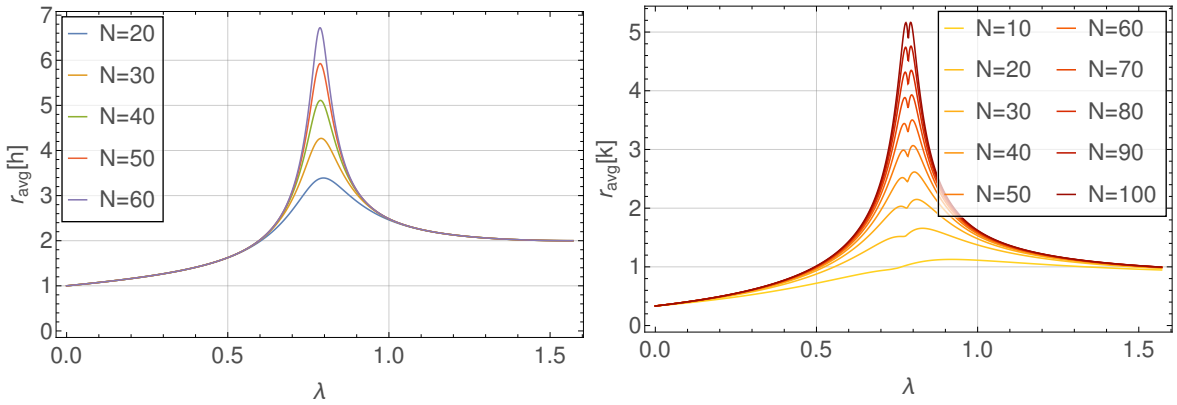

(a) (b)

Figure 5.9: Panel (a): effective interaction range of the non-projected adiabatic Hamiltonian. Panel (b): correlation range of $K_{ij}^{(N/2)}$.

5.5.3 *Non-projected adiabatic dynamics*

We have previously argued that the Hamiltonian evolution in Eq. (5.2) is a good candidate for IQA, since, in the adiabatic limit, it generates l-local PPHs for states with finite correlation length. In general, we can not numerically simulate this dynamics for large systems, and we resort to TDVP. This is not the case for Gaussian states. Hence, here we analyze its adiabatic solution of Eq. (5.2), which we call *non-projected* adiabatic Hamiltonian.

The non-projected adiabatic Hamiltonian corresponds to equation Eq. (5.6) for $l = N/2$. Indeed, Eq. (5.2) generates quadratic translation-invariant Hamiltonians. For these Hamiltonians $\mathcal{L}^{(N/2)}$ is a basis, and the projection of the TDVP acts as the identity. We know from Figure 5.5 ($l = N/2$) that the ground state of the non-projected adiabatic Hamiltonian exactly follows the target state $|\Psi(\lambda)\rangle$.

Here, we study the (effective) interaction range l of this Hamiltonian, to exemplify our previous statement about its relation with the correlation length of $|\Psi(\lambda)\rangle$. In Figure 5.8, we plot the total norm

$$\|h_r\| = \sqrt{\sum_{i:\text{range}(L_i^l)=r} h_i^2}$$

of the couplings of range r of this Hamiltonian at different values of λ, for a system of 30 and 60 sites. As predicted in Section 5.3, this norm exponentially decays with r for $\lambda \neq \lambda_c$, and the decay rate does not depend on the system size. We can confirm that Eq. (5.2) generates a local PPH, but only for non-critical states.

We can define an effective interaction range as

$$r_{\text{avg}}[h] \equiv \left(\sum_r r\|h_r\|\right) / \left(\sum_r \|h_r\|\right).$$

This range is represented in Figure 5.9 (a). We can see that, for sufficiently large N, it does not depend on the system size for non-critical states. However, it diverges linearly with the system size at $\lambda = \lambda_c$. This scaling is shared by the correlation length of $|\Psi(\lambda)\rangle$, and by the rescaled susceptibility in Figure 5.2.

To understand how the scaling behavior originated in the equation of motion, we look at the commutator matrix $K_{ij}^{(N/2)}$. We define a correlation range for this matrix

$$r_{\text{avg}}[k] \equiv \left(\sum_{i,j} |i-j||K_{ij}|\right) / \left(\sum_{ij} |K_{ij}|\right),$$

which measures the eventual exponential decay of non-diagonal elements. It is depicted in Figure 5.9 (b), and follows the same scaling behavior as the previously analyzed functions. We can conclude that, when the correlation length of states is finite, the non-projected dynamics weakly couples the local and non-local operators. Therefore, the Hamiltonian does not delocalize, allowing us to exploit the TDVP.

5.6 SUMMARY

Quantum annealing represents one of the major examples of the computational potential of quantum devices. Applications of this technique go far beyond condensed matter physics, allowing for an efficient solution to a large class of combinatorial optimization problems that are ubiquitous in everyday life, for example, the traveling salesman problem [80]. Analogously, reversing the perspective of quantum annealing could contribute to an equally large and important class of problems in science, mathematics, and engineering, i.e., the inverse problems. The capability of solving this kind of problem is indispensable for the inference of system parameters that can not be directly measured, and for the design of devices capable of implementing target classical and quantum states.

In this chapter, we defined an inverse quantum annealing technique for the reconstruction of PPHs, a task that in general is exponentially hard in the system size. It is based on

inverse dynamics for the Hamiltonian, generated by a path of target states, which in the adiabatic limit follows the PPHs of the target states. These Hamiltonians are guaranteed to be local for states with finite connected correlation lengths. The practical implementation of our method, based on a TDVP, allows for reconstructing local PPHs with a computational cost that weakly depends on the system size. Analogously to conventional quantum annealing, this approach fails at critical points.

In Section 5.5 we exemplified the functioning of the IQA on a path of Gaussian states. To ensure the existence of a local PPH, these have been chosen as the ground states of the Kitaev model. However, the extension to generic paths of Gaussian states is straightforward. In this context, we confirmed all the predictions about the strength and limits of our method. In the future, the next step could be testing the IQA on Tensor Network states.

Remarkably, our method only relies on the knowledge of local expectation values. This feature could be a precious ingredient for the application of IQA to the quantum marginal problem [84, 85]. For example, starting from local expectation values, one could look for PPHs through the IQA. Then, standard quantum annealing can be exploited to efficiently generate the target state and measure non-local expectation values.

In perspective, IQA raises two relevant questions. The first one is whether it is possible to design the path $|\psi(\lambda)\rangle$ towards a target state in a way that minimizes correlation lengths. Since the scaling Fubini-Study metrics are related to correlation lengths and quantum phase transitions [6, 117–120], the geodesics of this metric are a candidate solution to this problem. A second challenge consists of the direct implementation of Eq. 5.2 on a quantum annealer. This will result in an implementation of IQA capable of overcoming failure due to crossing critical states.

6

NON-STABILIZERNESS DYNAMICS IN MANY-BODY SYSTEMS

6.1 INTRODUCTION

Entanglement plays a fundamental role in defining the difference between classical and quantum systems at many levels. As shown by John Bell [175–178], entangled states are characterized by stronger correlation than classical states. This difference is so marked and significant that it has provided the basis for proving experimentally [179–181] that classical theories are not compatible with what we observe in nature [182]. Moreover, entanglement is a resource for quantum computational advantage, since it plays a fundamental role in quantum algorithms [9, 19, 132, 183–187]. The possibility of efficiently simulating slightly entangled systems through computational techniques such as Tensor Networks [88, 188] provides a further example of how entanglement determines the difference between classical and quantum physics. For all these reasons, entanglement has been widely studied in the context of many-body systems [189–191]. Also in the many-body inverse problem, it plays a fundamental role. Firstly, as motivation: since entanglement is a computational resource, being able to prepare PHs of entangled states helps us in quantum computation. But also as an obstacle, since for states with high entanglement it is harder to find local a PH, as seen in the Chapters 2 and 5.

Since we know that entanglement represents a fundamental resource for quantum computation, the question remains whether it is the only ingredient of the speed-up of quantum algorithms. One way to answer this question is to look at the simulatability of systems and wonder if there are highly entangled systems that can be simulated classically. The answer to this question is affirmative, and the key example is given by stabilizer states, defined as the common $+1$ eigenvector of a set of commuting Pauli operators. The Clifford group, generated by the Hadamard, S, and CNOT gates, transforms stabilizer states into stabilizer states. Remarkably, even if this group can generate states with the same entanglement entropy as random states [192], all the operations involving stabilizer states can be efficiently simulated [193]. Of course, the Clifford group cannot be used to generate universal quantum computation. To achieve this goal, it is necessary to add T gates to the group generators. In this sense, the number of T gates required to generate a state from stabilizer states can be considered as the second resource required, in addition to entanglement, to gain a quantum advantage. This resource has been called *non-stabilizerness*, or also *magic* [194–201].

Recently, the *stabilizer Rényi entropy* has been proposed amenable way of computing non-stabilizerness in many-body systems [198–201]. This quantity, based on the Rényi entropy associated with the decomposition of a state in the Pauli basis, has been also experimentally measured on a quantum processor [199]. The study of magic in many-body systems represents a fundamental goal, because it allows us to elaborate on the simulatability of these systems and their potential in the field of quantum computation, but also to study the interplay between non-stabilizerness and entanglement. For similar reasons to entanglement, non-stabilizerness also plays a fundamental role in the search for PHs. Firstly, the ability to construct PHs for non-stabilizer states allows us to implement them for quantum computation. Moreover, any stabilizer state is the unique ground state of a Hamiltonian defined simply as the negative sum of its stabilizer generators [202]. In this sense, just like entanglement, non-stabilizerness is a source of complexity for the inverse problem.

In this chapter, we study how non-stabilizerness evolves in many-body systems. Our goal is to understand how the Hamiltonians of these systems can be used as resources to dynamically generate non-stabilizerness, but also how this magic delocalizes over time. Indeed, in Refs. [203, 204] it has been shown that ground state magic is additive: taken sufficiently large subsystems, the total magic of the system is given by the sum of the magic of the subsystems. We could define this property as localization of magic. Corrections to this behavior characterize critical states, in analogy with corrections to area-law entanglement entropy [205], providing a first hint of the interplay between magic and entanglement at the origin of the unsimulability of quantum systems. During time evolution, entanglement ballistically spreads [206, 207]: the area law entanglement only affects subsystems that are larger than a size that increases linearly in time. We wonder if a similar delocalization process affects magic and if a ballistic spreading characterizes this process.

To achieve our goal, we focus our attention on the evolution generated by a quench of the transverse-field Ising model. However, our approach is suitable for the study of magic in any integrable spin system. Preliminarily, in Section 6.3 we analyze the behavior of the Loschmidt echo (LE) after a quench [208, 209], to be able to reconstruct the maximal group velocity of quasiparticles [210]. We also analyze subsystems' entropy and its time evolution, with particular attention to the ballistic growth of the entanglement length. At this point, we focus our attention on the non-stabilizerness dynamics. Firstly, in Section 6.4, we study how a T gate, responsible for non-stabilizerness, is delocalized after quenching the Hamiltonian. In Section 6.5, we study the time evolution of non-stabilizerness. In particular, we investigate how non-stabilizerness delocalizes during time evolution. Section 6.6 is devoted to summarizing our results.

6.2 NON-STABILIZERNESS OF INTEGRABLE SPIN CHAINS

As we show in Appendix D, a large class of integrable spin systems can be exactly simulated through a pseudo-spin formalism. In this formalism, Hamiltonians are written as non-interacting spins. As a consequence, their ground states are separable and the time-

evolution is efficiently calculated. Moreover, thanks to Wick's theorem, expectation values of Pauli strings can be calculated efficiently. Details of these calculations are illustrated in Appendix D. Once these expectation values are known, non-stabilizerness can be estimated through the stabilizer two Rényi entropy introduced in Ref. [199]:

$$\mathcal{M}_2(\rho) = -\log_2 \frac{\sum_{P\in\mathcal{P}} \mathrm{Tr}(\rho P)^4}{\sum_{P\in\mathcal{P}} \mathrm{Tr}(\rho P)^2}, \tag{6.1}$$

where $\mathcal{P}$ contains all the Pauli strings $\{\sigma_1^{\mu_1} \otimes \cdots \otimes \sigma_N^{\mu_N}\}$ acting on the whole system.

Analogously, the non-stabilizerness of any subsystem of size L is found by only measuring Pauli strings $\mathcal{P}_L = \{\sigma_1^{\mu_1} \otimes \cdots \otimes \sigma_L^{\mu_L}\}$ acting on the subsystem:

$$\mathcal{M}_2(\rho_L) = -\log_2 \frac{\sum_{P\in\mathcal{P}_L} \mathrm{Tr}(\rho P)^4}{\sum_{P\in\mathcal{P}_L} \mathrm{Tr}(\rho P)^2}. \tag{6.2}$$

Using this approach, magic can be evaluated for ground states of integrable spin chains, but also for time-dependent states under integrable dynamics. The principal computational obstacle is that, even if any Pauli string expectation value is efficiently calculated, the number of Pauli strings is exponential in the system size. In practice, this approach allows for evaluating the magic of systems of a few dozen of spins.

6.2.1 *Ground states non-stabilizerness*

In Ref. [203], exact diagonalization has been exploited to obtain a first investigation of non-stabilizerness in many-body systems. It consists of the study of two Rényi entropy of the Ising model ground states and their connected subsystems.

The one-dimension transverse-field Ising Hamiltonian has been previously introduced in Chapter 3 of this thesis. It reads:

$$H_{\mathrm{I}}(\lambda) = -\sum_n \left(\sigma_n^x \sigma_{n+1}^x + \lambda \sigma_n^z\right). \tag{6.3}$$

In pseudo-spin formalism, this Hamiltonian reads

$$H_{\mathrm{I}}(\lambda) = -\sum_{K\in\mathcal{K}^+} \epsilon_k(\lambda) \vec{v}_k(\lambda) \cdot \vec{\tilde{\sigma}}_k \tag{6.4}$$

where $\mathcal{K}^+ := \left\{k = \frac{(2n+1)\pi}{N}, \text{ with } n \in \{0, \ldots, N/2-1\}\right\}$ and

$$\begin{aligned}
\epsilon_k(\lambda) &:= 2\sqrt{\sin^2(k) + (\cos(k) - \lambda)^2} \\
\sin(\theta_k(\lambda)) &:= \sin(k)/\epsilon_k \\
\cos(\theta_k(\lambda)) &:= (\cos(k) - \lambda)/\epsilon_k \\
v_k^{\mu}(\lambda) &:= (\sin(\theta_k(\lambda)), 0, \cos(\theta_k(\lambda)).
\end{aligned}$$

The ground states are the separable ground states of a non-interacting spins Hamiltonian:

$$\rho(\lambda) = \bigotimes_{k\in\mathcal{K}^+} \left(\vec{v}_k(\lambda)\cdot\vec{\tilde{\sigma}}_k + \mathbb{1}\right)/2. \tag{6.5}$$

The main result of Ref. [203] is that the ground state magic is additive for non-critical states. Moreover, once the density of magic $\mathcal{M}_2(\rho_L)/L$ has been introduced, the relative error committed in approximating the non-stabilizerness density of a ground state as the sum of the non-stabilizerness density of subsystems of length L scales as $\mathcal{O}(1)$ for non-critical states, while it scales as $\mathcal{O}(L^{-1})$ for the critical state. This behavior suggests a link between the non-stabilizerness additivity and the area-law entanglement, which is affected by a logarithmic correction at critical states.

6.2.2 *Non-stabilizerness after a quantum quench*

There are two main reasons to study the dynamic properties of non-stabilizerness in many-body systems. The first reason is to understand if the Hamiltonians of these systems can be implemented to generate non-stabilizer states. Beyond the implications for the development of quantum algorithms, this investigation also provides an additional perspective on the study of quantum chaos. Indeed, in Refs. [198, 211, 212], it has been argued that quantum circuits capable of simulating chaotic systems must have a number of T gates larger than the system size N is the system size. Consequently, we expect that the study of the density of magic generated by a Hamiltonian should be able to distinguish between integrable systems and chaotic systems. In particular, integrable spin chains should generate a magic density $\mathcal{M}_2(\rho)/N < 1$, while non-integrable systems should produce more non-stabilizerness. The second reason is to investigate how the additivity of magic changes in time. This might also shed new light on the interplay between entanglement and magic, which are the two ingredients of quantum computational advantage.

We study the non-stabilizerness dynamics generated by the Ising Hamiltonian $H_{\rm I}(\lambda')$ acting on the ground state $\rho(\lambda)$ of $H_{\rm I}(\lambda)$. The Hamiltonian generates a rotation for each pseudo-spin as follows:

$$U(\lambda', t) = e^{-iH(\lambda')t} = \bigotimes_{K\in\mathcal{K}^+} e^{it\epsilon_k(\lambda')\vec{v}_k(\lambda')\cdot\vec{\tilde{\sigma}}}. \tag{6.6}$$

The effect of this rotation on the ground state $\rho(\lambda)$ of $H_{\rm I}(\lambda')$ can be calculated through the Rodrigues' rotation formula. This leads to the following evolution:

$$\rho(\lambda,\lambda',t) = U(\lambda',t)\rho(\lambda,\lambda',0)U(\lambda',-t) = \bigotimes_{K\in\mathcal{K}^+} \left(\vec{v}_k(\lambda,\lambda',t)\cdot\vec{\tilde{\sigma}}_k + \mathbb{1}\right)/2 \tag{6.7}$$

where

$$
\begin{aligned}
v_k^x(\lambda,\lambda',t) &= \cos(2t\epsilon_k')\sin(\theta_k) + (1-\cos(2t\epsilon_k'))\cos(\theta_k-\theta_k')\sin(\theta_k') \\
v_k^y(\lambda,\lambda',t) &= \sin(2t\epsilon_k')\sin(\theta_k-\theta_k') \\
v_k^z(\lambda,\lambda',t) &= \cos(2t\epsilon_k')\cos(\theta_k) + (1-\cos(2t\epsilon_k'))\cos(\theta_k-\theta_k')\cos(\theta_k')
\end{aligned}
$$

Here, we consider as the initial state the ground state corresponding to $\lambda \to \infty$. This is the state $|\uparrow \dots \uparrow\rangle$ of the computational basis, in which quantum computers are usually initialized. In the next sections, we study the evolution of this state after the Hamiltonian quench, with a focus on Loschmidt echo, subsystems' entropy, and subsystems' non-stabilizerness of the state $\rho(\lambda,\lambda',t)$.

6.3 LOSCHMIDT ECHO AND ENTANGLEMENT DYNAMICS

Before starting the investigation of magic dynamics, here we analyze the time scales that characterize evolution. Firstly, we look at the revival times. Revivals are brief detachments from the average value observables, whose magnitude decays in time as the equilibration process nears completion. During these detachments, the system state gets briefly closer to the initial state. Therefore, revivals can be detected by looking at the LE, that is, the squared fidelity between the evolved state and the initial state. The revival times are proportional to the system size, being related to maximal group velocity $v_{\max}$ of quasiparticles [210]. As shown in Ref. [210], this relation is also present in non-integrable local systems, where $v_{\max}$ generalizes into the Lieb-Robinson speed [213, 214]. We will see how this velocity affects many processes, from entanglement dynamics to the spreading of T gate.

Exploiting the pseudo-spin formalism, calculating the LE is straightforward:

$$
LE = \mathrm{Tr}(\rho(\lambda,\lambda',0)\rho(\lambda,\lambda',t)) = \prod_{k\in\mathcal{K}^+} \left(1+\vec{v}_k(\lambda,\lambda',t)\cdot\vec{v}_k(\lambda,\lambda',0)\right)/2. \tag{6.8}
$$

In Figure 6.1 we plot the LE evolution as a function of the rescaled time t/N, when the quench Hamiltonian $H_I(\lambda)$ evolves the initial state $|\uparrow \dots \uparrow\rangle$. We observe that the revival time is $T_{\mathrm{rev}} \approx N/4$ in the paramagnetic phase $\lambda > 1$, and $T_{\mathrm{rev}} \approx N/(\lambda 4)$ in the ferromagnetic phase $\lambda < 1$. Consequently, the associated velocity is $v_{\mathrm{rev}} = 4$ in the paramagnetic phase $\lambda > 1$, and $v_{\mathrm{rev}} = 4\lambda$ in the ferromagnetic phase $\lambda < 1$.

We can measure entanglement as the two Rényi entropy of entanglement $S_2(\rho_L) = -\log_2 \mathrm{Tr}(\rho_L^2)$ of the L spins connected subsystems ρ_L [189]. Since the Pauli strings in $\mathcal{P}$ are an orthogonal basis for the Hermitian operators and the purity $\mathrm{Tr}(\rho_L^2)$ is the squared norm of the operator ρ, the entanglement entropy can be written as a function of Pauli strings expectation values just like the non-stabilizerness:

$$
S_2 = L - \log_2 \sum_{P\in\mathcal{P}_L} \mathrm{Tr}(\rho P)^2. \tag{6.9}
$$

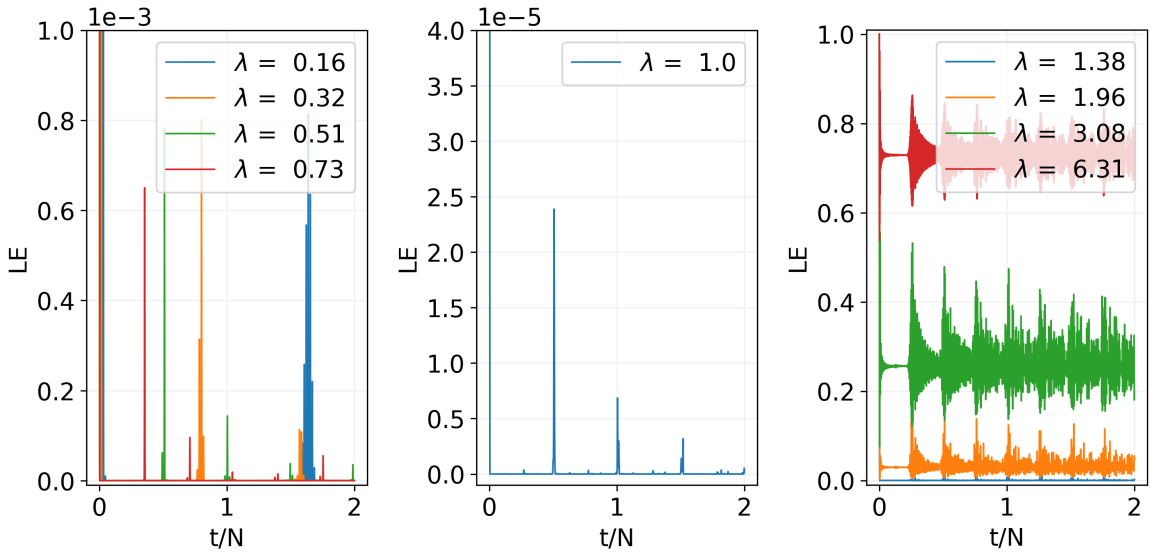

(a) (b) (c)

Figure 6.1: LE for a system of $N = 100$ spins and different values of the quench parameter. Panel (a) ferromagnetic phase, Panel (b) at the phase transition, Panel (c) paramagnetic phase.

In Figure 6.2 we plot the entanglement entropy of subsystems as a function of the time t, for a large number of spins ($N = 10000$). Different lines correspond to different subsystem sizes L. As shown in Ref. [206, 215], entanglement entropy increases in time after the quench until it reaches an equilibration value. Moreover, at any time t, we observe that a certain length $L_S(t)$ exists such that entanglement is linear in the system size (volume law) for subsystems smaller than $L_S(t)$, and independent of the system size (area law) for larger subsystems. We call $L_S(t)$ the *entanglement entropy length* (EEL) of the state. Investigating the dynamics of entanglement through the EEL is particularly convenient in our setting, since we can exploit a similar approach to define and investigate the delocalization of magic. The evolution of the EEL reflects the spreading of quantum correlations [90], since the exponential decay of correlations implies the area-law for the entanglement [216].

We define the EEL as a function of an error tolerance ϵ. Given the error tolerance ϵ, the state has EEL $L_S(\epsilon)$ when

$$\frac{|S_2(\rho_{N/2}) - S_2(\rho_L)|}{|S_2(\rho_{N/2})|} < \epsilon, \qquad \forall L \geq L_S(\epsilon). \tag{6.10}$$

Remarkably, the length L_S diverges for highly entangled states, whose subsystems density matrices ρ_L are the maximally mixed state with entropy L.

Due to limited computational resources, we can access only the entanglement of subsystems up to 16 spins. Therefore, to study the evolution of EEL, we analyze the behavior of the function $|S_2(L+1) - S_2(L)|$. In Figure 6.3 we observe the exponential decay of this function, which ensures the existence of a finite EEL. We estimate this length as the values of L such that $|S_2(L+1) - S_2(L)|$ is definitively upper-bounded by a tolerance ϵ. In this way, we can estimate how the EEL evolves with time for different values of the quench parameter λ. This evolution is depicted in Figure 6.4, where we observe that length in-

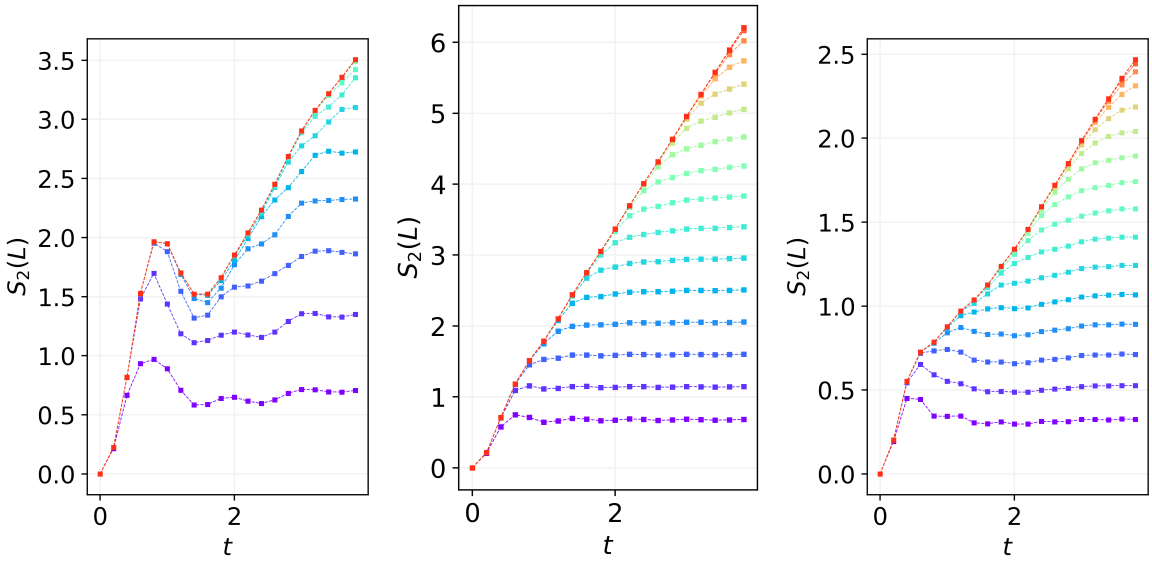

Figure 6.2: Evolution of the entanglement entropy of subsystems of sizes from $L = 1$ (purple lines) to $L = 16$ (red lines), for a system of $N = 10000$ spins. In Panel (a) $\lambda = 0.5$, in Panel (b) $\lambda = 1$, in Panel (c) $\lambda = 1.5$.

creases linearly in time as $L_S(t) \approx v(\lambda)t$. The speed $v(\lambda)$ is compatible with the revivals' velocity $v_{\text{rev}}(\lambda)$.

6.4 T SPREADING

As a first step towards the understanding of non-stabilizerness spreading, here we study how a T gate spreads out when evolved by the Hamiltonian $H_{\text{I}}(\lambda)$.

We consider a T gate acting on the spin $n = 0$ of the chain. This gate can be easily written in terms of pseudo-spins as follows:

$$T_n = \frac{1+e^{i\pi/4}}{2}\mathbb{1} + \frac{1-e^{i\pi/4}}{2}\sigma_0^z,$$
$$\sigma_0^z = \mathbb{1} - 2\frac{1}{N}\sum_k c_k^\dagger c_k = -\frac{2}{N}\sum_{k\in\mathcal{K}^+}\tilde{\sigma}_k^z.$$

Hence, the time evolution is

$$U^\dagger T_0 U = \frac{1+e^{i\pi/4}}{2}\mathbb{1} + \frac{1-e^{i\pi/4}}{2}U^\dagger\sigma_0^z U, \tag{6.11}$$

where

$$U^\dagger\sigma_0^z U = -\frac{2}{N}\sum_{k\in\mathcal{K}^+} U^\dagger\tilde{\sigma}_k^z U = -\frac{2}{N}\sum_{k\in\mathcal{K}^+}\vec{v}_k(-\infty,\lambda,t)\cdot\vec{\tilde{\sigma}}_k. \tag{6.12}$$

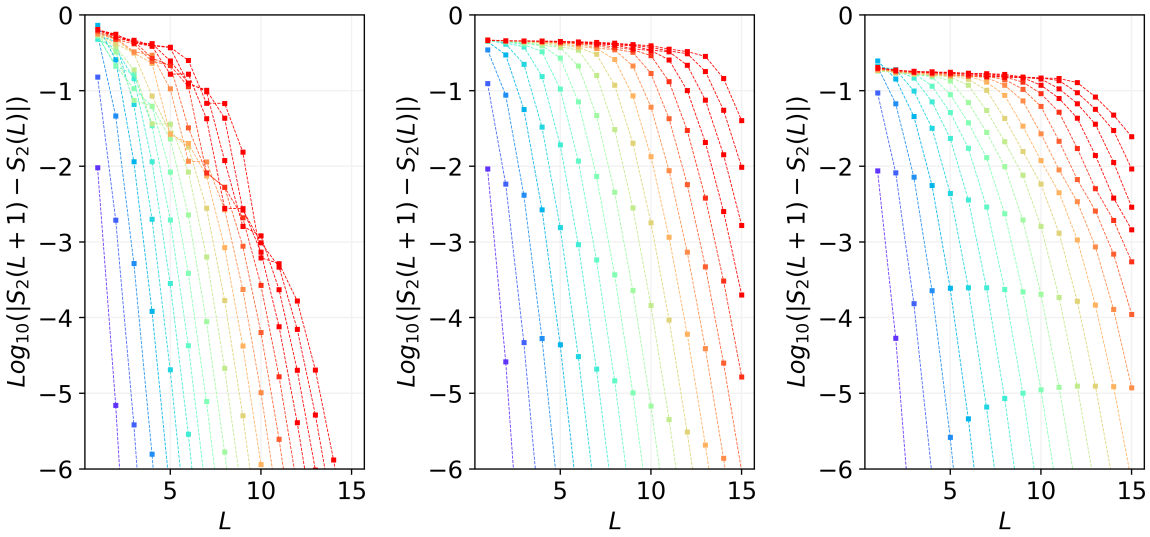

Figure 6.3: Logarithmic difference between the entanglement entropy of subsystems of sizes L and $L+1$, at different times for a system of $N = 10000$ spins. Time goes from 0 (purple lines) to 3.8 (red lines). In Panel (a) $\lambda = 0.5$, in Panel (b) $\lambda = 1$, in Panel (c) $\lambda = 1.5$.

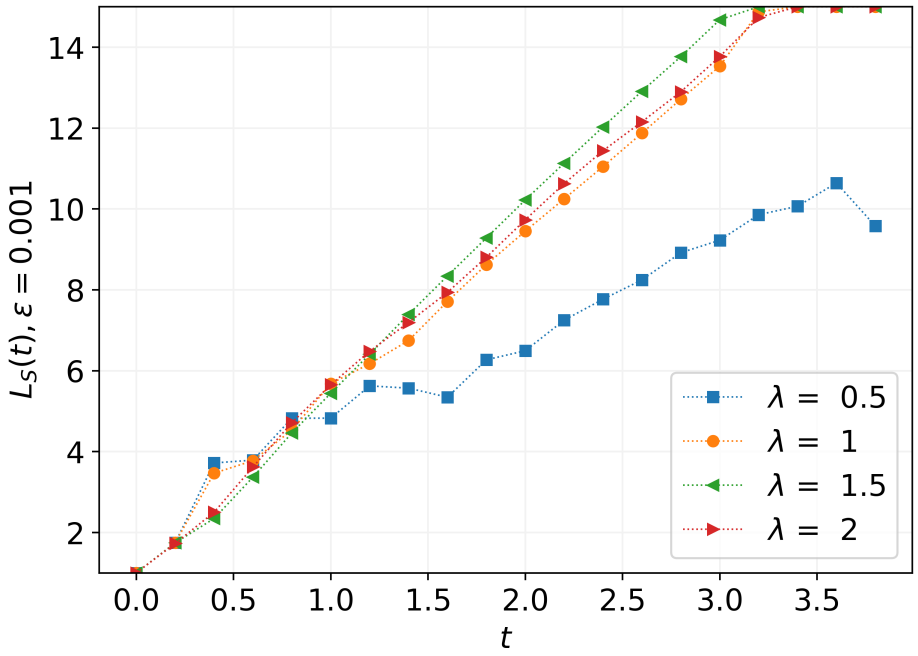

Figure 6.4: Evolution of the EEL for different values of the quench parameter λ, for a system of $N = 10000$ spins.

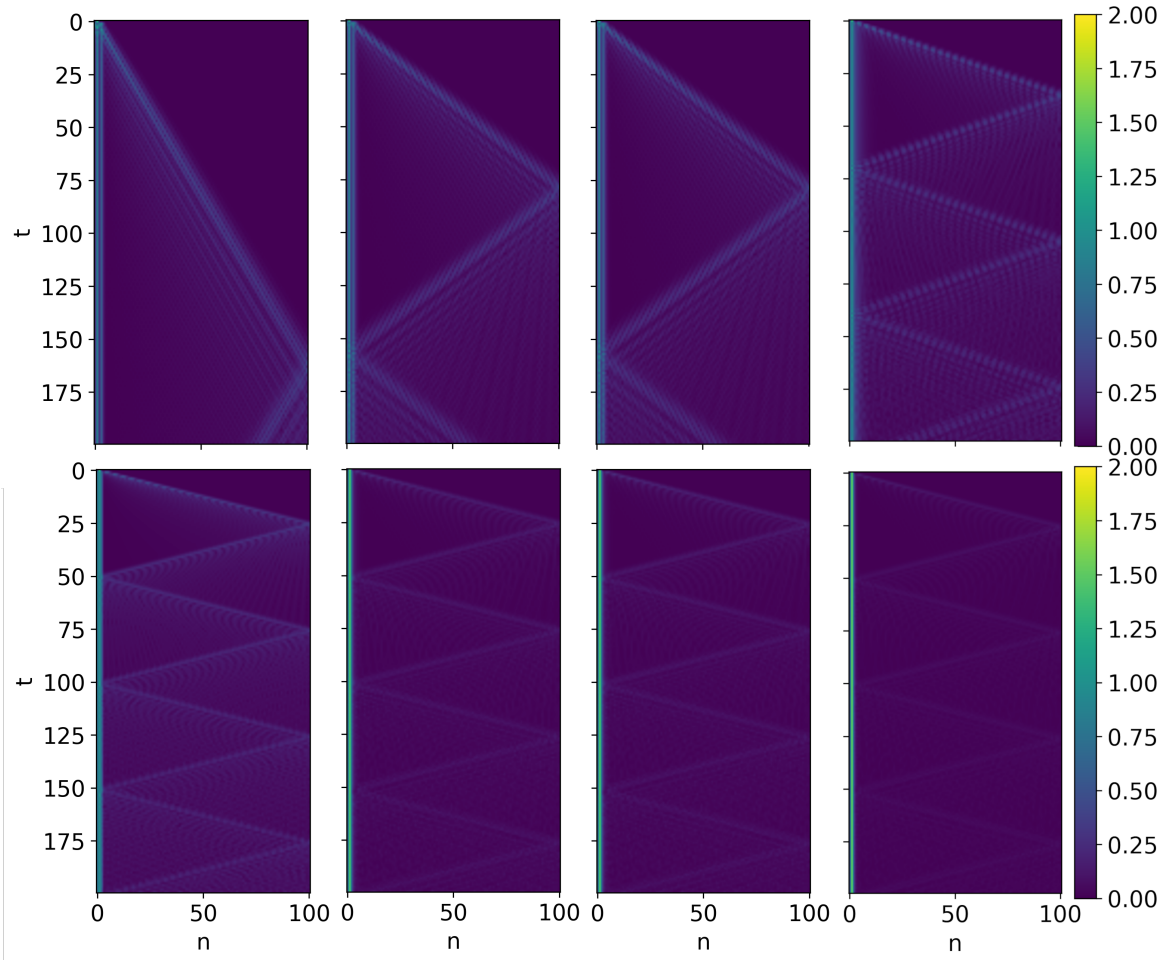

Figure 6.5: Weight of the Pauli strings of lenght m in the evolved T gate, for different values of the quench parameter $\lambda \in \{0.16, 0.32, 0.51, 0.73, 1., 1.38, 1.96, 3.08]\}$, for a system of $N = 200$ spins.

Finally, exploiting the methods in Appendices C and D, we can write the pseudo-spins in terms of spins. Finally, we obtain the evolution of the non-trivial part of the T gate:

$$U^\dagger \sigma_0^z U = -\frac{2}{N} \sum_{k \in \mathcal{K}^+} U^\dagger \tilde{\sigma}_k^z U = -\frac{2}{N} \sum_{0 \leq m \leq N/2} S_m^\mu \left(\sum_{k \in \mathcal{K}^+} v_k^\mu(-\infty, \lambda, t) F^\mu(mk) \right), \tag{6.13}$$

where

$$\begin{aligned}
S_0^Z &= -\frac{1}{2} \sum_n^N \sigma_n^z \\
S_m^X &= \frac{1}{4} \sum_n^N \left(\sigma_n^x \sigma_{n+1}^z \dots \sigma_{n+m-1}^z \sigma_{n+m}^x - \sigma_n^y \sigma_{n+1}^z \dots \sigma_{n+m-1}^z \sigma_{n+m}^y \right) \\
S_m^Y &= \frac{1}{4} \sum_n^N \left(\sigma_n^x \sigma_{n+1}^z \dots \sigma_{n+m-1}^z \sigma_{n+m}^y + \sigma_n^y \sigma_{n+1}^z \dots \sigma_{n+m-1}^z \sigma_{n+m}^x \right) \\
S_m^Z &= \frac{1}{4} \sum_n^N \left(\sigma_n^x \sigma_{n+1}^z \dots \sigma_{n+m-1}^z \sigma_{n+m}^x + \sigma_n^y \sigma_{n+1}^z \dots \sigma_{n+m-1}^z \sigma_{n+m}^y \right).
\end{aligned} \tag{6.14}$$

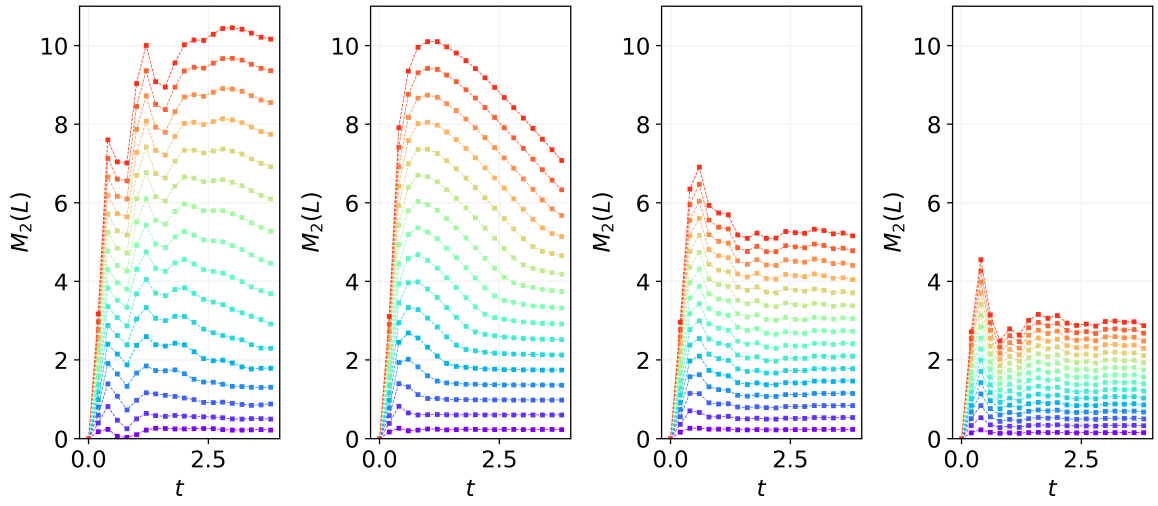

(a) (b) (c) (d)

Figure 6.6: Evolution of the non-stabilizerness of subsystems of sizes from $L = 1$ (purple lines) to $L = 16$ (red lines), for a system of $N = 10000$ spins. In Panel (a) $\lambda = 0.5$, in Panel (b) $\lambda = 1$, in Panel (c) $\lambda = 1.5$, in Panel (d) $\lambda = 2$.

The evolved T gate is the sum of Pauli strings acting non-trivially on connected blocks of n spins. For each value of n, we can look at the weight

$$d(n,t) = \sum_{\mu} \left[\left(\sum_{k \in \mathcal{K}^+} v_k^{\mu}(-\infty, \lambda, t) F^{\mu}(nk) \right)^2 \right] \tag{6.15}$$

of n-spins strings as a measure of delocalization of the T gate. The function $d(n,t)$ is depicted in Figure 6.5 for different values of λ. We observe that at each time strings of a given m^* length prevail in evolution. The function $m^*(t)$ is linear in time, i.e. $m^*(t) = vt$. The velocity v is compatible with the speed v_{rev} that characterizes the revivals time and the entanglement spreading.

6.5 NON-STABILIZERNESS DYNAMICS

In this section, we investigate the evolution of non-stabilizerness of the initial state $|\psi\rangle = |\uparrow \dots \uparrow\rangle$ with the quench Hamiltonian $H_{\text{I}}(\lambda)$. We consider a large system of $N = 10000$ spins, and analyze how the non-stabilizerness of subsystems up to 16 spins evolves for different values of the quench parameters $\lambda \in \{0.5, 1, 1.5, 2\}$.

In Figure 6.6 we show the evolution of magic for the different subsystems. We can observe that non-stabilzerness rapidly increases after the quench, and then it equilibrates to a non-null value. The equilibrating time increases with the size of the subsystem under exam. At the end of the process, the amount of non-stabilizerness is maximized when the ferromagnetic contribution of the quench Hamiltonian prevails, that is, for small values of the quench parameter λ. As expected from the integrability of the model under exam, the density of magic remains smaller than one during the evolution, as depicted in Figure 6.7.

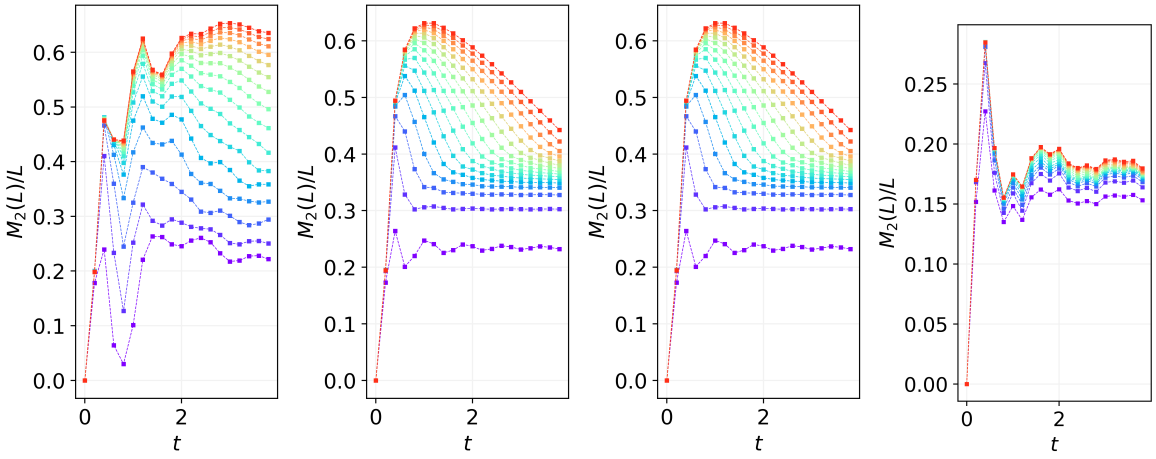

Figure 6.7: Evolution of the density of magic of subsystems of sizes from $L = 1$ (purple lines) to $L = 16$ (red lines), for a system of $N = 10000$ spins. In Panel (a) $\lambda = 0.5$, in Panel (b) $\lambda = 1$, in Panel (c) $\lambda = 1.5$, in Panel (d) $\lambda = 2$.

At a first look at Figues 6.6 and 6.7, the additivity seems to be preserved if we consider subsystems of size L, in a time interval that increases with L. In particular, at each time, the stabilizer Rényi entropy of the state is the sum of the stabilizer Rényi entropies of the subsystems larger than a given size L_M. We call this size *non-stabilizerness length*. Given an arbitrary small tolerance ϵ, we define the non-stabilizerness length as the subsystems size $L_M(\epsilon)$ such that

$$\frac{|\mathcal{M}_2(\rho)/N - \mathcal{M}_2(\rho_L)/L|}{|\mathcal{M}_2(\rho)/N|} < \epsilon, \qquad \forall L \geq L_M(\epsilon), \tag{6.16}$$

where $\mathcal{M}_2(\rho_L)$ the two Rényi entropy of a connected subsystem ρ_L of L spins.

In Section 6.3 we have seen that when the system evolves with the Hamiltonian $H_{\mathrm{I}}(\lambda)$, the EEL increases as $L_S(\lambda, t) = v(\lambda)t$, and $v(\lambda)$ is the speed of revivals. Now, we investigate the effect of time evolution on magic additivity. Looking at the non-stabilizerness length $L_M(t)$, we want to understand how magic delocalizes in time. To this aim, we look at the density of magic $\mathcal{M}_2(\rho_L(t))/L$. Indeed, based on Eq. 6.16, $L_M(t)$ can be defined as the length such that the density of magic is approximately constant for $L > L_M(t)$. We can apply the same approach of Section 6.3. Firstly, we look at the function $|\mathcal{M}_2(\rho_{L+1}(t))/(L+1) - \mathcal{M}_2(\rho_L(t))/L|$, depicted in Figure 6.8. If this function decreases exponentially, magic is additive. Then, in analogy with EEL, we estimate the non-stabilizerness length as the values of L such that $|\mathcal{M}_2(\rho_{L+1}(t))/(L+1) - \mathcal{M}_2(\rho_L(t))/L|$ is definitely smaller than a given tolerance ϵ.

Figure 6.8 suggests the expected exponential decrease for the function $|\mathcal{M}_2(\rho_{L+1}(t))/(L+1) - \mathcal{M}_2(\rho_L(t))/L|$, and therefore the robustness of magic additivity under time evolution. We also note that this decrease is slower than the one observed in Figure 6.9. In other words, non-stabilizerness spreads out faster than entanglement. As a consequence, estimating the behavior of $L_M(t)$ from small systems is harder. A first estimate is shown in Figure 6.9, where we observe that magic delocalizes at a finite speed,

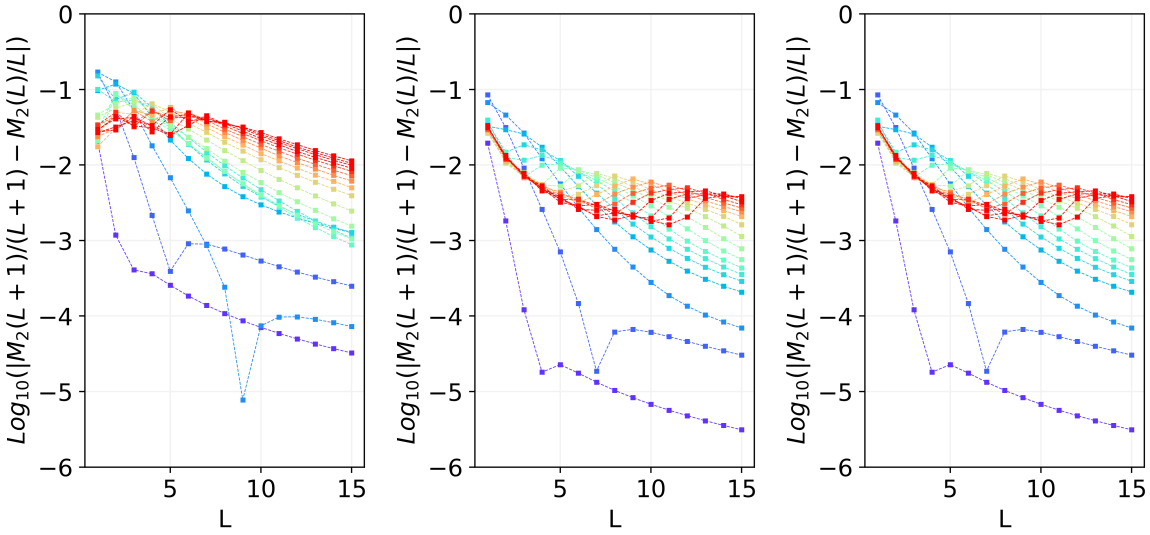

Figure 6.8: Logarithmic difference between the density of magic of subsystems of sizes L and $L+1$, at different times, for a system of $N = 10000$ spins. Times go from 0 (purple lines) to 3.8 (red lines). In Panel (a) $\lambda = 0.5$, in Panel (b) $\lambda = 1$, in Panel (c) $\lambda = 1.5$.

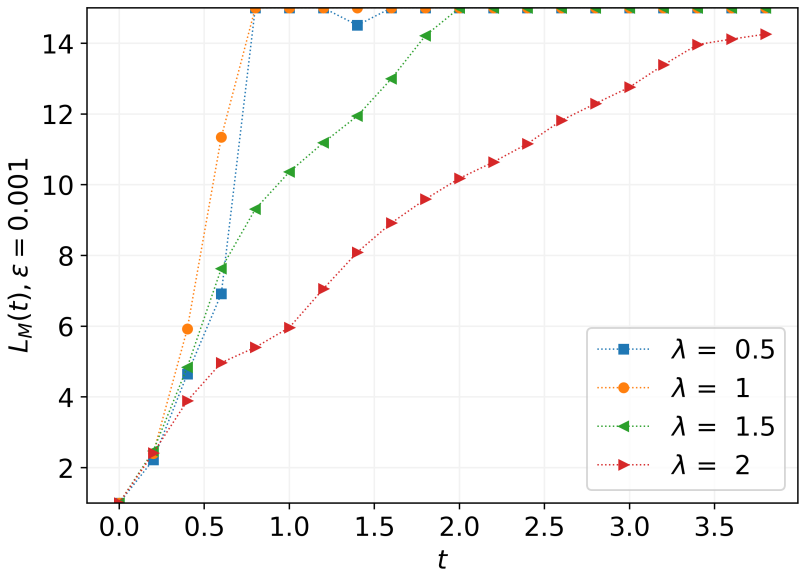

Figure 6.9: Evolution of the non-stabilizerness length for different values of the quench parameter λ, for a system of $N = 10000$ spins.

like entanglement. However, in both phases, this speed increases as the parameter λ decreases and the ferromagnetic term prevails.

6.6 SUMMARY

This chapter has been devoted to the study of the non-stabilizerness dynamics of an integrable spin chain. This investigation offers a novel point of view on the computational

power of many-body systems, and provides new tools for the investigation of the quantum chaos and of the spreading of quantum information.

We have investigated the evolution of a T gate, which is the source of non-stabilizerness. After the quantum quench, the T gate spreads over the system and is represented by the overlap of an increasing number of Pauli strings. The size of the leading term in this expansion increases linearly in time, and its speed is compatible with the maximum group velocity of quasiparticles.

We have shown that, after a quantum quench, the non-stabilizerness of subsystems increases towards a new equilibrium value, in analogy with entanglement entropy. During its evolution, the density of magic remains upper-bounded by one in the transverse field Ising model. This behavior is compatible with the integrability of the system, since a larger density of magic characterizes random states and signals a chaotic behavior [198].

We have also investigated the effect of time evolution on the additivity of magic. To analyze this effect, we have introduced a non-stabilizerness length, corresponding to the length of a connected subsystem whose density of magic well approximates the density of magic of the entire system. We have shown that the additivity of magic is preserved during the evolution, with a non-stabilizerness length that increases in time. This phenomenon is an example of magic delocalization. At a first analysis, the non-stabilizerness length evolves ballistically such as the length associated with entanglement entropy. However, the spreading of non-stabilizerness is faster than the spreading of entanglement.

The next step of this research consists in investigating the non-stabilizerness dynamics of a non-integrable system, for example, the Ising model in longitudinal field. Here, the production of a larger magic with respect to integrable spin chains would provide significant proof of the relationship between quantum chaos and non-stabilizerness [211] in the context of many-body systems.

7

CONCLUSIONS

In this thesis, we have addressed the inverse problem in many-body quantum systems [1]. This consists in the reconstruction of a many-body Hamiltonian given a quantum state. Such Hamiltonian must be realistic, i.e., it must satisfy the locality constraint, or has to be engineerable on a real quantum device. After introducing recent literature on the subject, we have focused our attention on our results about the inverse problem for time-dependent states [2–4].

Following Ref. [2], we began by analyzing the problem in its simplest form, which is finding a realistic generator for a given state evolution. We have shown how to seek an exact solution to the problem. In many cases, this exact solution is unrealistic, so we have introduced a cost function whose minimum defines an optimal generator for the target evolution. Defining the cost function in a space of Hamiltonians that can be implemented on a real device, this approach can be used to perform quantum state driving and Hamiltonian learning.

In this regard, we have analyzed how it is possible to perform Hamiltonian learning from measurements made on a single time-dependent state [3]. We have also analyzed the uncertainty that characterizes this reconstruction and its dependence on the evolution of the system. This has allowed us to prove that states with a lower inverse participation ratio in the eigenstates of the Hamiltonian minimize uncertainty in the inference process. In other words, ergodicity represents a resource for Hamiltonian learning. This result goes beyond our application to small-size systems and constitutes an important hint for the design of Hamiltonian learning algorithms that exploit the typical properties of many-body systems.

Finally, we have analyzed the adiabatic limit of the time-dependent inverse problem, with the goal of reconstructing a proper parent Hamiltonian for a certain path of quantum states [1]. To this end, we have defined an inverse quantum annealing process, swapping the role of the Hamiltonian and the state of the system in conventional quantum annealing. This new approach allows for an efficient reconstruction of the parent Hamiltonian for paths of states with finite correlation length. The efficiency of the proposed method, whose computational complexity weakly depends on the system size, allows its application to large-size systems and represents an important step forward for the state of the art on the inverse problem.

We have tested all the hypotheses and methods proposed through examples that are relevant on a technological level and paradigmatic for the study of many-body systems. Among these we have Hamiltonians describing realistic implementations of quantum

gates [148–151], and systems of interacting spins or fermions that exhibit phase transitions, such as the p-spin model [128–131], the Ising Hamiltonian in a transverse field [124], and the Kitaev model [174].

A dense network of connections with previous literature on parent Hamiltonians has been outlined, particularly regarding the role of the commutator matrix in the search for symmetries [56–61], optimal generators [2, 70, 71], and, finally, in the definition of inverse quantum annealing [4].

Our research has also intertwined with less directly related topics, such as the search for shortcuts to adiabaticity [100–109], the geometry of quantum information [6, 89, 114–120], and the quantum marginal problem [62, 84, 85]. We have shown how the search for solutions to the inverse problem can yield results equivalent to the search for shortcuts to adiabaticity through counterdiabatic potentials [110]. Additionally, we have seen that the Fubini-Study metric [89] plays a fundamental role in defining the effectiveness of the optimal generator in quantum state driving and that it may have a significant role in determining optimal paths for IQA. Finally, we have seen how the possibility and difficulty of reconstructing Hamiltonians from only local expectation values are related to the quantum marginal problem.

The last chapter of this thesis has been devoted to investigating the non-stabilizerness dynamics in the transverse field Ising model. We exploited the integrability of the model to estimate non-stabilizerness of subsystems of a large spin chain. We have measured the capability of the Hamiltonian under exam of generating this quantum resource, with a particular focus on how this capability is linked with the integrability of the model. We have also investigated the spreading of non-stabilizerness during the time evolution, measuring how T gate ballistically spread over larger spin strings, and how the additive behavior of non-stabilizerness changes over time. In particular, to estimate the non-stabilizerness of the entire system as the sum of non-stabilizerness of its subsystems, we have to consider increasingly larger subsystems. The next step in this research is to extend our consideration to a non-integrable spin chain. This would open a new perspective on the link between quantum chaos and simulability in many body-systems [211].

7.1 FUTURE PERSPECTIVES

In this work, we have had the opportunity to outline some future research perspectives. Here, we briefly analyze those that seem the most significant and fruitful.

7.1.1 *Accessibility*

In Chapter 4, we have introduced the *accessibility* of a path of states. It quantifies the error incurred when attempting to generate the path using limited resources, such as local interactions. This idea could be further developed and applied to contexts such as optimal control and the study of the accessible state space.

Starting from a set of states considered as free-resources, such as the separable states, the evolution that generates the target state with the highest accessibility can be identified. In this operation, it is necessary to take into account that the time available to generate the states is limited. Such approach allows defining the accessibility of a state.

The selection of the state path that maximizes accessibility represents a possible approach to optimal control, to be compared with other existing methods in order to establish limits and strengths.

More generally, the investigation of state accessibility allows us to study which part of the Hilbert space represents realistic states, as they can be realized through local interactions and finite temporal resources [53]. Additionally, the accessibility of paths towards a state may be linked to the quantum complexity, or the time required to access the state with a finite amount of resources, thus playing a fundamental role in the geometrization of quantum complexity [114–116].

7.1.2 *Learnability of many-body systems*

In Chapter 4, we have shown how ergodicity represents a resource for Hamiltonian learning, in the sense that the observation of ergodic systems allows reconstructing the Hamiltonian of a system more accurately. This phenomenon represents the first example of how certain characteristics of many-body systems favor their learnability.

There are other important properties of many-body systems that could be useful in this sense. Intuitively, the parameters of a system can be inferred with greater precision when the system is more sensitive to changes in those parameters. This intuitive idea is formalized in the Fisher information matrix presented in Section 2.7. There are behaviors of many-body systems that consist of a strong sensitivity to the variation of some parameters. In phase transitions, for example, the drastic response of the system to a change of the parent Hamiltonian is encoded in the Fubini-Study metric, which represents a quantum version of the Fisher information matrix.

Another example comes from the study of quantum chaos. It is the study of how quantum systems behave when they are highly sensitive to initial conditions, similar to how classical chaotic systems behave. An important indicator of quantum chaos is the Loschmidt echo (LE)[208, 209], which measures the spreading of quantum information. In a chaotic system, the LE decays exponentially with time, indicating a high degree of sensitivity to initial conditions. Out-of-time-ordered correlators (OTOCs) are other important indicators and measure the scrambling of quantum information [217–220].

By designing learning queries that involve phase transitions or chaotic evolutions, one could obtain an information matrix that is related to the Fubini-Study metric, or LE, or OTOCs. This would lead to a reduction of the learning uncertainty as an emergent behavior of many body systems.

7.1.3 *Implementing the IQA on a quantum computer*

The IQA has been introduced in Chapter 5 as an efficient algorithm to adiabatically generate a local Hamiltonian having a target state as the ground state. This algorithm is based on artificial inverse dynamics, where the role of the density matrix $\rho(t)$ and the Hamiltonian $H(t)$ in the Schrödinger evolution are swapped.

To implement the IQA, one needs to integrate the inverse dynamics in the adiabatic limit. Since we are dealing with a quantum evolution, this task is in general exponentially hard for a classical computer. We have shown how an efficient classical implementation of this dynamics is possible through a TDVP. However, if at some time the correlation length of $\rho(t)$ diverges, the TDVP fails to generate the correct parent Hamiltonian. This happens, for example, when the selected path of states crosses a phase transition, or when it is a linear interpolation of two states having finite correlation length.

To overcome this obstacle, one could try to simulate the IQA on a quantum computer, i.e., to implement the artificial inverse dynamics in Eq. 5.2 on an actual quantum system. To reach this goal, the first step is to map the Hamiltonian $H(t)$ in the system state $\sigma(t) \equiv (H(t) + E_0\mathbb{1})/\operatorname{Tr}(H(t) + E_0\mathbb{1})$. Then, the time-evolution generated by the density matrix of the state $\rho(t)$ can be implemented as a quantum circuit through the density matrix exponentiation algorithm [221, 222]. At the end of the process when $t = T$, the couplings of the Hamiltonian encoded in the state $\rho(T)$ are measured as expectation values of the local operators. The main obstacle to this implementation is that it requires the capability to prepare the initial state $\sigma(0)$ and the state $\rho(t)$, which is involved in the density matrix exponentiation algorithm. If we can overcome this obstacle, then we can perform a direct quantum implementation of the IQA.

7.1.4 *Solving the quantum marginal problem through IQA*

The quantum marginal problem consists of the reconstruction of non-local expectation values of a quantum state from only local expectation values.

In Chapter 5, we have shown that IQA allows to reconstruct the proper parent Hamiltonians of a given path of states knowing only the local expectation values of these states, contained in the commutator matrices. At this point, it is natural to wonder if a combination of inverse and direct annealing can be used to efficiently solve the inverse problem. Specifically, one could use IQA to construct engineerable PHs from the local expectation values of an unknown state $|\psi\rangle$, and then implement these proper parent Hamiltonians on a quantum annealer to prepare the state $|\psi\rangle$. At this point, the expectation values of non-local observables can be simply measured.

The biggest obstacle in implementing such an algorithm is the selection of the path of states, or more precisely, the path of commutator matrices suitable to generate the inverse annealing. At the moment, this is a topic still unexplored.

A

FUBINI-STUDY AND HILBERT-SCHMIDT METRIC AND QCM

In Chapter 3 we say that the Hilbert-Schmidt metric for pure states is equal to twice the Fubini-Study metric. Here we prove this statement.

Let $\{\hat{T}_n\}$ be a set of Hermitian generators for the basis $\{|\partial_n\psi\rangle\}$ of a tangent space for $|\psi\rangle$, that is, $|\partial_n\psi\rangle = i\,\hat{T}_n|\psi\rangle$ for each $|\partial_n\psi\rangle$. The derivative of a vector in an arbitrary direction can be written as

$$|d\psi\rangle = i\,\delta^n|\partial_n\psi\rangle = i\,\delta^n\hat{T}_n|\psi\rangle \tag{A.1}$$

where the δ^n are coordinates. The Fubini-Study metric is defined as

$$g(d\psi, d\psi) = \mathrm{Re}(\langle d\psi|d\psi\rangle - \langle\psi|d\psi\rangle\langle d\psi|\psi\rangle). \tag{A.2}$$

In the basis defined above, the coordinate representation of the Fubini-Study metric is the matrix g_{ij} such that

$$g(d\psi, d\psi) = \delta^n\delta^m g_{nm}. \tag{A.3}$$

We show that this matrix is proportional to the CQM V_{nm} of the operators $\{\hat{T}_n\}$:

$$\begin{aligned}
\delta^n\delta^m g_{nm} &= \mathrm{Re}(\langle d\psi|d\psi\rangle - \langle\psi|d\psi\rangle\langle d\psi|\psi\rangle) \\
&= \delta^n\delta^m\mathrm{Re}(\langle\psi|\hat{T}_n\hat{T}_m|\psi\rangle - \langle\psi|\hat{T}_n|\psi\rangle\langle\psi|\hat{T}_m|\psi\rangle) \\
&= \frac{\delta^n\delta^m}{2}\mathrm{Re}\left(\langle\psi|\{\hat{T}_n, \hat{T}_m\}|\psi\rangle - \langle\psi|\hat{T}_n|\psi\rangle\langle\psi|\hat{T}_m|\psi\rangle\right) \\
&= \frac{1}{2}\delta^n\delta^m V_{nm}.
\end{aligned} \tag{A.4}$$

The CQM V_{nm} is also the metric associated to the Hilbert-Schmidt length of tangent vectors:

$$\begin{aligned}
\|d\psi\|^2 &= \mathrm{Tr}\left[(|d\psi\rangle\langle\psi| + \mathrm{h.\,c.})^2\right] \\
&= \mathrm{Tr}\left[(i\,\delta^n[\hat{T}_n, \hat{\rho}])^2\right] \\
&= -\delta^n\delta^m\,\mathrm{Tr}\left[(\hat{T}_n\hat{\rho} - \hat{\rho}\hat{T}_n)(\hat{T}_m\hat{\rho} - \hat{\rho}\hat{T}_m)\right] \\
&= \delta^n\delta^m V_{nm}.
\end{aligned} \tag{A.5}$$

Therefore, the Hilbert-Schmidt length of tangent vectors is twice the Fubini-Study length, and the CQM associated to the operators $\hat{T}_n$ is twice the Fubini-Study metric on the tangent space with basis $\{i\,\hat{T}_n|\psi\rangle\}$.

B

DETAILS OF UNCERTAINTY ESTIMATION

In Chapter 4, we analyzed the uncertainty generated by a hypothetical Hamiltonian learning algorithm based on a single state time evolution. This analysis has been based on the bound in Eq. (4.4). Here, we illustrate the details of the derivation of this bound.

The uncertainty on B_i is

$$\delta B_i = \sqrt{\sum_{\gamma,m} \left(\frac{\partial B_i}{\partial r_\gamma(t_m)} \sigma(r_\gamma(t_m)) \right)^2} + \sum_m |\mathrm{Tr}\left(-i[L_i, \rho(t_m)] R_m\right)| \tag{B.1}$$

We want to find an upper bound on this uncertainty that does not depend on the states $\{\rho(t_m)\}$.

The first term in the previous equation contains the statistical uncertainty. In a spin system we can choose basis operators as normalized tensor products of Pauli operators, hence $O_\alpha^2 = \mathbb{1}/2^{N_q}$ and $\sigma(r_\alpha(t_n)) = 1/\sqrt{2^{N_q} N_M}$. It follows that

$$\delta B_i = \frac{1}{\sqrt{2^{N_q} N_M}} \sqrt{\sum_{\gamma,m} \left(\frac{\partial B_i}{\partial r_\gamma(t_m)} \right)^2} + \sum_m |\mathrm{Tr}\left(-i[L_i, \rho(t_m)] R_m\right)| \tag{B.2}$$

Since

$$B_i = \sum_{n\alpha\beta} \mathrm{Tr}\left(-i[L_i, O_\alpha] O_\beta\right) r_\alpha(t_n) (r_\beta(t_{n+1}) - r_\beta(t_n))/\delta t, \tag{B.3}$$

we can take the derivative to obtain

$$\begin{aligned}
\sum_{\gamma,m} \left(\frac{\partial B_i}{\partial r_\gamma(t_m)} \right)^2 &= \sum_{\gamma,m} \left(\sum_{n,\alpha\beta} \mathrm{Tr}(-i[L_i, O_\alpha] O_\beta) \left[\delta_{\alpha\gamma}\delta_{nm} \frac{r_\beta(t_{n+1}) - r_\beta(t_n)}{\delta t} + r_{\beta n}\delta_{\gamma\alpha} \frac{\delta_{mn} - \delta_{m,n+1}}{\delta t} \right] \right)^2 \\
&= \sum_{\gamma,m} \left(\sum_\beta \mathrm{Tr}(-i[L_i, O_\gamma] O_\beta) \left[\frac{r_\beta(t_{m+1}) - r_\beta(t_m)}{\delta t} + \frac{r_\beta(t_m) - r_\beta(t_{m-1})}{\delta t} \right] \right)^2 + o(N_T) \\
&\approx \sum_{\gamma,m} \left(\sum_\beta \mathrm{Tr}(-i[L_i, O_\beta] O_\gamma) \left[\frac{r_\beta(t_{m+1}) - r_\beta(t_{m-1})}{\delta t} \right] \right)^2 .
\end{aligned} \tag{B.4}$$

At this point we approximate the fraction with the derivative and exploit the fact that $\{O_\alpha\}$ is an orthonormal basis:

$$\begin{aligned}\sum_{\gamma,m}\left(\frac{\partial B_i}{\partial r_\gamma(t_m)}\right)^2 &\approx 4\sum_{\gamma,m}\left(\sum_\beta \mathrm{Tr}(-i[L_i,O_\beta]O_\gamma)\partial_t r_\beta(t_m)\right)^2\\ &= 4\sum_{\gamma,m}\left(\mathrm{Tr}(-i[L_i,\partial_t\rho(t_m)]O_\gamma)\right)^2\\ &= 4\sum_{\gamma,m}\left(\mathrm{Tr}\left(-i[L_i,\partial_t\rho(t_m)]\right)^2\right).\end{aligned} \tag{B.5}$$

Replacing this estimate of the statistical uncertainty and the Taylor remainder $R_n = \frac{-[H,[H,\rho(t_n^*)]]}{2}$ in the total uncertainty δB_i, we obtain

$$\delta B_i \approx \frac{2}{\sqrt{2^{N_q}N_M}}\sqrt{\sum_m\left(\mathrm{Tr}\left(-i[L_i,\partial_t\rho(t_m)]\right)^2\right)} + \frac{\delta t}{2}\sum_m\left|\mathrm{Tr}\left[\left(-i[L_i,\rho(t_m)]\right)\left(-[H,[H,\rho(t_m^*)]]\right)\right]\right|, \tag{B.6}$$

where H is the system Hamiltonian.

Considering the Cauchy-Schwarz inequality $|\mathrm{Tr}(AB)| \leq \sqrt{\mathrm{Tr}(AA)\,\mathrm{Tr}(BB)}$, this last estimate can be bounded as

$$\delta B_i \leq \frac{2}{\sqrt{2^{N_q}N_M}}\sqrt{\sum_m\left(\mathrm{Tr}\left(-i[L_i,-i[H,\rho(t_m)]]\right)^2\right)} + \frac{\delta t}{2}\sum_m\sqrt{\mathrm{Tr}\left(\left(i[L_i,\rho(t_m)]\right)^2\right)\mathrm{Tr}\left([H,[H,\rho(t_m^*)]]^2\right)}, \tag{B.7}$$

where we have taken into account that $\partial_t\rho(t_m) = -i[H,\rho(t_m)]$.

Now we need to understand how the commutator with an Hermitian operators changes the Frobenius norm of a given operator. In particular, given a Hermitian operator A with spectral decomposition $A = \sum_i a_i|i\rangle\langle i|$, we define $a_{\min} = \min(a_i)$, $a_{\max} = \max(a_i)$, and $A_\delta = A - a_{\min}\mathbb{1}$. Hence we can write

$$\begin{aligned}\mathrm{Tr}[(-i[A,X])^2] &= \mathrm{Tr}[(-i[A_\delta,X])^2]\\ &= 2[\mathrm{Tr}(XXA_\delta A_\delta) - \mathrm{Tr}(A_\delta X A_\delta X)]\\ &= 2\sum_{ij}(a_i-a_{\min})(a_i-a_j)|\langle i|X|j\rangle|^2\\ &\leq 2(a_{\max}-a_{\min})^2\sum_{ij}|\langle i|X|j\rangle|^2\\ &= 2\|A_\delta\|_{\mathrm{op}}^2\,\mathrm{Tr}(X^2),\end{aligned} \tag{B.8}$$

where $\|A_\delta\|_{\mathrm{op}}$ is the operator norm of A_δ.

Replacing this bound in our estimate of the uncertainty δB_i and considering that the purity of the state $\rho(t)$ is $\mathrm{Tr}(\rho(t)^2) \leq 1$ for each value of t, we obtain

$$\begin{aligned}\delta B_i &\leq \frac{2\|L_i\|_{\mathrm{op}}}{\sqrt{2^{N_q} N_T}} \sqrt{\sum_m 2\left(\mathrm{Tr}\left(-i[H,\rho(t_m)]\right)^2\right)} + \|L_{i,\delta}\|_{\mathrm{op}} \|H_\delta\|_{\mathrm{op}} \sum_m \sqrt{\mathrm{Tr}\left((-i[H,\rho(t_m^*)]\delta t)^2\right)} \\ &\leq \frac{4\|H_\delta\|_{\mathrm{op}}\|L_{i,\delta}\|_{\mathrm{op}}}{\sqrt{2^{N_q} N_M}} \sqrt{N_T} + \delta t \|L_{i,\delta}\|_{\mathrm{op}} \|H_\delta\|_{\mathrm{op}}^2 N_T, \end{aligned} \tag{B.9}$$

where $\|L_{i,\delta}\|_{\mathrm{op}}$ and $\|H_\delta\|_{\mathrm{op}}$ are the difference between the maximum and the minimum eigenvalues of H and L_i, respectively.

For a traceless operator $A = \sum_i a_i |i\rangle\langle i|$ we have that the maximum eigenvalue is positive and the minimum one is negative, therefore

$$\|A_\delta\|_{\mathrm{op}} = a_{\max} - a_{\min} = |a_{\max}| + |a_{\min}| \leq 2\max(|a_i|) = 2\|A\|_{\mathrm{op}}. \tag{B.10}$$

Hence, since both H and L_i are traceless and since we can choose without loss of generality $\|L_i\|_{\mathrm{op}} = \|L\|_{\mathrm{op}} \forall i$, the last inequality becomes

$$\delta B_i \leq \frac{16\|H\|_{\mathrm{op}}\|L\|_{\mathrm{op}}}{\sqrt{2^{N_q} N_M}} \sqrt{N_T} + 4\delta t \|L\|_{\mathrm{op}} \|H\|_{\mathrm{op}}^2 N_T. \tag{B.11}$$

An analogous bound on the uncertainty about the Hamiltonian couplings can be calculated propagating the uncertainty about B_i. When $\|V^{-1}\| \ll 1$ we obtain

$$\delta h_i = \sum_j (V^{-1})_{ij} \delta B_j. \tag{B.12}$$

and therefore

$$\|\vec{\delta} h\| \leq \sqrt{\mathrm{Tr}\left(V^{-2}\right)} \|L\|_{\mathrm{op}} \left(16\|H\|_{\mathrm{op}} \sqrt{\frac{N_T}{2^{N_q} N_M}} + 4N_T \|H\|_{\mathrm{op}}^2 \delta t\right). \tag{B.13}$$

When $\|V^{-1}\| \ll 1$ does not hold, this estimate for the uncertainty fails, but this is the case in which we have an uncertainty that is so large that finding the exact Hamiltonian is impossible.

Now, we want to derive a bound on the relative uncertainty on the couplings. Taking into account the triangular inequality and the relationship between p-norms, and defining l as the number of Hamiltonian couplings, we can write

$$\|H\|_{\mathrm{op}} = \|\sum_i h_i L_i\|_{\mathrm{op}} \leq \sum_i |h_i| \|L_i\|_{\mathrm{op}} = \|L\|_{\mathrm{op}} \sum_i |h_i| \leq \sqrt{l} \|L\|_{\mathrm{op}} \|\vec{h}\|, \tag{B.14}$$

from which we finally obtain

$$\frac{\|\vec{\delta} h\|}{\|\vec{h}\|} \leq \sqrt{l\,\mathrm{Tr}\left(V^{-2}\right)} \|L\|_{\mathrm{op}}^2 \left(16\sqrt{\frac{N_T}{2^{N_q} N_M}} + 4N_T \|H\|_{\mathrm{op}} \delta t\right). \tag{B.15}$$

C

TRANSLATIONALLY INVARIANT GAUSSIAN STATES

Quadratic fermionic Hamiltonians describe a wide range of systems, including interacting electrons in solid-state materials and ultracold atoms in optical lattices. These Hamiltonians take the form of a quadratic polynomial in the fermionic creation and annihilation operators and can be exactly diagonalized. The ground states of quadratic fermionic Hamiltonians are Gaussian states. These states can be described by a polynomial amount of information in the system size thanks to the Wick theorem, which allows for a simple calculation of many-body correlations from 2-body correlations [80]. From this point of view, Gaussian states are the simplest type of quantum state that can exhibit non-trivial quantum correlations and quantum phase transitions.

Quadratic Hamiltonians and Gaussian states have been the perfect playground to test some ideas of this thesis, such as inverse quantum annealing. In particular, we tested the inverse quantum annealing on a particular class of translationally invariant Gaussian states, that are described by separable pseudo-spin states. Following Refs. [80, 223], in this appendix, we illustrate the details of this approach. Moreover, we explain some statements exploited in Chapter 5, such as the choice of the basis $\mathcal{L}^{(l)}$ and the form of the commutator matrix.

C.1 BASIS DEFINITION

We define the basis $\mathcal{L}^{(l)}$ of a space of translation and reflection invariant interactions of range l as follows:

$$\mathcal{L}^{(l<N/2)} \equiv \{\Sigma_0^Z/\sqrt{2}, \Sigma_1^X, \Sigma_1^Y, \Sigma_1^Z, \ldots, \Sigma_{l-1}^X, \Sigma_{l-1}^Y, \Sigma_{l-1}^Z\}, \tag{C.1}$$

and

$$\mathcal{L}^{(N/2)} \equiv \mathcal{L}^{(N/2-1)} \cup \{\Sigma_{N/2}^X/\sqrt{2}, \Sigma_{N/2}^Y/\sqrt{2}\}, \tag{C.2}$$

where

$$\begin{aligned} \Sigma_m^X &= \tfrac{1}{2}\textstyle\sum_{n=1}^N \left(c_n^\dagger c_{n+m}^\dagger - c_n c_{n+m}\right) \\ \Sigma_m^Y &= \tfrac{i}{2}\textstyle\sum_{n=1}^N \left(c_n^\dagger c_{n+m}^\dagger + c_n c_{n+m}\right) \\ \Sigma_m^Z &= \tfrac{1}{2}\textstyle\sum_{n=1}^N \left(c_n^\dagger c_{n+m} - c_n c_{n+m}^\dagger\right) \end{aligned} \tag{C.3}$$

with $c_n^\dagger$ and c_n fermionic creation and annihilation operators in the physical space, with anti-periodic boundary conditions $c_{N+m} \equiv -c_m$.

Note that anti-periodic boundary conditions ensure that an eventual operator $\Sigma^Z_{N/2}$ is null, and eventual operators Σ^X_0 and Σ^Y_0 are null because of fermions commutation rules.

C.2 FOURIER TRANSFORM

Now, we introduce the fermionic operators $c_k^\dagger$ and c_k acting on the momenta space:

$$\begin{aligned} c_k &= \frac{e^{-i\pi/4}}{\sqrt{N}} \sum_{n=1}^{N} e^{-ikn} c_n, \\ c_n &= \frac{e^{i\pi/4}}{\sqrt{N}} \sum_{k\in\mathcal{K}} e^{ikn} c_k. \end{aligned} \tag{C.4}$$

The anti-periodic boundary condition $c_{N+m} = -c_m$ implies that $\sum_{k\in\mathcal{K}} e^{ik(N+m)} c_k = -\sum_{k\in\mathcal{K}} e^{ikm} c_k$, that is

$$k \in \mathcal{K} \equiv \Big\{ k = \frac{(2n+1)\pi}{N}, \text{ with } n \in \{-N, \dots, N-1\} \Big\}. \tag{C.5}$$

The operators in $\mathcal{L}^{(l)}$ can be written as :

$$\Sigma^X_m = -i \sum_{k\in\mathcal{K}} (e^{imk} c_k^\dagger c_{-k}^\dagger - e^{-imk} c_{-k} c_k)$$

$$\Sigma^Y_m = -\sum_{k\in\mathcal{K}} (e^{imk} c_k^\dagger c_{-k}^\dagger + e^{-imk} c_{-k} c_k) \tag{C.6}$$

$$\Sigma^Z_m = \sum_{k\in\mathcal{K}} e^{imk} (c_k^\dagger c_k + c_{-k}^\dagger c_{-k} - \mathbb{1}) \tag{C.7}$$

The quadratic interactions in the latter equation respect the following symmetry rules: $c_k^\dagger c_k + c_{-k}^\dagger c_{-k} = c_{-k}^\dagger c_{-k} + c_k^\dagger c_k$, $c_k^\dagger c_{-k}^\dagger = -c_{-k}^\dagger c_k^\dagger$, and $c_k c_{-k} = -c_{-k} c_k$. Thanks to these rules, we can simplify the previous equations:

$$\begin{aligned} \Sigma^X_m &= 2 \sum_{k\in\mathcal{K}^+} \sin(mk) (c_k^\dagger c_{-k}^\dagger + c_{-k} c_k) \\ \Sigma^Y_m &= -2i \sum_{k\in\mathcal{K}^+} \sin(mk) (c_k^\dagger c_{-k}^\dagger - c_{-k} c_k) \\ \Sigma^Z_m &= 2 \sum_{k\in\mathcal{K}^+} \cos(mk) (c_k^\dagger c_k + c_{-k}^\dagger c_{-k} - \mathbb{1}), \end{aligned} \tag{C.8}$$

where $\mathcal{K}^+$ contains only the positive values of $\mathcal{K}$. Now, each term in $\mathcal{L}^{(l)}$ is block-diagonal, and the Hilbert space is the sum of N non-interacting subspaces labeled by the momenta k.

C.3 ANDERSON PSEUDO-SPINS

At this point we note that the operators $\tilde{\sigma}^x_k := (c^\dagger_k c^\dagger_{-k} + c_{-k}c_k)$, $\tilde{\sigma}^y_k := -i(c^\dagger_k c^\dagger_{-k} - c_{-k}c_k)$ and $\tilde{\sigma}^z_k := (c^\dagger_k c_k + c^\dagger_{-k}c_{-k} - \mathbb{1})$ follow the spin commutation rules $[\tilde{\sigma}^\mu_k, \tilde{\sigma}^\nu_{k'}] = 2i\delta_{kk'}\sum_\gamma \varepsilon^{\mu\nu\gamma}\tilde{\sigma}_\gamma$. Hence we write

$$\begin{aligned}
\Sigma^X_m &= 2\sum_{k\in\mathcal{K}^+} \sin(mk)\tilde{\sigma}^x_k \\
\Sigma^Y_m &= 2\sum_{k\in\mathcal{K}^+} \sin(mk)\tilde{\sigma}^y_k \\
\Sigma^Z_m &= 2\sum_{k\in\mathcal{K}^+} \cos(mk)\tilde{\sigma}^z_k.
\end{aligned} \tag{C.9}$$

These equations can be summarized as

$$\begin{aligned}
\Sigma^X_m &= \sum_{k\in\mathcal{K}^+} F^\mu \tilde{\sigma}^x_k \\
F^\mu(x) &\equiv 2(\sin(x), \sin(x), \cos(x))
\end{aligned} \tag{C.10}$$

We can see that all the Hamiltonians spanned by $\mathcal{L}^{(l)}$ can be written as systems of non-interacting spins, called pseudo-spins. The set $\mathcal{L}^{(l)}$ and the set of all the single pseudo-spin operators $\{\tilde{\sigma}^\mu_k\}$ are linked by a Fourier transform, therefore they are two bases for the same space.

We can invert the Fourier transform as follows:

$$\begin{aligned}
\sum_{0\le m\le N/2-1} \cos(mk)\Sigma^z_m &= 2\sum_m \sum_{k\in\mathcal{K}^+} \cos(mk')\cos(mk)\tilde{\sigma}^z_{k'} \\
&= 2\sum_m \cos^2(mk)\tilde{\sigma}^z_k \\
&= 2\sum_m \cos^2(i_k 2\pi m/N + m\pi/N)\tilde{\sigma}^z_k \\
&= 2\frac{N}{2\pi}\int_0^\pi \cos^2[(i_k+1/2)x]\tilde{\sigma}^z_k \\
&= \frac{N}{2}\tilde{\sigma}^z_k
\end{aligned} \tag{C.11}$$

In this way, we obtain the inverse relations:

$$\tilde{\sigma}^\mu_k = \frac{1}{N}\sum_{0\le m\le N/2} F^\mu(mk)\Sigma^\mu_m \tag{C.12}$$

C.4 NORMALIZATION OF THE BASIS

Here we show that the operators in $\mathcal{L}^{(N/2)}$ are orthogonal and that they have the same norm. This is needed to implement the inverse quantum annealing through Eq. 5.6.

Firstly, let us remark that, since the $\tilde{\sigma}_k^\mu$ are pseudo-spin operators, $\mathrm{Tr}(\tilde{\sigma}_k^\mu \tilde{\sigma}_{k'}^\nu) = \mathrm{Tr}(\{\tilde{\sigma}_k^\mu, \tilde{\sigma}_{k'}^\nu\})/2 = \mathrm{Tr}(\mathbb{1})\delta_{kk'}\delta_{\mu\nu}$. Following Eq. (C.10), the scalar products of the operators Σ_m^μ are

$$\mathrm{Tr}\left(\Sigma_m^\mu \Sigma_l^\nu\right) = \sum_k \sum_{k'} \mathrm{Tr}(\tilde{\sigma}_k^\mu \tilde{\sigma}_{k'}^\nu) F^\mu(km) F^\nu(k'l) = \delta_{\mu\nu}\,\mathrm{Tr}(\mathbb{1}) \sum_k F^\mu(km) F^\mu(kl), \tag{C.13}$$

Considering the orthogonality of the Fourier basis, the latter equation becomes

$$\mathrm{Tr}\left(\Sigma_m^\mu \Sigma_l^\nu\right) = \delta_{\mu\nu}\delta_{ml}\frac{N}{2}\,\mathrm{Tr}(\mathbb{1}) \tag{C.14}$$

for $0 < m < N/2$ and

$$\mathrm{Tr}\left(\Sigma_m^\mu \Sigma_l^\nu\right) = \delta_{\mu\nu}\delta_{ml} N\,\mathrm{Tr}(\mathbb{1}) \tag{C.15}$$

for $m = 0$ and $m = N/2$.

Therefore,

$$\mathcal{L}^{(N/2)} \equiv \{\Sigma_0^Z/\sqrt{2}, \Sigma_1^X, \Sigma_1^Y, \Sigma_1^Z, \ldots, \Sigma_{N/2-1}^X, \Sigma_{N/2-1}^Y, \Sigma_{N/2-1}^Z, \Sigma_{N/2}^X/\sqrt{2}, \Sigma_{N/2}^Y/\sqrt{2}\}, \tag{C.16}$$

is a set of orthogonal vectors with the same norm.

C.5 FROM QUADRATIC FERMIONS TO NON-INTERACTING SPEUDO-SPINS

Following the scheme of the previous sections, any arbitrary Hamiltonian spanned by the interactions in $\mathcal{L}^{(l)}$ can be diagonalized as a non-interacting pseudo-spins system. As an example, here we diagonalize the Kitaev model exploited in Section. 5.5.

The Kitaev Hamiltonian is

$$H^{\mathrm{K}}(\lambda) = \sin(\lambda) \sum_{n=1}^{N} \left(c_n^\dagger c_{n+1}^\dagger + c_n^\dagger c_{n+1} + \mathrm{h.c.}\right) + \cos(\lambda) \sum_{n=1}^{N} \left(c_n^\dagger c_n - c_n c_n^\dagger\right). \tag{C.17}$$

This Hamiltonian, in terms of the operators in $\mathcal{L}^{(l)}$, reads

$$H^{\mathrm{K}}(\lambda) = 2\sin(\lambda)\left(\Sigma_1^Z + \Sigma_1^Z\right) + 2\cos(\lambda)\Sigma_0^Z. \tag{C.18}$$

Exploiting Eq. (C.10), the last equation is written in terms of non-interacting pseudo-spins as:

$$H^{\mathrm{K}}(\lambda) = 4 \sum_{k \in \mathcal{K}^+} \left[\cos(\lambda)\tilde{\sigma}_k^z + \sin(\lambda)\left(\sin(k)\tilde{\sigma}_k^x + \cos(k)\tilde{\sigma}_k^z\right)\right], \tag{C.19}$$

or, equivalently, as

$$H^{\mathrm{K}}(\lambda) = 4 \sum_{k \in \mathcal{K}^+} \epsilon_k \left(v_k^x \tilde{\sigma}_k^x + v_k^y \tilde{\sigma}_k^y + v_k^z \tilde{\sigma}_k^z\right), \tag{C.20}$$

where

$$\begin{aligned}\epsilon_k &= \sqrt{1+2\sin(\lambda)\cos(\lambda)\cos(k)}\\ v_k^x &= -\sin(\lambda)\sin(k)/\epsilon_k\\ v_k^y &= 0\\ v_k^z &= -\left(\cos(\lambda)+\sin(\lambda)\cos(k)\right)/\epsilon_k.\end{aligned} \tag{C.21}$$

In the same manner, any Hamiltonian spanned $\mathcal{L}^{(l)}$ can be written in this form, with different values of the vectors $\vec{v}_k$ and of the energies ϵ_k. Writing the ground state density matrix of these Hamiltonians is straightforward:

$$\Psi_{\text{gs}} \equiv \bigotimes_{k\in\mathcal{K}^+} \left(v_k^x\tilde{\sigma}_k^x + v_k^y\tilde{\sigma}_k^y + v_k^z\tilde{\sigma}_k^z + \mathbb{1}\right)/2. \tag{C.22}$$

C.6 COMMUTATOR MATRIX

Here, we calculate commutator matrix $K_{ij}^{(l)}(\Psi) = \langle\Psi| - i[\Sigma_m^\mu, \Sigma_n^\nu]|\Psi\rangle = K_{\{m,\mu\}\{n,\nu\}}^{(l)}(\Psi)$. The entries of this matrix are the commutators expectation values of the operators in $\mathcal{L}^{(l)}$ for the arbitrary ground states $|\Psi\rangle$ in Eq. C.22.

The commutator matrix is related to the pseudo-spins commutator matrix $K'_{\{k,\alpha\}\{k',\alpha'\}}(\Psi) \equiv \langle\Psi| - i[\tilde{\sigma}_k^\alpha, \tilde{\sigma}_{k'}^{\alpha'}]|\Psi\rangle$ as follows:

$$\begin{aligned}K_{\{m,\mu\}\{n,\nu\}}^{(l)} &= \langle\Psi| - i[\Sigma_m^\mu, \Sigma_n^\nu]|\Psi\rangle\\ &= \sum_{\{k,\alpha\}}^{k\in\mathcal{K}^+,\alpha\in\{X,Y,Z\}} \sum_{\{k',\alpha'\}}^{k'\in\mathcal{K}^+,\alpha'\in\{X,Y,Z\}} F_{\{m,\mu\}\{k,\alpha\}}^{(l)} F_{\{n,\nu\}\{k',\alpha'\}}^{(l)} K'_{\{k,\alpha\}\{k',\alpha'\}},\end{aligned} \tag{C.23}$$

where matrix F is a Fourier transform matrix.

In particular, for $l < N/2$ we have:

$$F^{(l)} = \begin{pmatrix} 0 & 0 & 1/\sqrt{2} & 0 & 0 & 1/\sqrt{2} & \dots\\ \sin(1k_1) & 0 & 0 & \sin(1k_2) & 0 & 0 & \dots\\ 0 & \sin(1k_1) & 0 & 0 & \sin(1k_2) & 0 & \dots\\ 0 & 0 & \cos(1k_1) & 0 & 0 & \cos(1k_2) & \dots\\ \dots & \dots & \dots & \dots & \dots & \dots & \dots\\ \sin(lk_1) & 0 & 0 & \sin(lk_2) & 0 & 0 & \dots\\ 0 & \sin(lk_1) & 0 & 0 & \sin(lk_2) & 0 & \dots\\ 0 & 0 & \cos(lk_1) & 0 & 0 & \cos(lk_2) & \dots \end{pmatrix}, \tag{C.24}$$

and for $l = N/2$:

$$F^{(N/2)} = \begin{pmatrix} 0 & 0 & 1/\sqrt{2} & \dots \\ \sin(1k_1) & 0 & 0 & \dots \\ 0 & \sin(1k_1) & 0 & \dots \\ 0 & 0 & \cos(1k_1) & \dots \\ \dots & \dots & \dots & \dots \\ \sin(\frac{N}{2}k_1 - k_1 & 0 & 0 & \dots \\ 0 & \sin(\frac{N}{2}k_1 - k_1) & 0 & \dots \\ 0 & 0 & \cos(\frac{N}{2}k_1 - k1) & \dots \\ \sin(Nk_1/2)/\sqrt{2} & 0 & 0 & \dots \\ 0 & \sin(Nk_1/2)/\sqrt{2} & 0 & \dots \end{pmatrix}. \tag{C.25}$$

The last step consists in calculating the elements of the matrix $K'(\Psi)$. Thanks to the simple commutation rules between pseudo-spins, this is a block-diagonal matrix:

$$K'(\Psi) = \begin{pmatrix} K_{k_1}(\Psi) & 0 & \dots \\ 0 & K_{k_2}(\Psi) & \dots \\ \dots & \dots & \dots \end{pmatrix}, \tag{C.26}$$

where the blocks are labeled by the elements of $\mathcal{K}^+$. Exploiting Eq. (C.22), we obtain the explicit form of the submatrices:

$$K_k(\Psi) = \begin{pmatrix} 0 & v_k^z(\Psi) & -v_k^y(\Psi) \\ -v_k^z(\Psi) & 0 & v_k^x(\Psi) \\ v_k^y(\Psi) & -v_k^x(\Psi) & 0 \end{pmatrix} \tag{C.27}$$

note that $K^{[w=0]}$ is the commutator matrix for the basis $\mathcal{L}^{[w=0]}$.

Now, the commutator matrix can be easily calculated through the Fourier transform of $K'(\Psi)$:

$$K^{(l)}(\Psi) = \left(F^{(l)}\right)\left(K'(\Psi)\right)\left(F^{(l)}\right)^T. \tag{C.28}$$

D

INTEGRABLE SPIN CHAINS

Numerous one-dimensional interacting spins systems can be exactly solved through mapping into the space of quadratic fermionic Hamiltonians. Examples of such models include the Ising model in transverse field [125], the XY model [126], and some cluster Hamiltonians [173].

Here, we define a set $\mathcal{S}$ of translationally invariant spins interactions that, exploiting the Jordan-Wigner transformations [124–126], are mapped to the basis $\{\Sigma^{\mu}_{m}\}$ studied in Appendix C. This equivalence allows for diagonalizing all the Hamiltonians spanned by $\mathcal{S}$ through a Jordan-Wigner transformation followed by the techniques of Appendix C. Finally, we show how the Wick theorem can be exploited to efficiently calculate the expectation values of any string of Pauli operators for an arbitrary ground state of these models.

D.1 BASIS DEFINITION

Let us define the operators $\mathcal{S} = \{S^{Z}_{0}, S^{X}_{1}, S^{Y}_{1}, S^{Z}_{1}, \dots, S^{X}_{N/2-1}, S^{Y}_{N/2-1}, S^{Z}_{N/2-1}, S^{X}_{N/2}, S^{Y}_{N/2}\}$ on a system of N spins, where

$$
\begin{aligned}
S^{Z}_{0} &= -\frac{1}{2}\sum_{n}^{N}\sigma^{z}_{n} \\
S^{X}_{m} &= \frac{1}{4}\sum_{n}^{N}\left(\sigma^{x}_{n}\sigma^{z}_{n+1}\dots\sigma^{z}_{n+m-1}\sigma^{x}_{n+m} - \sigma^{y}_{n}\sigma^{z}_{n+1}\dots\sigma^{z}_{n+m-1}\sigma^{y}_{n+m}\right) \\
S^{Y}_{m} &= \frac{1}{4}\sum_{n}^{N}\left(\sigma^{x}_{n}\sigma^{z}_{n+1}\dots\sigma^{z}_{n+m-1}\sigma^{y}_{n+m} + \sigma^{y}_{n}\sigma^{z}_{n+1}\dots\sigma^{z}_{n+m-1}\sigma^{x}_{n+m}\right) \\
S^{Z}_{m} &= \frac{1}{4}\sum_{n}^{N}\left(\sigma^{x}_{n}\sigma^{z}_{n+1}\dots\sigma^{z}_{n+m-1}\sigma^{x}_{n+m} + \sigma^{y}_{n}\sigma^{z}_{n+1}\dots\sigma^{z}_{n+m-1}\sigma^{y}_{n+m}\right).
\end{aligned}
\tag{D.1}
$$

Here the dots represent a string of σ^{z}_{i} operators.

We consider an even number of spins and periodic boundary conditions $\sigma^{\mu}_{i+N} = \sigma^{\mu}_{i}$. In this Appendix, we show that all these operators can be written as quadratic fermionic operators thanks to the Jordan-Wigner transformations [80].

Firstly, we consider the parity operator $P \equiv \prod_n \sigma_{n,z}$. P commutes with each element of $\mathcal{L}$, so we can divide the whole Hilbert space into two parity sectors and write the S_n^μ an a block diagonal form:

$$S_n^\mu = \begin{pmatrix} S_{n,0}^\mu & 0 \\ 0 & S_{n,1}^\mu \end{pmatrix}, \tag{D.2}$$

where the subscript index $p \in \{0,1\}$ is referred to the parity of the Hilbert subspace on which the operator acts (0 even, 1 odd).

The Jordan-Wigner transformations are defined as

$$\begin{aligned} K_n &= \prod_1^{n-1}(\mathbb{1} - 2c_n^\dagger c_n) \\ \sigma_n^z &= (\mathbb{1} - 2c_n^\dagger c_n) \\ \sigma_n^x &= K_n(c_n^\dagger + c_n) \\ \sigma_n^y &= i\,K_n(c_n^\dagger - c_n), \end{aligned} \tag{D.3}$$

where the $c_n^\dagger$'s and the c_n's are fermionic creation and annihilation operators in the positions space. Exploiting this mapping, one can write the elements of $\mathcal{S}$ as quadratic fermionic Hamiltonians. The action of these Hamiltonians changes on the different parity sectors of the Hilbert space [80]. In the even parity sector, which contains the ground states of the Hamiltonians spanned by $\mathcal{S}$, the representations of these elements coincide with the operators Σ_μ^Z introduced in Appendix C:

$$\begin{aligned} S_{0,0}^Z &= \Sigma_0^Z \\ S_{m,0}^X &= \Sigma_m^X \\ S_{m,0}^Y &= \Sigma_m^Y \\ S_{m,0}^Z &= \Sigma_m^Z. \end{aligned} \tag{D.4}$$

D.2 FROM INTERACTING SPINS TO NON-INTERACTING SPEUDO-SPINS

All the Hamiltonians spanned by $\mathcal{S}$ can be diagonalized through a Jordan-Wigner transformation followed by the techniques of Appendix C. As an example, let us consider the Ising Hamiltonian in transverse field introduced in Chapter 3:

$$H_{\mathrm{I}}(\lambda) = -\sum_{n=1}^{L} \sigma_n^x \sigma_{n+1}^x - \lambda \sum_{n=1}^{L} \sigma_n^z\,. \tag{D.5}$$

In terms of the operators in $\mathcal{S}$, this Hamiltonian is written as

$$H_{\mathrm{I}}(\lambda) = -2\sum_{n=1}^{L}(\Sigma_1^X + \Sigma_1^Z) + 2\lambda \sum_{n=1}^{L} \Sigma_0^Z\,. \tag{D.6}$$

The Jordan-Wigner transformation $S^{\mu}_{m} \rightarrow \Sigma^{\mu}_{m}$, maps this Hamiltonian in a Kiteav model that is analogous to the one diagonalized in Appendix C. This leads to a pseudo-spin representation of the Ising Hamiltonian in transverse field:

$$H_{\mathrm{I}} = -\sum_{k\in\mathcal{K}^{+}} \epsilon_k \left(v^x_k \tilde{\sigma}^x_k + v^y_k \tilde{\sigma}^y_k + v^z_k \tilde{\sigma}^z_k\right), \tag{D.7}$$

where

$$\mathcal{K}^{+} \equiv \left\{k = \frac{(2n+1)\pi}{L}, \text{ with } n \in \{0,\dots,L/2-1\}\right\}, \tag{D.8}$$

and

$$\begin{aligned}
\epsilon_k &= 2\sqrt{\sin^2(k) + (\cos(k)-\lambda)^2} \\
v^x_k &= \sin(k)/\epsilon_k \\
v^y_k &= 0 \\
v^z_k &= (\cos(k)-\lambda)/\epsilon_k.
\end{aligned} \tag{D.9}$$

D.3 PAULI STRINGS EXPECTATION VALUES

Let be $|\Psi\rangle$ the non-degenerate ground state of any linear combination of the operators in $\mathcal{S}$. We want to calculate the expectation values in $|\Psi\rangle$ of an arbitrary string of Pauli operators.

Let us define the operators

$$\begin{aligned}
A_j &= \bigotimes_{i<j} \sigma^z_i \sigma^x_j \\
B_j &= \bigotimes_{i<j} \sigma^z_i \sigma^y_j.
\end{aligned} \tag{D.10}$$

These are Majorana fermions, indeed

$$\begin{aligned}
\{A_i, A_j\} &= 2\delta_{ij}\mathbb{1} \\
\{B_i, B_j\} &= 2\delta_{ij}\mathbb{1} \\
\{A_i, B_j\} &= 0
\end{aligned} \tag{D.11}$$

As a consequence of the symmetries of the operators in $\mathcal{S}$, any Pauli string that contains a total odd number of σ_x and σ_y has a null expectation value in $|\Psi\rangle$. Moreover, after some algebra, one can show that all the other Pauli strings can be written as strings of Majorana fermions with an even number of fermions, multiplied by a phase factor:

	$m=0$	$m>0$	$m<0$
$A_jA_{j+m} =$	$\mathbb{1}$	$-i\sigma^y_j \bigotimes_{1\le i<m} \sigma^z_{j+i}\sigma^x_{j+m}$	$i\sigma^y_{j-\lvert m\rvert} \bigotimes_{1\le i<\lvert m\rvert} \sigma^z_{j-\lvert m\rvert+i}\sigma^x_j$
$B_jB_{j+m} =$	$\mathbb{1}$	$i\sigma^x_j \bigotimes_{1\le i<m} \sigma^z_{j+i}\sigma^y_{j+m}$	$-i\sigma^x_{j-\lvert m\rvert} \bigotimes_{1\le i<\lvert m\rvert} \sigma^z_{j-\lvert m\rvert+i}\sigma^y_j$
$A_jB_{j+m} =$	$i\sigma^z_j$	$-i\sigma^y_j \bigotimes_{1\le i<m} \sigma^z_{j+i}\sigma^y_{j+m}$	$-i\sigma^x_{j-\lvert m\rvert} \bigotimes_{1\le i<\lvert m\rvert} \sigma^z_{j-\lvert m\rvert+i}\sigma^x_j$

At this point, we call

$$C(\{i\}_k, \{j\}_l) \equiv \langle \Psi | A_{i_1}, \dots, A_{i_k}, B_{j_1}, \dots, B_{j_l} | \Psi \rangle \tag{D.12}$$

the expectation value on $|\Psi\rangle$ of an arbitrarily ordered product of Majorana fermions, where $\{i\}_k \equiv \{i_1, \dots, i_k | N > i_1 > \cdots > i_k > 1\}$ is a set of ordered indices ranging over all the sites. Any non-zero expectation value of a Pauli string in the state $|\Psi\rangle$ is equal to some $C(\{i\}_k, \{j\}_l)$ multiplied by a phase factor. Since we are dealing with Gaussian states, the computation of $C(\{i\}_k, \{j\}_l)$ can be done through the Wick theorem:

$$C(\{i\}_k, \{j\}_l) = \mathrm{Pf} \begin{pmatrix} \langle A_{i_1} A_{i_1} \rangle - 1 & \dots & \langle A_{i_1} A_{i_k} \rangle & \langle A_{i_1} B_{j_1} \rangle & \dots & \langle A_{i_1} B_{j_l} \rangle \\ \dots & \dots & \dots & \dots & \dots & \dots \\ \langle A_{i_k} A_{i_1} \rangle & \dots & \langle A_{i_k} A_{i_k} \rangle - 1 & \langle A_{i_k} B_{j_1} \rangle & \dots & \langle A_{i_k} B_{j_l} \rangle \\ \langle B_{j_1} A_{i_1} \rangle & \dots & \langle B_{j_1} A_{i_k} \rangle & \langle B_{j_1} B_{j_1} \rangle - 1 & \dots & \langle B_{j_1} B_{j_l} \rangle \\ \dots & \dots & \dots & \dots & \dots & \dots \\ \langle B_{j_l} A_{i_1} \rangle & \dots & \langle B_{j_l} A_{i_k} \rangle & \langle B_{j_l} B_{j_1} \rangle & \dots & \langle B_{j_l} B_{j_l} \rangle - 1, \end{pmatrix}, \tag{D.13}$$

where Pf indicates the Pfaffian of the matrix.

If we define the matrices

$$\begin{aligned} \gamma^{AA}_{j,j+m}(\Psi) &\equiv \langle \Psi | A_j A_{j+m} | \Psi \rangle - \delta_{m0} = -\langle \Psi | B_j B_{j+m} | \Psi \rangle + \delta_{m0} \\ \gamma^{AB}_{j,j+m}(\Psi) &\equiv \langle \Psi | A_j B_{j+m} | \Psi \rangle, \end{aligned} \tag{D.14}$$

we can write

$$C(\{i\}_k, \{j\}_l) = \mathrm{Pf} \begin{pmatrix} \gamma^{AA}_{\{i\}_k \{i\}_k} & -\gamma^{AB}_{\{i\}_k \{j\}_l} \\ -\left(\gamma^{AB}_{\{i\}_k \{j\}_l}\right)^T & -\gamma^{AA}_{\{j\}_l \{j\}_l}. \end{pmatrix} \tag{D.15}$$

In this way, once the two-point correlation functions that define the matrices $\gamma^{AA}_{j,j+m}$ and $\gamma^{AB}_{j,j+m}$ have been calculated, any non-null Pauli string expectation values can be found in polynomial time through the Pfaffian technique.

To estimate these matrices, we exploit the translational and reflection invariance. Firstly, we note that due to the translation invariance $\gamma^{AA}_{j,j+m} = \sum_j \gamma^{AA}_{j,j+m}/N$ and $\gamma^{AB}_{j,j+m} = \sum_j \gamma^{AB}_{1,1+m}/N$. Considering the definition of the operators in $\mathcal{S}$, we obtain

$$\begin{aligned} \gamma^{BB}_m(\Psi) &= -\gamma^{AA}_m(\Psi) \\ \gamma^{AA}_0(\Psi) &= 0 \\ \gamma^{AB}_0(\Psi) &= -i\langle \Psi | S^Z_0 | \Psi \rangle / N \\ \gamma^{AA}_{m>0}(\Psi) &= i\langle \Psi | S^Y_m | \Psi \rangle / N \\ \gamma^{AB}_{m>0}(\Psi) &= i\langle \Psi | S^X_m - S^Z_m | \Psi \rangle / N \\ \gamma^{AA}_{m<0}(\Psi) &= -i\langle \Psi | S^Y_{|m|} | \Psi \rangle / N \\ \gamma^{AB}_{m<0}(\Psi) &= -i\langle \Psi | S^X_{|m|} + S^Z_{|m|} | \Psi \rangle / N \end{aligned}$$

These expectation values can be evaluated by exploiting the pseudo-spin representation of the operators in $\mathcal{S}$:

$$\begin{aligned}\gamma_m^{AA}(\Psi) &= 2i \sum_{k\in\mathcal{K}^+} \langle\Psi| \sin(mk)\tilde{\sigma}_k^y|\Psi\rangle / N \\ \gamma_m^{AB}(\Psi) &= 2i \sum_{k\in\mathcal{K}^+} \langle\Psi| \sin(mk)\tilde{\sigma}_k^x - \cos(mk)\tilde{\sigma}_k^z|\Psi\rangle / N. \end{aligned} \tag{D.16}$$

Similarly, we have shown that the ground states of integrable spin systems are represented in pseudo-spins formalism through Eq. C.22. Finally, this leads to

$$\begin{aligned}\gamma_m^{AA}(\Psi) &= 2i \sum_{k\in\mathcal{K}^+} \sin(mk)v_k^y / N \\ \gamma_m^{AB}(\Psi) &= 2i \sum_{k\in\mathcal{K}^+} \left(\sin(mk)v_k^x - \cos(mk)v_k^z\right) / N. \end{aligned} \tag{D.17}$$

BIBLIOGRAPHY

[1] D. Rattacaso, G. Passarelli, P. Lucignano and R. Fazio, 'Optimal parent hamiltonians for many-body states', in *Entanglement in Spin Chains: From Theory to Quantum Technology Applications*, A. Bayat, S. Bose and H. Johannesson, Eds., Cham: Springer International Publishing, 2022, pp. 189–209, ISBN: 978-3-031-03998-0.

[2] D. Rattacaso, G. Passarelli, A. Mezzacapo, P. Lucignano and R. Fazio, 'Optimal parent hamiltonians for time-dependent states', *Physical Review A*, vol. 104, no. 2, Aug. 2021, ISSN: 2469-9934.

[3] D. Rattacaso, G. Passarelli and P. Lucignano, 'High-accuracy hamiltonian learning via delocalized quantum state evolutions', *Quantum*, vol. 7, p. 905, Jan. 2023.

[4] D. Rattacaso, G. Passarelli, A. Russomanno, G. Santoro, P. Lucignano and R. Fazio, *Parent hamiltonian searching by inverse quantum annealing*, [In preparation].

[5] D. Rattacaso, S. F. O. Lorenzo Leone, P. Lucignano, R. Fazio and A. Hamma, *Non-stabilizerness dynamics in quantum spin chains*, [In preparation].

[6] D. Rattacaso, P. Vitale and A. Hamma, 'Quantum geometric tensor away from equilibrium', *Journal of Physics Communications*, vol. 4, no. 5, p. 055 017, 2020.

[7] ——, 'Towards a geometrization of quantum complexity and chaos', in *Geometric Science of Information*, F. Nielsen and F. Barbaresco, Eds., Cham: Springer International Publishing, 2021, pp. 163–171, ISBN: 978-3-030-80209-7.

[8] R. P. Feynman, 'Simulating physics with computers', *International Journal of Theoretical Physics*, vol. 21, no. 6, pp. 467–488, Jun. 1982, ISSN: 1572-9575.

[9] M. A. Nielsen and I. Chuang, 'Quantum computation and quantum information', *American Journal of Physics*, vol. 70, no. 5, pp. 558–559, 2002.

[10] I. Buluta, S. Ashhab and F. Nori, 'Natural and artificial atoms for quantum computation', *Reports on Progress in Physics*, vol. 74, no. 10, p. 104 401, Sep. 2011.

[11] Zoller, P. *et al.*, 'Quantum information processing and communication - strategic report on current status, visions and goals for research in europe', *Eur. Phys. J. D*, vol. 36, no. 2, pp. 203–228, 2005.

[12] J. Preskill, 'Quantum computing in the nisq era and beyond', *Quantum*, vol. 2, p. 79, Aug. 2018, ISSN: 2521-327X.

[13] I. H. Deutsch, 'Harnessing the power of the second quantum revolution', *PRX Quantum*, vol. 1, p. 020 101, 2 Nov. 2020.

[14] R. Blatt and C. F. Roos, 'Quantum simulations with trapped ions', *Nature Physics*, vol. 8, no. 4, pp. 277–284, Apr. 2012, ISSN: 1745-2481.

[15] D. Leibfried, R. Blatt, C. Monroe and D. Wineland, 'Quantum dynamics of single trapped ions', *Rev. Mod. Phys.*, vol. 75, pp. 281–324, 1 Mar. 2003.

[16] H. Häffner, C. Roos and R. Blatt, 'Quantum computing with trapped ions', *Physics Reports*, vol. 469, no. 4, pp. 155–203, 2008, ISSN: 0370-1573.

[17] J. I. Cirac and P. Zoller, 'Quantum computations with cold trapped ions', *Phys. Rev. Lett.*, vol. 74, pp. 4091–4094, 20 May 1995.

[18] J. T. Barreiro *et al.*, 'An open-system quantum simulator with trapped ions', *Nature*, vol. 470, no. 7335, pp. 486–491, Feb. 2011.

[19] C. S. Adams, J. D. Pritchard and J. P. Shaffer, 'Rydberg atom quantum technologies', *Journal of Physics B: Atomic, Molecular and Optical Physics*, vol. 53, no. 1, p. 012 002, Dec. 2019.

[20] M. Saffman, 'Quantum computing with atomic qubits and rydberg interactions: Progress and challenges', *Journal of Physics B: Atomic, Molecular and Optical Physics*, vol. 49, no. 20, p. 202 001, Oct. 2016.

[21] H.-L. Huang, D. Wu, D. Fan and X. Zhu, 'Superconducting quantum computing: A review', *Science China Information Sciences*, vol. 63, p. 180 501, Jul. 2020, ISSN: 1869-1919.

[22] J. M. Gambetta, J. M. Chow and M. Steffen, 'Building logical qubits in a superconducting quantum computing system', *npj Quantum Information*, vol. 3, no. 1, p. 2, Jan. 2017, ISSN: 2056-6387.

[23] J. Clarke and F. K. Wilhelm, 'Superconducting quantum bits', *Nature*, vol. 453, no. 7198, pp. 1031–1042, Jun. 2008, ISSN: 1476-4687.

[24] J. L. O'Brien, A. Furusawa and J. Vučković, 'Photonic quantum technologies', *Nature Photonics*, vol. 3, no. 12, pp. 687–695, Dec. 2009.

[25] A. Gheorghiu, T. Kapourniotis and E. Kashefi, 'Verification of quantum computation: An overview of existing approaches', *Theory of Computing Systems*, vol. 63, no. 4, pp. 715–808, Jul. 2018, ISSN: 1433-0490.

[26] I. H. Deutsch, 'Harnessing the power of the second quantum revolution', *PRX Quantum*, vol. 1, p. 020 101, 2 Nov. 2020.

[27] J. Eisert *et al.*, 'Quantum certification and benchmarking', *Nature Reviews Physics*, vol. 2, no. 7, pp. 382–390, Jun. 2020, ISSN: 2522-5820.

[28] I. Šupić and J. Bowles, 'Self-testing of quantum systems: A review', *Quantum*, vol. 4, p. 337, Sep. 2020, ISSN: 2521-327X.

[29] J. Carrasco, A. Elben, C. Kokail, B. Kraus and P. Zoller, 'Theoretical and experimental perspectives of quantum verification', *PRX Quantum*, vol. 2, p. 010 102, 1 Mar. 2021.

[30] M. Kliesch and I. Roth, 'Theory of quantum system certification', *PRX Quantum*, vol. 2, p. 010 201, 1 Jan. 2021.

[31] N. Wiebe, C. Granade, C. Ferrie and D. G. Cory, 'Hamiltonian learning and certification using quantum resources', *Physical Review Letters*, vol. 112, no. 19, May 2014, ISSN: 1079-7114.

[32] J. Wang *et al.*, 'Experimental quantum hamiltonian learning', *Nature Physics*, vol. 13, no. 6, pp. 551–555, Mar. 2017, ISSN: 1745-2481.

[33] T. Bertalan, F. Dietrich, I. Mezić and I. G. Kevrekidis, 'On learning hamiltonian systems from data', *Chaos: An Interdisciplinary Journal of Nonlinear Science*, vol. 29, no. 12, p. 121 107, 2019.

[34] P. Bienias, A. Seif and M. Hafezi, *Meta hamiltonian learning*, 2021.

[35] J. H. Cole, S. G. Schirmer, A. D. Greentree, C. J. Wellard, D. K. L. Oi and L. C. L. Hollenberg, 'Identifying an experimental two-state hamiltonian to arbitrary accuracy', *Phys. Rev. A*, vol. 71, p. 062 312, 6 Jun. 2005.

[36] J. H. Cole, A. D. Greentree, D. K. L. Oi, S. G. Schirmer, C. J. Wellard and L. C. L. Hollenberg, 'Identifying a two-state hamiltonian in the presence of decoherence', *Physical Review A*, vol. 73, no. 6, Jun. 2006, ISSN: 1094-1622.

[37] D. Burgarth and K. Yuasa, 'Quantum system identification', *Phys. Rev. Lett.*, vol. 108, p. 080 502, 8 Feb. 2012.

[38] R. B. Laughlin, 'Anomalous quantum hall effect: An incompressible quantum fluid with fractionally charged excitations', *Phys. Rev. Lett.*, vol. 50, pp. 1395–1398, 18 May 1983.

[39] I. H. Deutsch and P. S. Jessen, 'Quantum-state control in optical lattices', *Phys. Rev. A*, vol. 57, pp. 1972–1986, 3 Mar. 1998.

[40] R. van Handel, J. K. Stockton and H. Mabuchi, 'Modelling and feedback control design for quantum state preparation', *Journal of Optics B: Quantum and Semiclassical Optics*, vol. 7, no. 10, S179–S197, Sep. 2005.

[41] F. Verstraete, M. M. Wolf and J. Ignacio Cirac, 'Quantum computation and quantum-state engineering driven by dissipation', *Nature Physics*, vol. 5, no. 9, pp. 633–636, Sep. 2009, ISSN: 1745-2481.

[42] M. Plesch and C. Č. Brukner, 'Quantum-state preparation with universal gate decompositions', *Phys. Rev. A*, vol. 83, p. 032 302, 3 Mar. 2011.

[43] J. Werschnik and E. K. U. Gross, 'Quantum optimal control theory', *J. Phys. B: At. Mol. Opt. Phys.*, vol. 40, no. 18, R175–R211, Sep. 2007.

[44] C. Brif, R. Chakrabarti and H. Rabitz, 'Control of quantum phenomena: Past, present and future', *New Journal of Physics*, vol. 12, no. 7, p. 075 008, Jul. 2010, ISSN: 1367-2630.

[45] D. Dong and I. Petersen, 'Quantum control theory and applications: A survey', *IET Control Theory & Applications*, vol. 4, no. 12, pp. 2651–2671, Dec. 2010, ISSN: 1751-8652.

[46] S. J. Glaser *et al.*, 'Training schrödinger's cat: Quantum optimal control', *The European Physical Journal D*, vol. 69, no. 12, Dec. 2015, ISSN: 1434-6079.

[47] C. P. Koch, 'Controlling open quantum systems: Tools, achievements, and limitations', *Journal of Physics: Condensed Matter*, vol. 28, no. 21, p. 213 001, May 2016, ISSN: 1361-648X.

[48] S. Deffner and S. Campbell, 'Quantum speed limits: From heisenberg's uncertainty principle to optimal quantum control', *Journal of Physics A: Mathematical and Theoretical*, vol. 50, no. 45, p. 453 001, Oct. 2017, ISSN: 1751-8121.

[49] Koch, Christiane P. *et al.*, 'Quantum optimal control in quantum technologies. strategic report on current status, visions and goals for research in europe', *EPJ Quantum Technol.*, vol. 9, no. 1, p. 19, 2022.

[50] P. Doria, T. Calarco and S. Montangero, 'Optimal control technique for many-body quantum dynamics', *Phys. Rev. Lett.*, vol. 106, p. 190 501, 19 May 2011.

[51] T. Caneva *et al.*, 'Optimal control at the quantum speed limit', *Phys. Rev. Lett.*, vol. 103, p. 240 501, 24 Dec. 2009.

[52] J. R. Garrison and T. Grover, 'Does a single eigenstate encode the full hamiltonian?', *Phys. Rev. X*, vol. 8, p. 021 026, 2 Apr. 2018.

[53] D. Poulin, A. Qarry, R. Somma and F. Verstraete, 'Quantum simulation of time-dependent hamiltonians and the convenient illusion of hilbert space', *Physical Review Letters*, vol. 106, no. 17, Apr. 2011, ISSN: 1079-7114.

[54] E. F. Dumitrescu and P. Lougovski, 'Hamiltonian assignment for open quantum systems', *Phys. Rev. Research*, vol. 2, p. 033 251, 3 Aug. 2020.

[55] E. Bairey, C. Guo, D. Poletti, N. H. Lindner and I. Arad, 'Learning the dynamics of open quantum systems from their steady states', *New Journal of Physics*, vol. 22, no. 3, p. 032 001, Mar. 2020, ISSN: 1367-2630.

[56] X.-L. Qi and D. Ranard, 'Determining a local Hamiltonian from a single eigenstate', *Quantum*, vol. 3, p. 159, Jul. 2019, ISSN: 2521-327X.

[57] E. Chertkov and B. K. Clark, 'Computational inverse method for constructing spaces of quantum models from wave functions', *Phys. Rev. X*, vol. 8, p. 031 029, 3 Jul. 2018.

[58] M. Greiter, V. Schnells and R. Thomale, 'Method to identify parent hamiltonians for trial states', *Phys. Rev. B*, vol. 98, p. 081 113, 8 Aug. 2018.

[59] E. Bairey, I. Arad and N. H. Lindner, 'Learning a local hamiltonian from local measurements', *Physical Review Letters*, vol. 122, no. 2, Jan. 2019, ISSN: 1079-7114.

[60] S.-Y. Hou, N. Cao, S. Lu, Y. Shen, Y.-T. Poon and B. Zeng, 'Determining system hamiltonian from eigenstate measurements without correlation functions', *New Journal of Physics*, vol. 22, no. 8, p. 083 088, Sep. 2020, ISSN: 1367-2630.

[61] C. Cao, S.-Y. Hou, N. Cao and B. Zeng, 'Supervised learning in hamiltonian reconstruction from local measurements on eigenstates', *Journal of Physics: Condensed Matter*, vol. 33, no. 6, p. 064 002, Feb. 2020, ISSN: 1361-648X.

[62] J. Chen, Z. Ji, B. Zeng and D. L. Zhou, 'From ground states to local hamiltonians', *Phys. Rev. A*, vol. 86, p. 022 339, 2 Aug. 2012.

[63] C. Fernández-González, N. Schuch, M. M. Wolf, J. I. Cirac and D. Pérez-García, 'Frustration free gapless hamiltonians for matrix product states', *Communications in Mathematical Physics*, vol. 333, no. 1, pp. 299–333, Nov. 2014, ISSN: 1432-0916.

[64] X. Turkeshi, T. Mendes-Santos, G. Giudici and M. Dalmonte, 'Entanglement-guided search for parent hamiltonians', *Phys. Rev. Lett.*, vol. 122, p. 150 606, 15 Apr. 2019.

[65] X. Turkeshi and M. Dalmonte, 'Parent Hamiltonian Reconstruction of Jastrow-Gutzwiller Wavefunctions', *SciPost Phys.*, vol. 8, p. 42, 3 2020.

[66] H. Wang, 'Quantum algorithm for preparing the ground state of a system via resonance transition', *Scientific Reports*, vol. 7, no. 1, p. 16 342, Nov. 2017, ISSN: 2045-2322.

[67] D. Lee *et al.*, 'Projected cooling algorithm for quantum computation', *Physics Letters B*, vol. 807, p. 135 536, 2020, ISSN: 0370-2693.

[68] L. Lin and Y. Tong, 'Near-optimal ground state preparation', *Quantum*, vol. 4, p. 372, Dec. 2020, ISSN: 2521-327X.

[69] M. Raghunandan, F. Wolf, C. Ospelkaus, P. O. Schmidt and H. Weimer, 'Initialization of quantum simulators by sympathetic cooling', *Science Advances*, vol. 6, no. 10, eaaw9268, 2020.

[70] A. Zubida, E. Yitzhaki, N. H. Lindner and E. Bairey, *Optimal short-time measurements for hamiltonian learning*, 2021.

[71] D. Hangleiter, I. Roth, J. Eisert and P. Roushan, *Precise hamiltonian identification of a superconducting quantum processor*, 2021.

[72] E. H. Lieb and R. Seiringer, *The Stability of Matter in Quantum Mechanics*. Cambridge University Press, 2009.

[73] Y. Cao, S. Jiang, D. Perouli and S. Kais, 'Solving set cover with pairs problem using quantum annealing', *Scientific Reports*, vol. 6, Aug. 2016.

[74] S. Somaroo, C. H. Tseng, T. F. Havel, R. Laflamme and D. G. Cory, 'Quantum simulations on a quantum computer', *Phys. Rev. Lett.*, vol. 82, pp. 5381–5384, 26 Jun. 1999.

[75] I. M. Georgescu, S. Ashhab and F. Nori, 'Quantum simulation', *Rev. Mod. Phys.*, vol. 86, pp. 153–185, 1 Mar. 2014.

[76] E. Farhi, J. Goldstone, S. Gutmann and M. Sipser, 'Quantum computation by adiabatic evolution', 2000.

[77] J. Brooke, D. Bitko, T. F., null Rosenbaum and G. Aeppli, 'Quantum annealing of a disordered magnet', *Science*, vol. 284, no. 5415, pp. 779–781, 1999.

[78] J. Brooke, T. F. Rosenbaum and G. Aeppli, 'Tunable quantum tunnelling of magnetic domain walls', *Nature*, vol. 413, no. 6856, pp. 610–613, Oct. 2001, ISSN: 1476-4687.

[79] T. Albash and D. A. Lidar, 'Adiabatic quantum computation', *Rev. Mod. Phys.*, vol. 90, p. 015 002, 1 Jan. 2018.

[80] G. E. Santoro and E. Tosatti, 'Optimization using quantum mechanics: Quantum annealing through adiabatic evolution', *Journal of Physics A: Mathematical and General*, vol. 39, no. 36, R393, Aug. 2006.

[81] E. T. Campbell, B. M. Terhal and C. Vuillot, 'Roads towards fault-tolerant universal quantum computation', *Nature*, vol. 549, no. 7671, pp. 172–179, Sep. 2017, ISSN: 1476-4687.

[82] W. Lechner, P. Hauke and P. Zoller, 'A quantum annealing architecture with all-to-all connectivity from local interactions', *Science Advances*, vol. 1, no. 9, e1500838, 2015.

[83] K. Boothby, P. Bunyk, J. Raymond and A. Roy, 'Next-generation topology of d-wave quantum processors', 2020.

[84] N. Linden and W. K. Wootters, 'The parts determine the whole in a generic pure quantum state', *Phys. Rev. Lett.*, vol. 89, p. 277 906, 27 Dec. 2002.

[85] D. L. Zhou, 'Irreducible multiparty correlations in quantum states without maximal rank', *Physical Review Letters*, vol. 101, no. 18, Oct. 2008, ISSN: 1079-7114.

[86] M. P. da Silva, O. Landon-Cardinal and D. Poulin, 'Practical characterization of quantum devices without tomography', *Phys. Rev. Lett.*, vol. 107, p. 210 404, 21 Nov. 2011.

[87] A. Dutt *et al.*, *Active learning of quantum system hamiltonians yields query advantage*, 2021.

[88] R. Orús, 'A practical introduction to tensor networks: Matrix product states and projected entangled pair states', *Annals of Physics*, vol. 349, pp. 117–158, 2014, ISSN: 0003-4916.

[89] W. K. Wootters, 'Statistical distance and hilbert space', *Phys. Rev. D*, vol. 23, pp. 357–362, 2 Jan. 1981.

[90] S. Bravyi, M. B. Hastings and F. Verstraete, 'Lieb-robinson bounds and the generation of correlations and topological quantum order', *Phys. Rev. Lett.*, vol. 97, p. 050 401, 5 Jul. 2006.

[91] V. Giovannetti, S. Lloyd and L. Maccone, 'Quantum-enhanced measurements: Beating the standard quantum limit', *Science*, vol. 306, no. 5700, pp. 1330–1336, 2004.

[92] M. Zwierz, C. A. Pé rez-Delgado and P. Kok, 'General optimality of the heisenberg limit for quantum metrology', *Physical Review Letters*, vol. 105, no. 18, Oct. 2010.

[93] V. Giovannetti, S. Lloyd and L. Maccone, 'Advances in quantum metrology', *Nature Photonics*, vol. 5, no. 4, pp. 222–229, Mar. 2011.

[94] G. Tóth and I. Apellaniz, 'Quantum metrology from a quantum information science perspective', *Journal of Physics A: Mathematical and Theoretical*, vol. 47, no. 42, p. 424 006, Oct. 2014.

[95] L. Pezzè, A. Smerzi, M. K. Oberthaler, R. Schmied and P. Treutlein, 'Quantum metrology with nonclassical states of atomic ensembles', *Rev. Mod. Phys.*, vol. 90, p. 035 005, 3 Sep. 2018.

[96] H. Cramér and K. M. R. Collection, *Mathematical Methods of Statistics*, ser. Goldstine Printed Materials. Princeton University Press, 1946, ISBN: 9780691080048.

[97] D. D. Lewis and W. A. Gale, *A sequential algorithm for training text classifiers*, 1994.

[98] B. Settles, 'Active learning literature survey', 2009.

[99] M. V. Berry, 'Transitionless quantum driving', *Journal of Physics A Mathematical General*, vol. 42, no. 36, 365303, p. 365 303, Sep. 2009.

[100] M. Demirplak and S. A. Rice, 'Adiabatic population transfer with control fields', *The Journal of Physical Chemistry A*, vol. 107, no. 46, pp. 9937–9945, Nov. 2003, ISSN: 1089-5639.

[101] ——, 'Assisted adiabatic passage revisited', *The Journal of Physical Chemistry B*, vol. 109, no. 14, pp. 6838–6844, Apr. 2005, ISSN: 1520-6106.

[102] A. del Campo, 'Shortcuts to adiabaticity by counterdiabatic driving', *Phys. Rev. Lett.*, vol. 111, p. 100 502, 10 Sep. 2013.

[103] S. Deffner, C. Jarzynski and A. del Campo, 'Classical and quantum shortcuts to adiabaticity for scale-invariant driving', *Phys. Rev. X*, vol. 4, p. 021 013, 2 Apr. 2014.

[104] S. An, D. Lv, A. del Campo and K. Kim, 'Shortcuts to adiabaticity by counterdiabatic driving for trapped-ion displacement in phase space', *Nature Communications*, vol. 7, no. 1, p. 12 999, Sep. 2016, ISSN: 2041-1723.

[105] K. Funo, J.-N. Zhang, C. Chatou, K. Kim, M. Ueda and A. del Campo, 'Universal work fluctuations during shortcuts to adiabaticity by counterdiabatic driving', *Phys. Rev. Lett.*, vol. 118, p. 100 602, 10 Mar. 2017.

[106] C. W. Duncan and A. d. Campo, 'Shortcuts to adiabaticity assisted by counterdiabatic born–oppenheimer dynamics', *New Journal of Physics*, vol. 20, no. 8, p. 085 003, Aug. 2018, ISSN: 1367-2630.

[107] D. Guéry-Odelin, A. Ruschhaupt, A. Kiely, E. Torrontegui, S. Martınez-Garaot and J. G. Muga, 'Shortcuts to adiabaticity: Concepts, methods, and applications', *Rev. Mod. Phys.*, vol. 91, p. 045 001, 4 Oct. 2019.

[108] G. Passarelli, G. De Filippis, V. Cataudella and P. Lucignano, 'Dissipative environment may improve the quantum annealing performances of the ferromagnetic p-spin model', *Physical Review A*, vol. 97, no. 2, Feb. 2018, ISSN: 2469-9934.

[109] G. Passarelli, V. Cataudella and P. Lucignano, 'Improving quantum annealing of the ferromagnetic *p*-spin model through pausing', *Phys. Rev. B*, vol. 100, p. 024 302, 2 Jul. 2019.

[110] D. Sels and A. Polkovnikov, 'Minimizing irreversible losses in quantum systems by local counterdiabatic driving', *Proceedings of the National Academy of Sciences*, vol. 114, no. 20, E3909–E3916, 2017, ISSN: 0027-8424.

[111] E. J. Heller, 'Time dependent variational approach to semiclassical dynamics', *The Journal of Chemical Physics*, vol. 64, no. 1, pp. 63–73, 1976.

[112] J. Haegeman, J. I. Cirac, T. J. Osborne, I. Pi žorn, H. Verschelde and F. Verstraete, 'Time-dependent variational principle for quantum lattices', *Phys. Rev. Lett.*, vol. 107, p. 070 601, 7 Aug. 2011.

[113] E. Caurier and B. Grammaticos, 'Extreme level repulsion for chaotic quantum hamiltonians', *Physics Letters A*, vol. 136, no. 7, pp. 387–390, 1989, ISSN: 0375-9601.

[114] M. A. Nielsen, *A geometric approach to quantum circuit lower bounds*, 2005.

[115] M. A. Nielsen, M. R. Dowling, M. Gu and A. C. Doherty, 'Quantum computation as geometry', *Science*, vol. 311, no. 5764, pp. 1133–1135, Feb. 2006.

[116] A. R. Brown and L. Susskind, 'Complexity geometry of a single qubit', *Phys. Rev. D*, vol. 100, p. 046 020, 4 Aug. 2019.

[117] P. Zanardi, P. Giorda and M. Cozzini, 'Information-theoretic differential geometry of quantum phase transitions', *Phys. Rev. Lett.*, vol. 99, p. 100 603, 10 Sep. 2007.

[118] L. Campos Venuti and P. Zanardi, 'Quantum critical scaling of the geometric tensors', *Phys. Rev. Lett.*, vol. 99, p. 095 701, 9 Aug. 2007.

[119] D. F. Abasto, A. Hamma and P. Zanardi, 'Fidelity analysis of topological quantum phase transitions', *Phys. Rev. A*, vol. 78, p. 010 301, 1 Jul. 2008.

[120] P. Zanardi, L. Campos Venuti and P. Giorda, 'Bures metric over thermal state manifolds and quantum criticality', *Phys. Rev. A*, vol. 76, p. 062 318, 6 Dec. 2007.

[121] A. Carlini, A. Hosoya, T. Koike and Y. Okudaira, 'Time-optimal quantum evolution', *Phys. Rev. Lett.*, vol. 96, p. 060 503, 6 Feb. 2006.

[122] A. T. Rezakhani, W.-J. Kuo, A. Hamma, D. A. Lidar and P. Zanardi, 'Quantum adiabatic brachistochrone', *Phys. Rev. Lett.*, vol. 103, p. 080 502, 8 Aug. 2009.

[123] J. I. Latorre and R. Orús, 'Adiabatic quantum computation and quantum phase transitions', *Phys. Rev. A*, vol. 69, p. 062 302, 6 Jun. 2004.

[124] G. B. Mbeng, A. Russomanno and G. E. Santoro, *The quantum ising chain for beginners*, 2020.

[125] P. Pfeuty, 'The one-dimensional ising model with a transverse field', *Annals of Physics*, vol. 57, no. 1, pp. 79–90, 1970, ISSN: 0003-4916.

[126] E. Lieb, T. Schultz and D. Mattis, 'Two soluble models of an antiferromagnetic chain', *Annals of Physics*, vol. 16, no. 3, pp. 407–466, 1961, ISSN: 0003-4916.

[127] A. del Campo, M. M. Rams and W. H. Zurek, 'Assisted finite-rate adiabatic passage across a quantum critical point: Exact solution for the quantum ising model', *Phys. Rev. Lett.*, vol. 109, p. 115 703, 11 Sep. 2012.

[128] D. Gross and M. Mezard, 'The simplest spin glass', *Nuclear Physics B*, vol. 240, no. 4, pp. 431–452, 1984, ISSN: 0550-3213.

[129] E. Gardner, 'Spin glasses with p-spin interactions', *Nuclear Physics B*, vol. 257, pp. 747–765, 1985, ISSN: 0550-3213.

[130] T. R. Kirkpatrick and D. Thirumalai, 'Dynamics of the structural glass transition and the *p*-spin—interaction spin-glass model', *Phys. Rev. Lett.*, vol. 58, pp. 2091–2094, 20 May 1987.

[131] ——, 'P-spin-interaction spin-glass models: Connections with the structural glass problem', *Phys. Rev. B*, vol. 36, pp. 5388–5397, 10 Oct. 1987.

[132] L. K. Grover, *A fast quantum mechanical algorithm for database search*, 1996.

[133] G. Passarelli, K.-W. Yip, D. A. Lidar, H. Nishimori and P. Lucignano, 'Reverse quantum annealing of the *p*-spin model with relaxation', *Phys. Rev. A*, vol. 101, p. 022 331, 2 Feb. 2020.

[134] G. Passarelli, V. Cataudella, R. Fazio and P. Lucignano, 'Counterdiabatic driving in the quantum annealing of the *p*-spin model: A variational approach', *Phys. Rev. Research*, vol. 2, p. 013 283, 1 Mar. 2020.

[135] L. Prielinger, A. Hartmann, Y. Yamashiro, K. Nishimura, W. Lechner and H. Nishimori, 'Two-parameter counter-diabatic driving in quantum annealing', *Phys. Rev. Research*, vol. 3, p. 013 227, 1 Mar. 2021.

[136] A. Russomanno, R. Fazio and G. E. Santoro, 'Thermalization in a periodically driven fully connected quantum ising ferromagnet', *Europhysics Letters*, vol. 110, no. 3, p. 37 005, May 2015.

[137] M. M. Wauters, G. B. Mbeng and G. E. Santoro, 'Polynomial scaling of the quantum approximate optimization algorithm for ground-state preparation of the fully connected *p*-spin ferromagnet in a transverse field', *Phys. Rev. A*, vol. 102, p. 062 404, 6 Dec. 2020.

[138] M. M. Wauters, R. Fazio, H. Nishimori and G. E. Santoro, 'Direct comparison of quantum and simulated annealing on a fully connected ising ferromagnet', *Phys. Rev. A*, vol. 96, p. 022 326, 2 Aug. 2017.

[139] C. Gogolin and J. Eisert, 'Equilibration, thermalisation, and the emergence of statistical mechanics in closed quantum systems', *Reports on Progress in Physics*, vol. 79, no. 5, p. 056 001, Apr. 2016, ISSN: 1361-6633.

[140] C. Neuenhahn and F. Marquardt, 'Thermalization of interacting fermions and delocalization in fock space', *Physical Review E*, vol. 85, no. 6, Jun. 2012, ISSN: 1550-2376.

[141] E. Canovi, D. Rossini, R. Fazio, G. E. Santoro and A. Silva, 'Quantum quenches, thermalization, and many-body localization', *Phys. Rev. B*, vol. 83, p. 094 431, 9 Mar. 2011.

[142] A. Polkovnikov, K. Sengupta, A. Silva and M. Vengalattore, 'Colloquium: Nonequilibrium dynamics of closed interacting quantum systems', *Reviews of Modern Physics*, vol. 83, no. 3, pp. 863–883, Aug. 2011, ISSN: 1539-0756.

[143] T. M. Cover and J. A. Thomas, *Elements of Information Theory 2nd Edition (Wiley Series in Telecommunications and Signal Processing)*. Wiley-Interscience, Jul. 2006, ISBN: 0471241954.

[144] P. Reimann, 'Foundation of statistical mechanics under experimentally realistic conditions', *Phys. Rev. Lett.*, vol. 101, p. 190 403, 19 Nov. 2008.

[145] N. Linden, S. Popescu, A. J. Short and A. Winter, 'Quantum mechanical evolution towards thermal equilibrium', *Phys. Rev. E*, vol. 79, p. 061 103, 6 Jun. 2009.

[146] A. J. Short, 'Equilibration of quantum systems and subsystems', *New Journal of Physics*, vol. 13, no. 5, p. 053 009, May 2011.

[147] M. S. ANIS *et al.*, *Qiskit: An open-source framework for quantum computing*, 2021.

[148] C. Rigetti and M. Devoret, 'Fully microwave-tunable universal gates in superconducting qubits with linear couplings and fixed transition frequencies', *Phys. Rev. B*, vol. 81, p. 134 507, 13 Apr. 2010.

[149] J. M. Chow *et al.*, 'Simple all-microwave entangling gate for fixed-frequency superconducting qubits', *Phys. Rev. Lett.*, vol. 107, p. 080 502, 8 Aug. 2011.

[150] S. Sheldon, E. Magesan, J. M. Chow and J. M. Gambetta, 'Procedure for systematically tuning up cross-talk in the cross-resonance gate', *Phys. Rev. A*, vol. 93, p. 060 302, 6 Jun. 2016.

[151] E. Magesan and J. M. Gambetta, 'Effective hamiltonian models of the cross-resonance gate', *Phys. Rev. A*, vol. 101, p. 052 308, 5 May 2020.

[152] *Hamiltonian tomography*, Accessed: 2022-03-29.

[153] M. Berry, 'Quantum chaology, not quantum chaos', *Physica Scripta*, vol. 40, no. 3, p. 335, Sep. 1989.

[154] F. Haake, 'Quantum signatures of chaos', in *Quantum Coherence in Mesoscopic Systems*, Springer, 1991, pp. 583–595.

[155] S. Kirkpatrick, C. D. Gelatt and M. P. Vecchi, 'Optimization by simulated annealing', *Science*, vol. 220, no. 4598, pp. 671–680, 1983.

[156] P. J. M. van Laarhoven and E. H. L. Aarts, 'Simulated annealing', in *Simulated Annealing: Theory and Applications*, Dordrecht: Springer Netherlands, 1987, pp. 7–15, ISBN: 978-94-015-7744-1.

[157] R. Rutenbar, 'Simulated annealing algorithms: An overview', *IEEE Circuits and Devices Magazine*, vol. 5, no. 1, pp. 19–26, 1989.

[158] S. R. White, 'Density matrix formulation for quantum renormalization groups', *Phys. Rev. Lett.*, vol. 69, pp. 2863–2866, 19 Nov. 1992.

[159] ——, 'Density-matrix algorithms for quantum renormalization groups', *Phys. Rev. B*, vol. 48, pp. 10 345–10 356, 14 Oct. 1993.

[160] U. Schollwöck, 'The density-matrix renormalization group', *Rev. Mod. Phys.*, vol. 77, pp. 259–315, 1 Apr. 2005.

[161] U. Schollwöck, 'The density-matrix renormalization group in the age of matrix product states', *Annals of Physics*, vol. 326, no. 1, pp. 96–192, Jan. 2011.

[162] E. Farhi, J. Goldstone and S. Gutmann, *A quantum approximate optimization algorithm*, 2014.

[163] E. Farhi and A. W. Harrow, *Quantum supremacy through the quantum approximate optimization algorithm*, 2016.

[164] L. Zhou, S.-T. Wang, S. Choi, H. Pichler and M. D. Lukin, 'Quantum approximate optimization algorithm: Performance, mechanism, and implementation on near-term devices', *Phys. Rev. X*, vol. 10, p. 021 067, 2 Jun. 2020.

[165] A. Messiah, *Quantum Mechanics*, ser. Dover books on physics v. 2. Dover Publications, 1999, ISBN: 9780486409245.

[166] F. Wilczek and A. Zee, 'Appearance of gauge structure in simple dynamical systems', *Phys. Rev. Lett.*, vol. 52, pp. 2111–2114, 24 Jun. 1984.

[167] G. Rigolin and G. Ortiz, 'Adiabatic perturbation theory and geometric phases for degenerate systems', *Phys. Rev. Lett.*, vol. 104, p. 170 406, 17 Apr. 2010.

[168] ——, 'Adiabatic theorem for quantum systems with spectral degeneracy', *Phys. Rev. A*, vol. 85, p. 062 111, 6 Jun. 2012.

[169] S. M. Giampaolo, G. Adesso and F. Illuminati, 'Theory of ground state factorization in quantum cooperative systems', *Phys. Rev. Lett.*, vol. 100, p. 197 201, 19 May 2008.

[170] B. Tomasello, D. Rossini, A. Hamma and L. Amico, 'Ground-state factorization and correlations with broken symmetry', *EPL (Europhysics Letters)*, vol. 96, no. 2, p. 27 002, 2011.

[171] S. M. Giampaolo, G. Adesso and F. Illuminati, 'Separability and ground-state factorization in quantum spin systems', *Phys. Rev. B*, vol. 79, p. 224 434, 22 Jun. 2009.

[172] G. L. Giorgi, 'Ground-state factorization and quantum phase transition in dimerized spin chains', *Phys. Rev. B*, vol. 79, p. 060 405, 6 Feb. 2009.

[173] S. Montes and A. Hamma, 'Phase diagram and quench dynamics of the cluster-XY spin chain', *Phys. Rev. E*, vol. 86, p. 021 101, 2 Aug. 2012.

[174] A. Y. Kitaev, 'Unpaired majorana fermions in quantum wires', *Physics-Uspekhi*, vol. 44, no. 10S, pp. 131–136, Oct. 2001.

[175] J. S. Bell, 'On the einstein podolsky rosen paradox', *Physics Physique Fizika*, vol. 1, no. 3, p. 195, 1964.

[176] A. Fine, 'Hidden variables, joint probability, and the bell inequalities', *Phys. Rev. Lett.*, vol. 48, pp. 291–295, 5 Feb. 1982.

[177] B. M. Terhal, 'Bell inequalities and the separability criterion', *Physics Letters A*, vol. 271, no. 5-6, pp. 319–326, Jul. 2000.

[178] R. F. Werner and M. M. Wolf, *Bell inequalities and entanglement*, 2001.

[179] A. Aspect, P. Grangier and G. Roger, 'Experimental tests of realistic local theories via bell's theorem', *Phys. Rev. Lett.*, vol. 47, pp. 460–463, 7 Aug. 1981.

[180] ——, 'Experimental realization of einstein-podolsky-rosen-bohm gedankenexperiment: A new violation of bell's inequalities', *Phys. Rev. Lett.*, vol. 49, pp. 91–94, 2 Jul. 1982.

[181] A. Aspect, J. Dalibard and G. Roger, 'Experimental test of bell's inequalities using time-varying analyzers', *Phys. Rev. Lett.*, vol. 49, pp. 1804–1807, 25 Dec. 1982.

[182] A. Peres, *Quantum mechanics: Concepts and methods*, 1993.

[183] R. Jozsa, *Entanglement and quantum computation*, 1997.

[184] A. Steane, 'Quantum computing', *Reports on Progress in Physics*, vol. 61, no. 2, p. 117, 1998.

[185] R. Jozsa and N. Linden, 'On the role of entanglement in quantum-computational speed-up', *Proceedings of the Royal Society of London. Series A: Mathematical, Physical and Engineering Sciences*, vol. 459, no. 2036, pp. 2011–2032, Aug. 2003.

[186] D. Deutsch and R. Jozsa, 'Rapid solution of problems by quantum computation', *Proceedings of the Royal Society of London. Series A: Mathematical and Physical Sciences*, vol. 439, no. 1907, pp. 553–558, 1992.

[187] P. W. Shor, 'Polynomial-time algorithms for prime factorization and discrete logarithms on a quantum computer', *SIAM review*, vol. 41, no. 2, pp. 303–332, 1999.

[188] J. I. Latorre, E. Rico and G. Vidal, 'Ground state entanglement in quantum spin chains', 2003.

[189] L. Amico, R. Fazio, A. Osterloh and V. Vedral, 'Entanglement in many-body systems', *Rev. Mod. Phys.*, vol. 80, pp. 517–576, 2 May 2008.

[190] G. Vidal, J. I. Latorre, E. Rico and A. Kitaev, 'Entanglement in quantum critical phenomena', *Phys. Rev. Lett.*, vol. 90, p. 227 902, 22 Jun. 2003.

[191] A. Osterloh, L. Amico, G. Falci and R. Fazio, 'Scaling of entanglement close to a quantum phase transition', *Nature*, vol. 416, no. 6881, pp. 608–610, Apr. 2002.

[192] D. N. Page, 'Average entropy of a subsystem', *Phys. Rev. Lett.*, vol. 71, pp. 1291–1294, 9 Aug. 1993.

[193] D. Gottesman, 'The heisenberg representation of quantum computers', 1998.

[194] V. Veitch, S. A. H. Mousavian, D. Gottesman and J. Emerson, 'The resource theory of stabilizer quantum computation', *New Journal of Physics*, vol. 16, no. 1, p. 013 009, Jan. 2014.

[195] M. Howard and E. Campbell, 'Application of a resource theory for magic states to fault-tolerant quantum computing', *Phys. Rev. Lett.*, vol. 118, p. 090 501, 9 Mar. 2017.

[196] E. T. Campbell, H. Anwar and D. E. Browne, 'Magic-state distillation in all prime dimensions using quantum reed-muller codes', *Phys. Rev. X*, vol. 2, p. 041 021, 4 Dec. 2012.

[197] E. T. Campbell and D. E. Browne, 'Bound states for magic state distillation in fault-tolerant quantum computation', *Phys. Rev. Lett.*, vol. 104, p. 030 503, 3 Jan. 2010.

[198] L. Leone, S. F. E. Oliviero and A. Hamma, 'Stabilizer rényi entropy', *Phys. Rev. Lett.*, vol. 128, p. 050 402, 5 Feb. 2022.

[199] S. F. E. Oliviero, L. Leone, A. Hamma and S. Lloyd, 'Measuring magic on a quantum processor', *npj Quantum Information*, vol. 8, no. 1, Dec. 2022.

[200] T. Haug and M. S. Kim, *Scalable measures of magic resource for quantum computers*, 2022.

[201] L. Leone, S. F. E. Oliviero and A. Hamma, *Magic determines the hardness of direct fidelity estimation*, 2022.

[202] A. S. Darmawan and S. D. Bartlett, 'Graph states as ground states of two-body frustration-free hamiltonians', *New Journal of Physics*, vol. 16, no. 7, p. 073 013, 2014.

[203] S. F. E. Oliviero, L. Leone and A. Hamma, 'Magic-state resource theory for the ground state of the transverse-field ising model', *Physical Review A*, vol. 106, no. 4, Oct. 2022.

[204] T. Haug and L. Piroli, *Quantifying nonstabilizerness of matrix product states*, 2022.

[205] J. Eisert, M. Cramer and M. B. Plenio, 'Colloquium: Area laws for the entanglement entropy', *Rev. Mod. Phys.*, vol. 82, pp. 277–306, 1 Feb. 2010.

[206] P. Calabrese and J. Cardy, 'Evolution of entanglement entropy in one-dimensional systems', *Journal of Statistical Mechanics: Theory and Experiment*, vol. 2005, no. 04, P04010, 2005.

[207] H. Kim and D. A. Huse, 'Ballistic spreading of entanglement in a diffusive nonintegrable system', *Physical Review Letters*, vol. 111, no. 12, Sep. 2013.

[208] R. A. Jalabert and H. M. Pastawski, 'Environment-independent decoherence rate in classically chaotic systems', *Phys. Rev. Lett.*, vol. 86, pp. 2490–2493, 12 Mar. 2001.

[209] A. Peres, 'Stability of quantum motion in chaotic and regular systems', *Phys. Rev. A*, vol. 30, pp. 1610–1615, 4 Oct. 1984.

[210] J. Häppölä, G. B. Halász and A. Hamma, 'Universality and robustness of revivals in the transverse field xy model', *Physical Review A*, vol. 85, no. 3, Mar. 2012.

[211] L. Leone, S. F. Oliviero, Y. Zhou and A. Hamma, 'Quantum chaos is quantum', *Quantum*, vol. 5, p. 453, 2021.

[212] S. F. E. Oliviero, L. Leone, S. Lloyd and A. Hamma, *Black hole complexity, unscrambling, and stabilizer thermal machines*, 2022.

[213] E. H. Lieb and D. W. Robinson, 'The finite group velocity of quantum spin systems', *Communications in Mathematical Physics*, vol. 28, no. 3, pp. 251–257, Sep. 1972, ISSN: 1432-0916.

[214] B. Nachtergaele, Y. Ogata and R. Sims, 'Propagation of correlations in quantum lattice systems', *Journal of Statistical Physics*, vol. 124, no. 1, pp. 1–13, Jul. 2006.

[215] G. D. Chiara, S. Montangero, P. Calabrese and R. Fazio, 'Entanglement entropy dynamics of heisenberg chains', *Journal of Statistical Mechanics: Theory and Experiment*, vol. 2006, no. 03, P03001–P03001, Mar. 2006.

[216] F. G. S. L. Brandão and M. Horodecki, 'Exponential decay of correlations implies area law', *Communications in Mathematical Physics*, vol. 333, no. 2, pp. 761–798, Nov. 2014.

[217] A. I. Larkin and Y. N. Ovchinnikov, 'Quasiclassical Method in the Theory of Superconductivity', *Soviet Journal of Experimental and Theoretical Physics*, vol. 28, p. 1200, Jun. 1969.

[218] A. Kitaev, 'Hidden correlations in the hawking radiation and thermal noise', in *Talk given at the Fundamental Physics Prize Symposium*, vol. 10, 2014.

[219] D. A. Roberts and B. Yoshida, 'Chaos and complexity by design', *Journal of High Energy Physics*, vol. 2017, no. 4, p. 121, Apr. 2017, ISSN: 1029-8479.

[220] K. Hashimoto, K. Murata and R. Yoshii, 'Out-of-time-order correlators in quantum mechanics', *Journal of High Energy Physics*, vol. 2017, no. 10, p. 138, Oct. 2017, ISSN: 1029-8479.

[221] S. Lloyd, M. Mohseni and P. Rebentrost, 'Quantum principal component analysis', *Nature Physics*, vol. 10, no. 9, pp. 631–633, 2014.

[222] M. Kjaergaard *et al.*, 'Demonstration of density matrix exponentiation using a superconducting quantum processor', *Phys. Rev. X*, vol. 12, p. 011 005, 1 Jan. 2022.

[223] J. Surace and L. Tagliacozzo, 'Fermionic gaussian states: An introduction to numerical approaches', *SciPost Physics Lecture Notes*, May 2022.